



UNITED NATIONS
UNIVERSITY

GEOHERMAL TRAINING PROGRAMME

ORKUSTOFNUN



Hot spring at Ölkelduháls in the Hengill area

Sylvia Joan Malimo

**AQUIFER FLUID MODELLING AND ASSESSMENT OF
MINERAL-GAS-LIQUID EQUILIBRIA IN THE
NÁMAFJALL GEOTHERMAL SYSTEM, NE-ICELAND**

Report 3
November 2012



**UNITED NATIONS
UNIVERSITY**

GEOHERMAL TRAINING PROGRAMME
Orkustofnun, Grensásvegur 9,
IS-108 Reykjavík, Iceland

Reports 2012
Number 3

AQUIFER FLUID MODELLING AND ASSESSMENT OF MINERAL-GAS-LIQUID EQUILIBRIA IN THE NÁMAFJALL GEOTHERMAL SYSTEM, NE-ICELAND

MSc thesis

School of Engineering and Natural Sciences
Faculty of Earth Sciences
University of Iceland

by

Sylvia Joan Malimo

Geothermal Development Company Ltd - GDC
P.O. Box 17700 - 20100
Nakuru
KENYA
smalimo@gdc.co.ke, malimosj@gmail.com

United Nations University
Geothermal Training Programme
Reykjavík, Iceland
Published in November 2012

ISBN 978-9979-68-322-3
ISSN 1670-7427

This MSc thesis has also been published in April 2012 by the
School of Engineering and Natural Sciences,
Faculty of Earth Sciences
University of Iceland

INTRODUCTION

The Geothermal Training Programme of the United Nations University (UNU) has operated in Iceland since 1979 with six month annual courses for professionals from developing countries. The aim is to assist developing countries with significant geothermal potential to build up groups of specialists that cover most aspects of geothermal exploration and development. During 1979-2012, 515 scientists and engineers from 53 developing countries have completed the six month courses. They have come from Asia (40%), Africa (32%), Central America (16%), Central and Eastern Europe (12%), and Oceania (0.4%) There is a steady flow of requests from all over the world for the six month training and we can only meet a portion of the requests. Most of the trainees are awarded UNU Fellowships financed by the UNU and the Government of Iceland.

Candidates for the six month specialized training must have at least a BSc degree and a minimum of one year practical experience in geothermal work in their home countries prior to the training. Many of our trainees have already completed their MSc or PhD degrees when they come to Iceland, but several excellent students who have only BSc degrees have made requests to come again to Iceland for a higher academic degree. In 1999, it was decided to start admitting UNU Fellows to continue their studies and study for MSc degrees in geothermal science or engineering in co-operation with the University of Iceland. An agreement to this effect was signed with the University of Iceland. The six month studies at the UNU Geothermal Training Programme form a part of the graduate programme.

It is a pleasure to introduce the 31st UNU Fellow to complete the MSc studies at the University of Iceland under the co-operation agreement. Sylvia J. Malimo, BSc in Chemistry and Mathematics, of the Geothermal Development Company – GDC, Kenya, completed the six month specialized training in Chemistry of Thermal Fluids at the UNU Geothermal Training Programme in October 2009. Her research report was entitled: “Interpretation of geochemical well test data for wells OW-903B, OW-904B and OW-909, Olkaria Domes, Kenya”. After one year of geothermal research work in Kenya, she came back to Iceland for MSc studies at the Faculty of Earth Sciences of the University of Iceland in August 2010. In April 2012, she defended her MSc thesis presented here, entitled “Aquifer fluid modelling and assessment of mineral-gas-liquid equilibria in the Námafjall geothermal system, NE-Iceland”. Her studies in Iceland were financed by the Government of Iceland through a UNU-GTP Fellowship from the UNU Geothermal Training Programme. We congratulate her on her achievements and wish her all the best for the future. We thank the Faculty of Earth Sciences at the School of Engineering and Natural Sciences of the University of Iceland for the co-operation, and her supervisors for the dedication.

Finally, I would like to mention that Sylvia’s MSc thesis with the figures in colour is available for downloading on our website www.unugtp.is under publications.

With warmest wishes from Iceland,

Ingvar B. Fridleifsson, director
United Nations University
Geothermal Training Programme

ACKNOWLEDGEMENTS

I acknowledge and thank the following for their support and contributions to this study:

... Government of Iceland for awarding me this Fellowship through the United Nations University Geothermal Training Programme (UNU-GTP).

... UNU-GTP staff: Ingvar Birgir Fridleifsson, Lúdvík S. Georgsson, Thórhildur Ísberg, Ingimar G. Haraldsson, Markús A.G. Wilde and Málfrídur Ómarsdóttir.

... Geothermal Development Company Ltd., Kenya for granting me the time off work to pursue this study.

... To my supervisors: Dr. Thráinn Fridriksson and Prof. Stefán Arnórsson who have had the enthusiasm and made the time for discussions towards this study. Your views and eagerness to provide me with meticulous comments on the principles in the chapters have been admirable, and certainly contributed to a clearer presentation of ideas.

... Landsvirkjun, Orkustofnun, ÍSOR and Kemia Ltd for providing the data on which this study is based.

... Dr. Andri Stefánsson and Nicole Keller at the Institute of Earth Sciences, University of Iceland for various inputs and discussions.

... Orkustofnun and ÍSOR staff with special thanks to Rósa S. Jónsdóttir, Magnús Ólafsson and Sigrídur Sif Gylfadóttir.

My family and friends for their love, support and encouragement.

DEDICATION

For Rhoda James, my "antique" girl.

ABSTRACT

This study presents a geochemical evaluation of the Námafjall high-temperature geothermal field with respect to the chemical and physical processes that account for the fluid concentrations of volatile and non-volatile components, and the mineral assemblages controlling equilibrium in the aquifer. Aquifer fluid compositions and aqueous species distribution, for 25 samples collected from 7 wet-steam well discharges, were calculated from water- and steam-phase analyses and discharge enthalpies using the WATCH 2.1 speciation program according to the phase segregation model. Phase segregation pressures calculated at ~80% volume fraction of the flowing vapour are selected in view of the fact that liquid saturation at this pressures relate to residual liquid saturation of 0.2. The modelled aquifer fluid compositions were used to assess how closely equilibrium is approached between solution and various minerals. H₂S and H₂ concentrations were used to evaluate the presence of equilibrium vapour fraction in the initial aquifer fluid, calculated as 0-3.9% by weight with a field average of 0.79% by weight. At inferred Námafjall aquifer temperatures (200-300°C), the concentration of H₂S in the initial aquifer fluids is somewhat higher than predicted at equilibrium with hydrothermal mineral assemblage consisting of pyrite, pyrrhotite, prehnite and epidote, while concentration of H₂ closely approaches equilibrium for the excess enthalpy wells unlike for the liquid enthalpy wells. With respect to CO₂ the calculated chemical compositions of initial aquifer fluid show a close approach to equilibrium (for liquid enthalpy wells) but lower than equilibrium for the excess enthalpy wells with the hydrothermal alteration minerals clinozoisite, calcite, quartz and prehnite. The shallower aquifer at Námafjall are higher in gas (H₂S, H₂, CO₂ and N₂) indicating that gaseous steam from deeper aquifers has condensed in the shallower ones signifying that they are, at least partly, steam-heated. The main uncertainty involved in calculating mineral saturation indices, particularly in the case of excess enthalpy well discharges, lies in the model adopted to calculate the aquifer water composition and its aqueous species distribution and in the quality of the thermodynamic data on the aqueous species and the minerals especially those that involve Fe-bearing species. In the deep aquifers, chemical equilibrium has been rather closely approached between dissolved solids, H₂S and H₂ on one hand and hydrothermal minerals on the other.

TABLE OF CONTENTS

	Page
1. INTRODUCTION	1
2. NÁMAFJALL GEOTHERMAL FIELD	5
2.1 Geology.....	5
2.2 Hydrology	7
2.3 Geophysical review.....	8
2.4 Geochemical review	9
2.5 Reservoir characteristics	11
3. METHODOLOGY.....	12
3.1 Sampling and analysis	12
3.2 Data handling.....	14
3.3 Aquifer fluid modelling	14
3.3.1 ‘Excess’ enthalpy and phase segregation	14
3.3.2 Aquifer fluid temperature.....	16
3.3.3 Phase segregation pressure.....	19
3.3.4 Thermodynamics of the phase segregation model	21
3.4 Equilibrium vapour fraction.....	30
4. MINERAL-GAS-LIQUID EQUILIBRIA	34
4.1 Alteration mineralogy and thermodynamic data.....	34
4.2 Mineral-gas equilibria.....	37
4.2.1 H ₂ S and H ₂	38
4.2.2 CO ₂	39
4.3 Mineral-solute equilibria.....	40
4.3.1 Calcite, wollastonite and anhydrite	41
4.3.2 Epidote-clinozoisite, grossular and prehnite	42
4.3.3 Magnetite, pyrite and pyrrhotite	43
5. SUMMARY AND CONCLUSIONS	46
REFERENCES.....	49
APPENDIX I: Temperature profiles of Námafjall wells	56
APPENDIX II: Fluid/gas characteristics and selected constituent concentrations at 10 bar-a	57

LIST OF FIGURES

1. Simplified geological map of Iceland.	1
2. Location of wells in the Námafjall geothermal field.....	3
3. Structural map of Krafla and Námafjall geothermal areas.....	5
4. Geological map of the Námafjall area	6
5. Possible groundwater flow model to Námafjall and Krafla	7
6. General resistivity structure and alteration of basaltic crust in Iceland.	8
7. Resistivity structure of Námafjall	9
8. Reservoir temperature contours based on geothermometry	10
9. Changes during the production period in the concentrations of Cl, SO ₄ and SiO ₂ at 10 bar-a	10
10. The basic grid of the Námafjall model.....	11
11. Mass recharge into the reservoir	11
12. Relationship between p/T and enthalpy of saturated steam in the range 100-300°C	14

	Page
13. Fluid characteristics and concentration of Námafjall wells at 10 bar-a	15
14. Discharge enthalpy of wells in Námafjall field.....	16
15. Variation in silica content in separated waters and total discharge of excess enthalpy wells.....	17
16. Relationship between geothermometer temperatures in Námafjall wells.....	18
17. Relative permeability functions relating liquid saturation to relative permeability.....	20
18. Calculated liquid saturation at segregation pressures considered at ~80% volume fraction	20
19. Relative $V^{f,t}$ of initial inflowing aquifer fluid as a function of $h^{d,t}$	23
20. Relative calculated concentration of a non-volatile component ($m_r^{f,t}$) in initial aquifer fluid	24
21. Relative calculated concentration of volatile components ($m_s^{f,t}$) in initial aquifer fluid.....	28
22. Calculated SiO_2 concentration of excess enthalpy wells in the initial aquifer fluid.....	29
23. Calculated concentration of volatiles (CO_2 , H_2S and H_2) in the initial aquifer fluid.....	29
24. Calculated equilibrium vapour fractions ($X_{\text{H}_2\text{S}-\text{H}_2}^{f,v}$) for Námafjall wells.....	31
25. Calculated equilibrium vapour fractions, $X_{\text{H}_2\text{S}-\text{H}_2}^{f,v}$ as a function of selected fluid temperature..	32
26. Potential mineral buffers controlling H_2S gas concentrations in the initial aquifer fluid.	38
27. Potential mineral buffers controlling H_2 gas concentrations in the initial aquifer fluid.....	38
28. Potential mineral buffers controlling CO_2 gas concentrations in the initial aquifer fluid.	39
29. Saturation state of aquifer waters with respect to calcite, wollastonite and anhydrite.....	41
30. Saturation state of calcite, wollastonite and anhydrite as a function of aquifer water pH	42
31. $\text{Ca}^{+2}/[\text{H}^+]^2$ activity ratios versus initial aquifer fluid temperature.....	42
32. Saturation indices of Ca-Al silicate minerals in the initial aquifer fluid.....	43
33. Saturation indices of Fe-bearing minerals in the initial aquifer fluid.....	44
34. $\text{Fe}(\text{OH})_4^-/\text{OH}^-$ activity ratios versus initial aquifer fluid temperatures.....	45
35. Calculated $\text{H}_2\text{S}/\text{H}_2$ activity ratios at equilibrium with pyr+mag and pyr+pyrr.....	45

LIST OF TABLES

1. Boreholes in Námafjall geothermal field.	2
2. Measured discharge enthalpies, sampling pressures and analysis of elements	13
3. Geothermometer equations valid in the range 0-350°C at P_{sat}	17
4. Geothermometer temperatures (°C) and aquifer temperature logs for Námafjall wells.	18
5. Conservation equations and equations to calculate individual component concentrations.....	21
6. Henry's law constants and equations	25
7. Composition of initial aquifer fluid for Námafjall wells.....	27
8. Calculated equilibrium vapor fractions for Námafjall wells.....	31
9. Composition of initial aquifer liquid taking into account the presence of $X^{f,v}$	33
10. Temperature equations for equilibrium constants for individual mineral dissolution reactions ..	35
11. Mineral pairs and assemblage reactions that control activity ratios and gas concentrations	36

ABBREVIATIONS

μ_i	Dynamic viscosity of phase i
$\rho^{e,l}$	Liquid density at the point of phase segregation
$\rho^{e,v}$	Vapour density at the point of phase segregation
D_s^e	Distribution coefficient for volatile species s at the point of phase segregation
D_s^f	Distribution coefficient for volatile species s in initial aquifer fluid
$h^{d,l}$	Enthalpy of saturated liquid at sampling pressure SP (kJ/kg)
$h^{d,t}$	Total enthalpy of well discharge (kJ/kg)
$h^{d,v}$	Enthalpy of saturated vapour at sampling pressure SP (kJ/kg)
$h^{e,l}$	Enthalpy of saturated liquid at phase segregation pressure P^e (kJ/kg)
$h^{e,v}$	Enthalpy of saturated vapour at phase segregation pressure P^e (kJ/kg)
$h^{f,l}$	Enthalpy of saturated liquid at initial aquifer fluid conditions (kJ/kg)
$h^{f,t}$	Total enthalpy of initial aquifer fluid. If $X^{f,v}$ is assumed to be 0, $h^{f,t} = h^{f,l}$ (kJ/kg)
$h^{f,v}$	Enthalpy of saturated vapour at initial aquifer fluid conditions (kJ/kg)
$K_{H,S}$	Henry's Law solubility constant for volatile species s
k_{ri}	Relative permeability of phase i
k_a	Intrinsic permeability
$m_i^{d,l}$	Concentration of chemical component i in liquid phase at sampling pressure, SP (moles/kg)
$m_i^{d,t}$	Concentration of chemical component i in total well discharge (moles/kg)
$m_i^{d,v}$	Concentration of chemical component i in vapour phase at sampling pressure, SP (moles/kg)
$m_i^{e,l}$	Concentration of chemical component i in liquid phase at phase segregation pressure P^e (moles/kg)
$m_i^{e,t}$	Concentration of chemical component i in total fluid immediately before phase segregation (moles/kg)
$m_i^{e,v}$	Concentration of chemical component i in vapour phase at phase segregation pressure P^e (moles/kg)
$m_i^{f,l}$	Concentration of chemical component i in liquid phase of initial aquifer fluid (moles/kg)
$m_i^{f,t}$	Concentration of chemical component i in initial aquifer fluid. If $X^{f,v} = 0$, $m_i^{f,t} = m_i^{f,l}$ (moles/kg)
$m_r^{d,t}$	Concentration of non-volatile r in total well discharge (moles/kg)
$m_r^{e,l}$	Concentration of non-volatile r in liquid phase at phase segregation pressure P^e (moles/kg)
$m_r^{f,l}$	Concentration of non-volatile species, r, in liquid phase of initial aquifer fluid (moles/kg)
$m_r^{f,t}$	Concentration of non-volatile species, r, in total initial aquifer fluid. If $X^{f,v} = 0$, $m_r^{f,t} = m_r^{f,l}$
$m_s^{d,t}$	Concentration of volatile species s in total well discharge (moles/kg)
$m_s^{e,l}$	Concentration of volatile species s in liquid phase at phase segregation pressure P^e (moles/kg)
$m_s^{f,l}$	Concentration of volatile species s in liquid phase of the initial aquifer fluid (moles/kg)
$m_s^{f,t}$	Concentration of volatile species s in total initial aquifer fluid (moles/kg)
M_i	Mass flow of phase i (kg/s)
$M^{d,l}$	Mass flow of liquid in wet-steam well discharge (kg/s)
$M^{d,t}$	Mass flow of liquid and steam in wet-steam well discharge (kg/s)
$M^{d,v}$	Mass flow of steam in wet-steam well discharge (kg/s)
$M^{e,l}$	Mass flow of boiled aquifer liquid which separates from steam flowing into well (kg/s)
$M^{f,t}$	Mass flow of total initial aquifer fluid into well (kg/s)
$\Delta p/L$	Pressure gradient
P^e	Vapour pressure at which phase segregation is assumed to occur (bar-a)
P^f	Vapour pressure of the initial aquifer (bar-a)
$S^{e,l}$	Liquid saturation at phase segregation pressure P^e
SP	Vapour pressure as read from gauge atop Webre separator (bar-g)
T^e	Temperature at phase segregation pressure P^e ($^{\circ}C$)
T^f	Selected temperature of initial aquifer fluid ($^{\circ}C$) taken as the average of T_{qtz} and $T_{Na/K}$.

$T_{\text{Na/K}}$	Fluid temperature (°C) as determined using the Na/K concentration ratio at equilibrium with pure low-albite and pure microcline according to Arnórsson and Stefánsson (1999) and Arnórsson et al. (2000)
T_{qtz}	Fluid temperature (°C) based on unionized silica concentration in water initially in equilibrium with quartz after adiabatic boiling to 180°C (10 bar-a vapour pressure) according to Gudmundsson and Arnórsson (2002)
$V^{e,l}$	Relative mass of boiled water retained in aquifer upon phase segregation to well discharge ($M^{e,l,r} / M^{d,t}$)
$V^{f,t}$	Relative mass of total inflowing initial aquifer fluid to well discharge ($M^{f,t} / M^{d,t}$)
$X^{d,v}$	Vapour mass fraction at sampling pressure SP
$X^{e,v}$	Vapour mass fraction immediately prior to phase segregation
$X^{f,v}$	Vapour mass fraction present in the initial aquifer fluid
$X_{\text{H}_2\text{S}}^{f,v}$	Calculated equilibrium vapour fraction assuming equilibrium of H ₂ S concentration in aquifer liquid phase
$X_{\text{H}_2}^{f,v}$	Calculated equilibrium vapour fraction assuming equilibrium of H ₂ concentration in aquifer liquid phase
$X_{\text{H}_2\text{S-H}_2}^{f,v}$	Calculated equilibrium vapour fraction assuming equilibrium of H ₂ S and H ₂ concentrations in aquifer liquid phase

1. INTRODUCTION

Volcanic activity in Iceland is confined to the active volcanic zones composed of volcanic systems which consists a central volcano and a fissure swarm that may extend tens of kilometres along strike in both directions away from the central volcano (Figure 1). Iceland has 30 identified volcanic systems of which 16 have been active after 870 AD (Gudmundsson et al., 2008; Thordarson and Larsen, 2007). Most eruptions occur within central volcanoes, which have often developed calderas that frequently host active geothermal systems, and erupt a range of magma compositions from basalts to rhyolites although basalts or basaltic andesites are usually volumetrically dominant in their products (Jakobsson, 1979; Saemundsson, 1979; Thordarson and Larsen, 2007). Although of less frequent occurrence, fissure eruptions produce basalts and tend to be larger than eruptions confined to the central volcanoes and extend up to several kilometres. Many of the largest volcanic events are fires: a series of eruptions occurring along the same fissure over a period of several months or years. Volcanic geothermal systems are commonly associated with ring structures or calderas – a product of rapid emptying of a shallow magma body. High temperature geothermal systems are associated with central volcanoes.

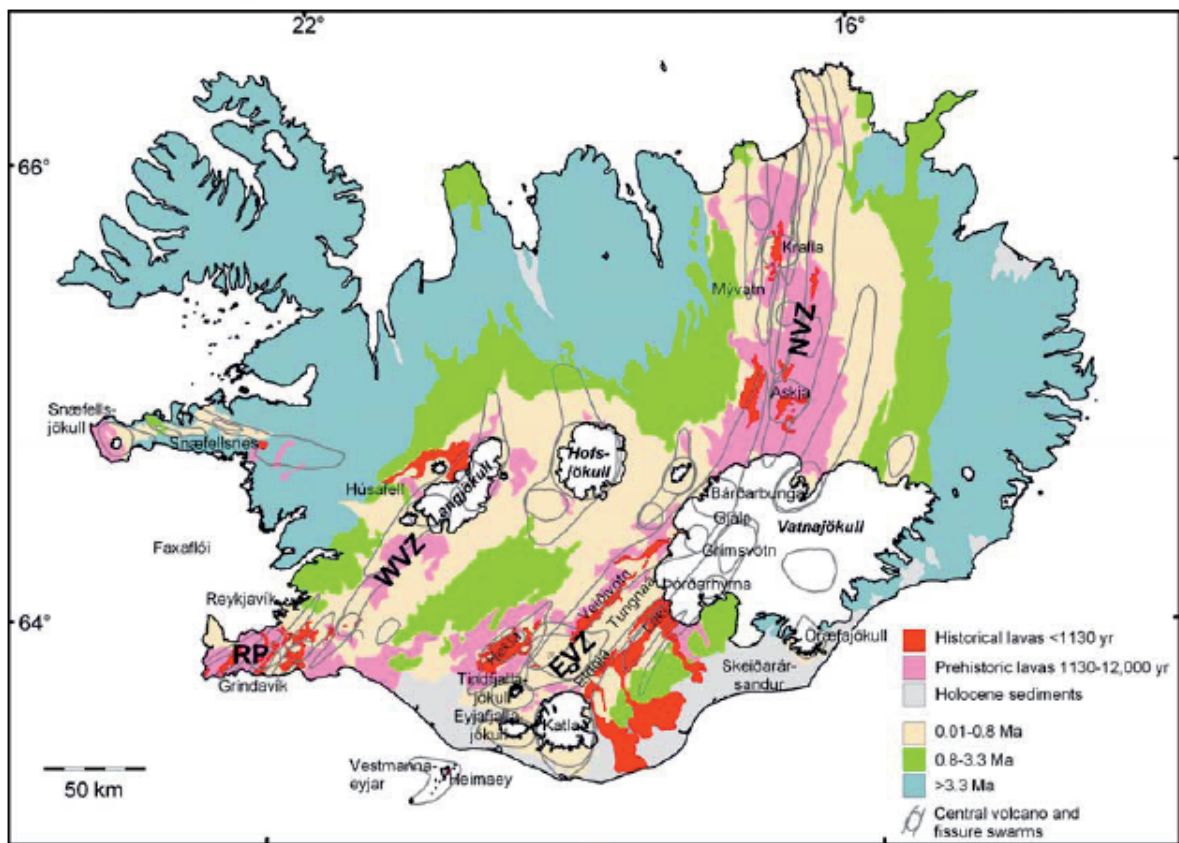


FIGURE 1: Simplified geological map of Iceland showing historical and Holocene lava flows, glaciers, and the main chronologically-defined units. RP – Reykjanes peninsula; WVZ – Western volcanic zone; EVZ – Eastern volcanic zone and NVZ – Northern volcanic zone; modified from Jóhannesson and Saemundsson (1998)

Námafjall high-temperature geothermal field is located in NE-Iceland in the southern half of the Krafla fissure swarm, and is associated with the Krafla central volcano (Pálmason and Saemundsson, 1974; Gudmundsson and Arnórsson, 2002; 2005). The Krafla system is located in the rift zone at the plate boundary where the American and Eurasian plates drift apart. The Krafla area geology is characterized by active rifting, forming a graben zone through its center, where volcanic craters, volcanic pyroclastics and lava flows, all of basaltic composition, dominate. In postglacial times some 18 eruptions have occurred in the Krafla caldera and its nearest surroundings and about 15 in the

Námafjall area (Saemundsson, 1991). The fissure swarm that intersects the Krafla central volcano is part of the neo-volcanic zone of axial rifting in N-Iceland.

‘Námafjall’ is a composite of two Icelandic words, to mean *mountain of mines*; as a reference to the sulphur mined in the area from time to time. For centuries sulphur was an important export from Iceland, the first record of it being mined in 1198 and shipped to Bergen, Norway (Sverris saga, 1920). Námafjall was one of the places which were mined for sulphur. Following the discovery of rich deposits of high grade diatomite on the bottom of Lake Mývatn, the Government of Iceland initiated simultaneously exploration of the nearby Námafjall geothermal high-temperature area with continued technical and economic feasibility study of the diatomite mining and processing. Drilling of wells started in 1963 (Table 1 and Figure 2) and a 3 MWe pilot plant was commissioned in early 1969. In the early 1970s, a central heating system for the Reykjahlíd village and nearby farms was constructed based on direct utilization of the fluid, but this turned out to be unfeasible because of a corrosive fluid inflowing the wells. This was improved in 1984 by the installation of a heat exchanger.

An account of the exploration, development and utilization of the geothermal field has been given by Ármannsson, (2011); Gudmundsson et al. (2010); and Ragnars et al. (1970).

The 1975-1984 ‘Krafla fires’ volcanic episode affected the Námafjall area, in particular during two events in 1977, when magma intruded to the south along the fissure swarm (Brandsdóttir and Einarsson, 1979; Larsen et al., 1978). Subsidence and expansion of the ground occurred between Grjótagjá to the west and Krummaskard to the east in addition to transient pressure changes and a temperature increase in the upper part of the groundwater system. During this volcanic episode, information gathered were utilized in the development of the conceptual model on which the most recent exploration drilling in Námafjall was based. In addition, an extensive scientific research program was carried out concerning the volcanism, geothermal areas and the relationship between them. The outcome of this exploration program was drilling of three directional wells (BJ-13, BJ-14 and BJ-15), in the years 2006 to 2008, to confirm the location of up-flow zones and improve the data input for Námafjall’s numerical model. The key numbers for the utilization area are that the geothermal anomaly is 20 km², enthalpy of the borehole fluid 1600-2400 kJ/kg, gas concentration <1 wt% , TDS of the geothermal fluid ~1000 ppm and maximum downhole recorded reservoir temperature is 320°C (Gudmundsson and Arnórsson, 2002).

TABLE 1: Boreholes in Námafjall geothermal field (Gudmundsson et al., 2010)

Well no.	Drilling year	Prod. c. shoe	Liner	Dia.	Depth
B-1	1963-1965	107	-	4 3/4	342*
B-2	1963-1965	207	-	4 3/4	492**
B-3	1966-1968	596	-	4 3/4	683
B-4	1968	625		6 ¼	630 (1138)***
B-5	1968-1969	478		8 3/4	638**
B-6	1969	577	550-953	6 ¼	1193*
B-7	1969	582		6 ¼	1206*
B-8	1970	537.5		6 ¼	1312*
B-9	1970	600	570-819****	6 ¼	843 (1311)
B-10	1975	598	558-1780	8 3/4	1809*
BJ-11	1979	619.6	604-1915	8 ½	1923
BJ-12	1980	686	631-1955	8 ½	1999
BJ-13	2006	851.7	816-2155	8 ½	2174 *****
BJ-14	2008	840.5	801.7-2479	8 ½	2506 *****
BJ-15	2008	846	806.9-2655.6	8 ½	2690 *****

*Collapsed 1977

**Monitoring well

***Lava intruded through the bottom aquifer

****Slotted liner 621-641 m

*****Directionally drilled

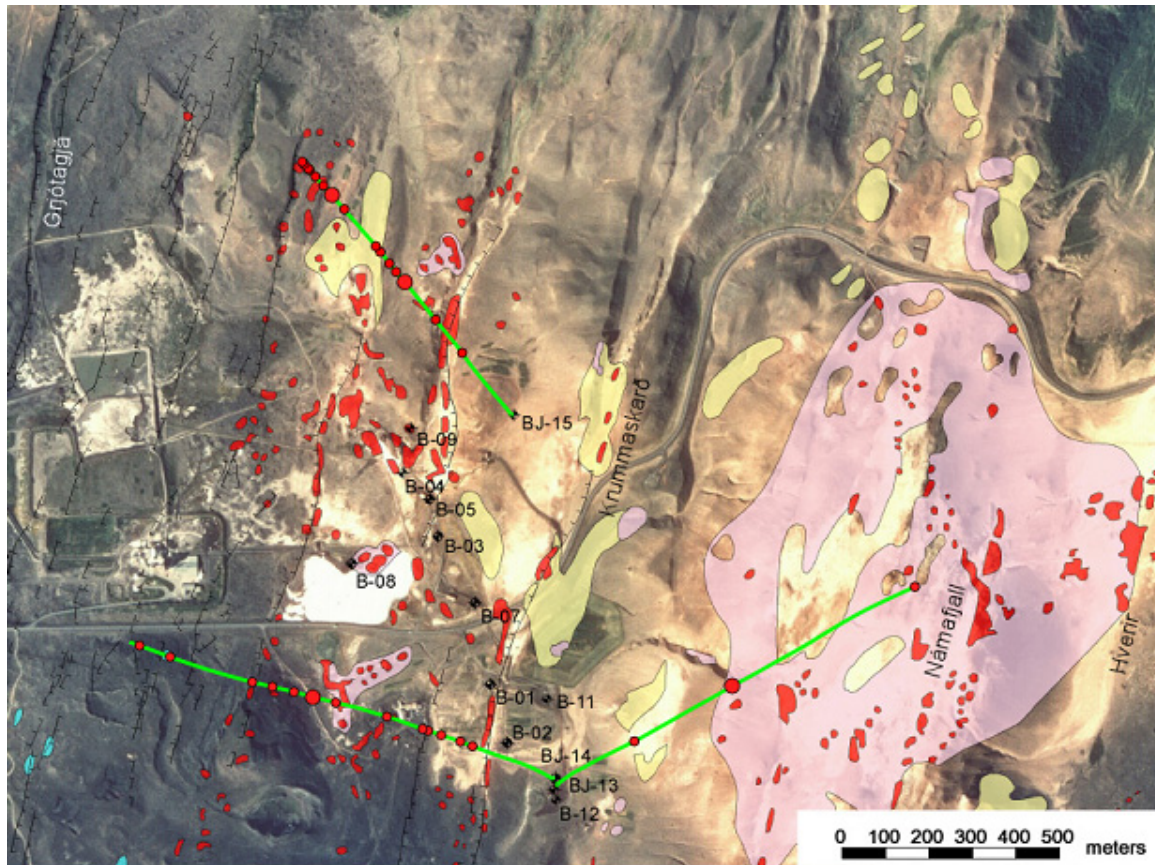


FIGURE 2: Location of wells in the Námafjall geothermal field; from Gudmundsson et al. 2010

Further surface investigation of the Námafjall area and deep drilling exploration complemented the conceptual and natural state model of the area. Concurrently, a design for a 90 MWe geothermal power plant has been worked out and assessment of environmental impact completed (Hönnun, 1996; 2003; Noorollahi, 2005; Orkustofnun and VGK, 1994; Rodas, 2010 and Sólnes et al., 1995). Landsvirkjun, the owner of the power plant at Námafjall, has the privilege to exploit the area according to an agreement with the state and landowners. The size of the power plant currently at Námafjall is 3 MWe and the energy generated by the station amounts to approximately 18 GWh per year. Operation of the current power plant at Námafjall will continue until construction of the planned 90 MWe power plant is completed.

Geothermal geochemistry is used to identify the origin of geothermal fluids and to quantify the processes that govern their compositions and the associated chemical and mineralogical transformations of the rocks with which the fluids interact. The subject has a strong applied component: geothermal chemistry constitutes an important tool for the exploration of geothermal resources and in assessing the production characteristics of drilled geothermal reservoirs and their response to production. Understanding the chemical processes within active geothermal systems has been advanced by thermodynamic and kinetic experiments and numerical modelling of fluid flow (Arnórsson et al., 2007). Deep drillings for geothermal energy have provided important information on the sources and composition of geothermal fluids, their reaction with rock-forming minerals, migration of the fluids, fluid phase separation and fluid mixing processes. The high-temperature, high-pressure, volatile-rich two phase fluids discharged from wet-steam wells in volcanic geothermal systems pose unique challenges in terms of chemical analysis and modelling of initial aquifer fluid compositions. Geochemical assessments of geothermal fluids have provided insights on current reservoir conditions in different parts of the world after prolonged production thus creating further understanding on the behaviour of wells in geothermal systems; resulting in insights for formulating resource management

strategies (e.g. Angcoy, 2010; Arnórsson et al., 2007, 2010; Gudmundsson and Arnórsson, 2002; 2005; Karingithi, 2010; Scott, 2011).

Geochemical monitoring of the Námafjall geothermal field during the last 20–25 years has revealed decreases in the Cl concentrations in the water discharged from most of the wells with more than 10 years production. The suspected cause is enhanced recharge of colder water into the producing aquifers due to depressurization by fluid withdrawal from the geothermal reservoir (Gudmundsson and Arnórsson, 2002). The incursion of cold groundwater into the reservoir was particularly intense subsequent the volcanic-rifting event in the area in 1977. Solute (quartz, Na/K, Na/K/Ca) geothermometry temperatures have decreased significantly in those wells where Cl concentrations have decreased but only to a limited extent in those wells which have remained constant in Cl. Aqueous SO₄ concentrations increase as Cl concentrations decrease. Increase in SO₄ concentrations is a reflection of cooling as anhydrite has retrograde solubility with respect to temperature. According to Gudmundsson and Arnórsson (2002), H₂S-temperatures are similar to the solute geothermometry temperatures for wells with a single feed zone but higher for wells with multiple feeds, if the feed zones have significantly different temperatures. H₂-temperatures are anomalously high for most wells due to the presence of equilibrium steam in the producing aquifers. The equilibrium steam fraction has been found to amount 0–2.2 % by weight of the aquifer fluid. The depth level of producing aquifers in individual wells at Námafjall has been evaluated by combining data on temperature and pressure logs and geothermometry results.

Encounters with wells whose discharge enthalpies are higher than that of steam-saturated water at the feed zone temperature are common in the Icelandic geothermal experience. Wells with excess discharge enthalpies pose a particular challenge for those interested in modelling aquifer fluid compositions, and several non-isolated system models accounting for the boiling processes between aquifer and wellhead have been developed (Arnórsson et al., 2007; 2010). The excess discharge enthalpies are dominantly attributed to the process of phase segregation, the result of adhesion of liquid water to mineral grain surfaces due to capillary forces. The chemistry of fluids in volcanic geothermal systems should be considered in light of the heat transfer mechanism. The mechanism of heat transfer from the magma heat source of volcanic geothermal systems to the circulating fluid envisages deep circulation of fluid above and to the sides of a magmatic heat source with a thin layer between the magma and the base of fluid circulation, through which heat is transferred conductively. Some heat may also be transferred to the geothermal system by convection of saline fluids in a closed loop between the geothermal system and the magma heat source. Close proximity of the circulating fluid to the magmatic heat source also implies closeness of the circulating fluid to gaseous magma components. At magmatic temperatures, these components include H₂O, CO₂, SO₂, H₂, HCl, HF, and many metal-chloride and metal-fluoride species, which upon deposition can form ore deposits (Arnórsson et al., 2007).

This study attempts to model the aquifer fluid of the Námafjall geothermal field with respect to geochemistry as aided by discharge fluid (two-phase) analysis, temperature and pressure logs, solute geothermometers, and mineral-gas and mineral-solution equilibria. Modeling will involve evaluating specific mineral-gas and mineral-solution equilibria that may potentially control the concentrations of the prevalent reactive gases (CO₂, H₂S and H₂) in well discharges. The sensitivity of calculated aquifer fluid compositions to assumed phase segregation pressure for 4 out of the 7 wet-steam well discharges sampled at the Námafjall geothermal field since drilling to recent dates will be shown. Literature review of Námafjall geothermal field with production history are dealt with in Chapter 2. Description of phase segregation and its application in modelling aquifer fluid compositions, including physical description, supporting proof for the occurrence of phase segregation in the Námafjall field, a mathematical depiction and the practical procedure that can be used to integrate phase segregation calculations into modelling using WATCH 2.1 are dealt with in Chapter 3. Chapter 4 accounts for the thermodynamic database used to model aquifer mineral-gas-solution equilibria, presents the state of chemical equilibria between the main hydrothermal alteration minerals and solution, and discusses the results obtained from the modelling. Chapter 5 presents my conclusions.

2. NÁMAFJALL GEOTHERMAL FIELD

2.1 Geology

As mentioned in the introductory chapter, Námafjall high-temperature geothermal field is located in NE-Iceland about 5 km northeast of Lake Mývatn in the southern half of the Krafla fissure swarm, at an elevation of 300-400 m.a.s.l., and is associated with the Krafla central volcano (Pálmason and Saemundsson, 1974). The Krafla system is located in the rift zone at the plate boundary where the American and Eurasian plates drift apart. The Krafla area geology is characterized by active rifting, forming a graben zone through its center, where volcanic craters, volcanic pyroclastics and lava flows, all of basaltic composition, dominate. In postglacial times some 18 eruptions have occurred in the Krafla caldera and its nearest surroundings and about 15 in the Námafjall area. The fissure swarm that intersects the Krafla central volcano (100 km long and 5 to 8 km wide) is part of the neo-volcanic zone of axial rifting in N-Iceland (Figures 3 and 4, Saemundsson, 1991).

Námafjall geothermal system is perceived a parasitic system to the Krafla field (Arnórsson, 1995):

magma from the Krafla caldera travelled horizontally in the SSW direction along the fissures and fractures all the way down to Námafjall, serving as the heat source for the hydrothermal system. Supporting evidence for this is that during the Krafla eruption in 1977, well BN-04 in Námafjall discharged magma (Larsen et al., 1978). The 1975-84 volcanic episode suggests that the heat source to the Námafjall geothermal system is characterized by dykes formed by magma intrusion into tensional fissures from the magma body in the roots of the Krafla system. The aquifer rock at Námafjall is the same as at Krafla (basaltic, sub-aerially erupted lavas, sub-glacially erupted hyaloclastites, and small intrusive bodies of basalt, dolerite, gabbro and granophyres) except that silicic rocks are absent. Intrusive formations dominate below about 1500 m depth. The Námafjall field is characterized by the Námafjall ridge - about 2.5 km long and 0.5 km wide - composed of hyaloclastites formed during the last glaciation period as a product of sub-glacial eruptions. The sides of the Námafjall ridge are covered with postglacial basaltic flows, coming from

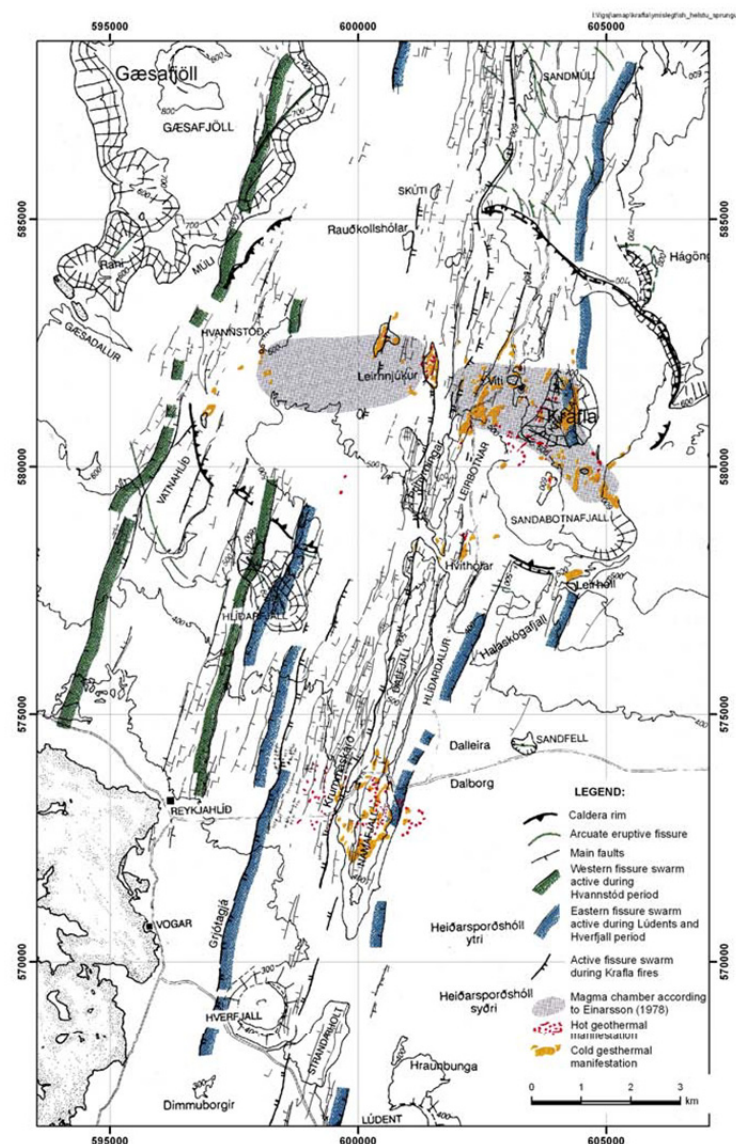


FIGURE 3: Structural map of Krafla and Námafjall geothermal areas showing the Krafla caldera and associated fissure swarm. Based on mapping by Saemundsson (1991)

fissure volcanoes in the area. The area is marked by several fractures and faults, like Krummaskard and Grjótagjá, and often surface manifestations are clearly aligned with the fractures. The geological characteristics of the Námafjall field indicate that the Námafjall ridge is part of the Námafjall-Dalfjall-Leirhnjúkur ridge, having an overall length of about 15 km and width of about 1 km (Ragnars et al., 1970).

The thermal manifestations at Námafjall are limited to the Námafjall hill (150 m above surroundings) and the low ground east and west of it and is divided into two sectors located to the east and west of the Námafjall Ridge, Hverarönd and Bjarnarflag, respectively (Figures 3 and 4). Surface manifestations of geothermal activity - steaming grounds, mud pools, fumaroles and sulphur deposits -

are distributed over an area of 3 to 4 km² (Ármannsson, 2011; Ármannsson et al., 1987; Mortensen et al., 2008; Ragnars et al., 1970). Hot springs are mostly located along the fractures and faults, while the altered grounds are located mainly on both sides of the Krummaskard fault.

Petrological studies in the Krafla-Námafjall area show a range of rock composition from olivine tholeiites to rhyolites erupted in postglacial times (Nicholson et al., 1991). The basalts formed by fissure eruptions, however, are predominantly quartz normative tholeiites, which appear to be closely similar in composition irrespective of the eruption site. The geological units in the area, as seen in drill cuttings, can be divided in an upper and a lower succession. The upper succession extends from the surface to about 1100 m depth, composed mainly of hyaloclastites (70%) and lava flow interlayers. The lower succession is composed mainly of lava from shield volcanoes intercalated with hyaloclastite layers. Below 1700m, intrusives constitute about 50% of the rock volume. Some of the intrusives exhibit

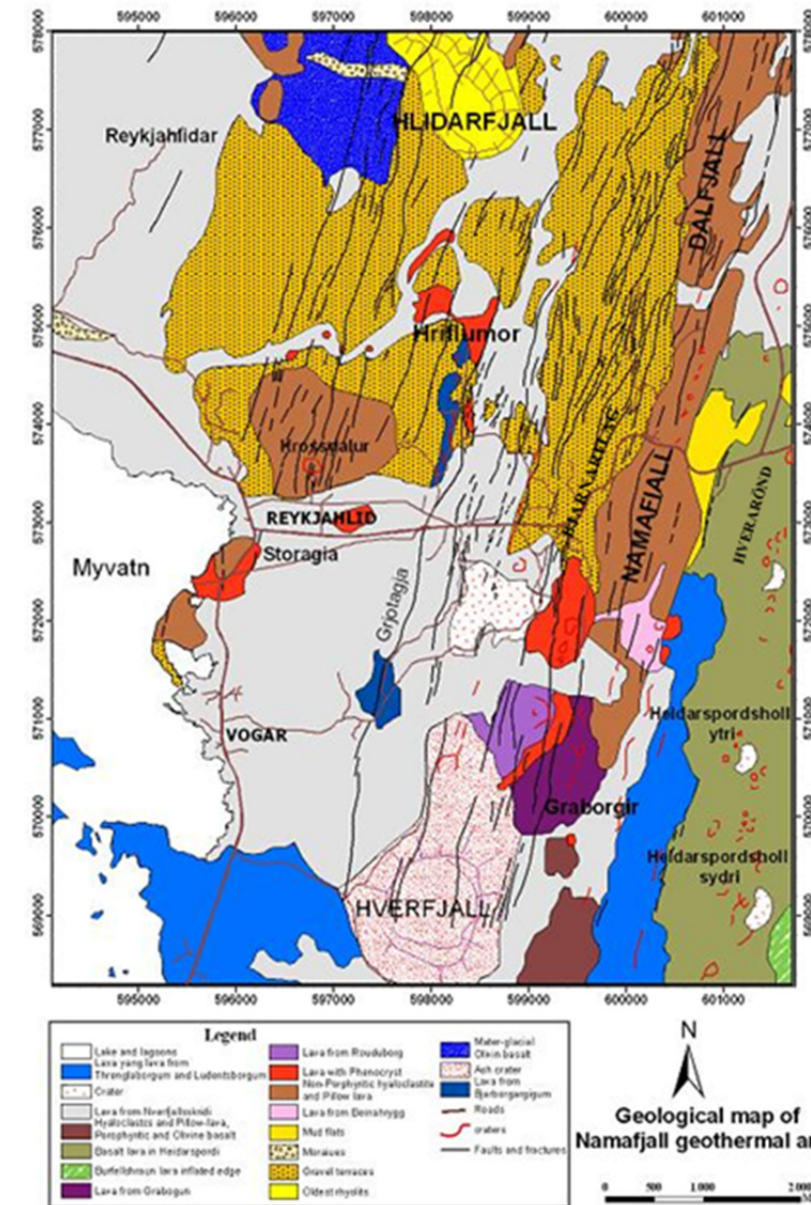


FIGURE 4: Geological map of the Námafjall area; Saemundsson (1991)

considerable degree of alteration but some of them are fresh. Tectonic movements during the Krafla eruptions of 1977 were confined between the Krummaskard and Grjótagjá faults and subsurface alteration reveal that the temperature has reached ca. 300°C at 1000 m depth and increases slightly with depth (Ármannsson, 1993; Gudmundsson, 1993; Isabirye, 1994).

2.2 Hydrology

The surface rocks in the study area are highly permeable, consisting of recently formed lava fields where surface runoff is almost negligible. There is hardly any surface water in the area because it is covered by young and porous lava fields and transacted by numerous faults. Almost no creeks and rivers exist and nearly all the precipitation within the area seeps underground. The water is exposed in depressions where the land surface intersects the groundwater table or where aquifers are interrupted by tectonic faults and fissures (Kristmannsdóttir and Ármannsson, 2004). Part of Lake Mývatn is located in the study area. Lake Mývatn is a fresh water lake that was protected by law in 1974, and in 1978 designated to the Ramsar list of wetlands of international importance. Numerous bays and creeks line its coastline and the lake has some fifty islands and islets. The lake has an average depth of 2.5 m, and a maximum depth of 4 m. Moreover there are small lakes and pools in the area which are important for social and environmental reasons.

As seen from Figure 4, the area geology indicates that different basaltic lava flows are of postglacial age, and are bound in the north by glacial moraines, in the east by older lava flows and by the Pleistocene hyaloclastites of the Námafjall ridge (Thórarinnsson, 1979). The postglacial lava flow act as good aquifers and numerous open fissures and large active faults with a NNE/SSW strike, like Grjótagjá and Stóragjá, add to the already permeable nature of the lavas. From the profiles of the boreholes that have been drilled in the area it can be concluded that the uppermost layer consists mainly of lava to a depth of 20 to 25 m. This layer is underlain by a sequence of scoria layers interbedded with lavas, thus acting as aquifers. Ground water will flow preferentially from north to south through the north-south faults and from east to west according to the directions of the lava flows. The scoria layers probably act as more a homogeneous aquifer (De Zeeuw and Gíslason, 1988).

The flashed geothermal water at Námafjall enters the shallow groundwater system through active open faults and fissures.

From Námafjall the groundwater flow in a southwesterly direction and reaches Lake Mývatn in three main tongues (Figure 5). The relation between the direction of the lava flows and the direction of groundwater flow is probably caused by the fact that fissures, which developed during the cooling of the lava, are mostly parallel to the direction of the lava flow. It might also be due to the general dip of

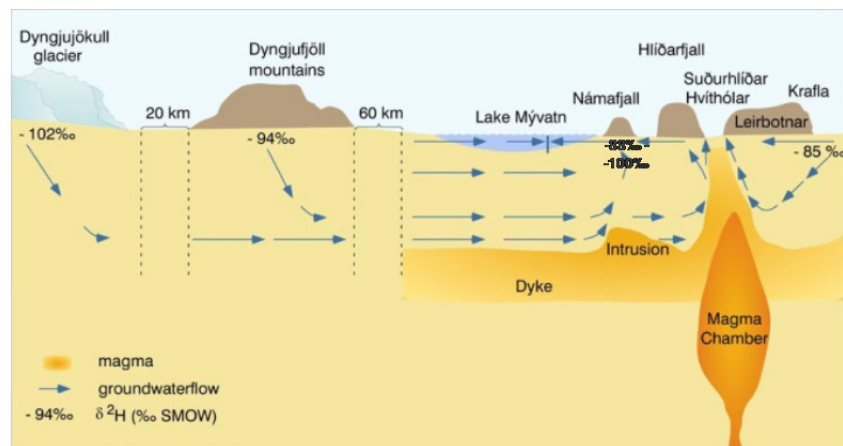


FIGURE 5: Possible groundwater flow model to Námafjall and Krafla; modified from Gudmundsson et al., 2010

the lava and scoria layers toward the southwest. The large NS faults like Stóragjá and Grjótagjá do not form a barrier to groundwater flow (Thórarinnsson, 1979; De Zeeuw and Gíslason, 1988; and Noorollahi, 2005). Measurements of the flow velocity in Grjótagjá fissure suggest that the surface flow in the top layer of the groundwater in the fissures is fast, ~3.5 m/s, but at a depth of 2-4 m the flow becomes disturbed and obvious mixing occurs (Thoroddsson and Sigbjarnarson, 1983). The groundwater chemistry studies by De Zeeuw and Gíslason (1988) show that mixing of hot and cold groundwater is only important near the hot and cold water boundary zones.

Based on the value of deuterium isotopes, the origin of the geothermal fluid is considered to be precipitation at high elevation, probably in the vicinity of the Vatnajökull glacier to the south (Dyngjujökull glacier). The $\delta^2\text{H}$ values of the aquifer water at Námafjall fall into two distinct groups, at about -88‰ and -100‰. Ármannsson (1993) and Darling and Ármannsson (1989) considered this,

on the basis of the deuterium precipitation map of Árnason (1976), to indicate two distinct flows into the geothermal system: a shallow inflow of local groundwater, corresponding to the less negative $\delta^2\text{H}$ value, and a deep inflow from a distant source, most likely from the Vatnajökull area, corresponding to the more negative $\delta^2\text{H}$ value. Arnórsson (1995) proposed that recharge into the Námafjall geothermal system at deep levels largely occurs by downward plunging of cold groundwater on both sides of the geothermal field in the N–S fissure swarm that runs through it.

2.3 Geophysical review

Geophysical measurements in geothermal resource investigations deal with the physical properties of the earth, with emphasis on parameters sensitive to temperature and fluid content of the rocks, or on parameters that may reveal structures that influence the properties of the geothermal system. Electrical resistivity of rocks in geothermal surroundings reflects the properties of the geothermal system, or its history. Resistivity methods have for a long time proven a success in geothermal exploration (Georgsson and Karlsdóttir, 2009; Flóvenz, 2011; Rosenkjaer, 2011). A good knowledge on resistivity relates the fact that the resistivity of rocks is chiefly controlled by parameters that correlate to the geothermal activity, such as porosity and pore structure (inter-granular, fracture and vugular porosity); rock alteration due to water-rock interaction; fluid salinity; temperature; water (i.e. saturation or steam content) and pressure (Georgsson, 2010; Hersir and Árnason, 2009; Flóvenz, 2011).

Over the past two decades, Transient Electro Magnetic resistivity measurements (TEM) have been considered the most effective first phase surveying tool for Icelandic environment, as basaltic formations conduct electrical currents better with temperature up to 230-240°C, reflecting progressive changes in alteration of clay minerals until stable chlorite is formed, which leads up to higher resistivity signatures. TEM (transient electric measurements) is the most common method used to measure electrical resistivity in the Earth's upper most 1 km (Flóvenz, 2011). The TEM layout is such that current transmitted in a transmitter loop on the surface creates stationary magnetic field. A secondary magnetic field is created when the current is turned off, which decays with time and is measured by the receiver coil at the surface. The rate of decay depends on the resistivity of the underlying rock, and from this rate of decay, the resistivity as function of depth can be calculated.

The resistivity structure of many high-temperature geothermal systems has been reported to have similar characteristics (e.g. Árnason et al., 2000; Pálsson et al., 2010). Typically, there is a low resistivity cap on the outer limits of the geothermal system with a more resistive core towards the center of the system. This character is found both in fresh water and saline geothermal systems but the overall resistivity is lower in saline systems (Figure 6). Árnason et al., (2000) show that resistivity measurements reflect the subsurface alteration and indicate the extent of the geothermal system thus relating alteration minerals to formation temperature (as illustrated by Flóvenz et al. (2005) in Figure 6). A correlation between the resistivity structure and the hydrothermal alteration of the rocks in geothermal systems is discussed in Árnason et al. (2000) and Flóvenz et al. (2005). The boundary of the low resistivity cap and the higher resistivity core

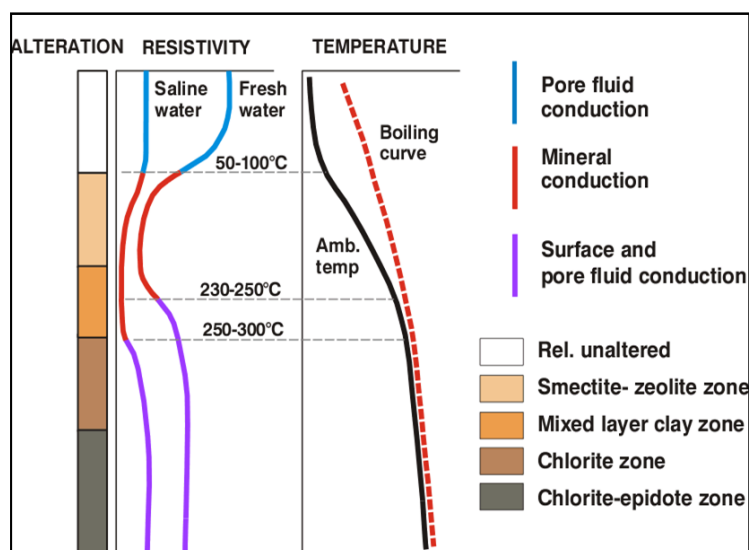


FIGURE 6: General resistivity structure and alteration of basaltic crust in Iceland; from Flóvenz et al. (2005)

is lower in saline systems (Figure 6). Árnason et al., (2000) show that resistivity measurements reflect the subsurface alteration and indicate the extent of the geothermal system thus relating alteration minerals to formation temperature (as illustrated by Flóvenz et al. (2005) in Figure 6). A correlation between the resistivity structure and the hydrothermal alteration of the rocks in geothermal systems is discussed in Árnason et al. (2000) and Flóvenz et al. (2005). The boundary of the low resistivity cap and the higher resistivity core

has been found to correlate with the change from smectite to chlorite dominated alterations. This alteration change is known to occur at a temperature of approximately 230°C. The transition from smectite to chlorite indicates increasing temperatures above 100-240°C. Chlorite becomes stable at 230-240°C, but is less conductive than smectite and mixed layer clays.

A TEM-resistivity survey was carried out to map the low resistivity cover around a high resistivity core in the Námafjall field (Figure 7; Karlsdóttir, 2002). The extension of the anomaly was estimated around 20km² at 800m depth according to this interpretation, compared to 8 km² based on previous Schlumberger - method measurements. Two TEM-resistivity surveys were carried out in the Námafjall area by ÍSOR in 1992 and winter 2000/2001, and the interpretation done by Karlsdóttir (1993, 2002).

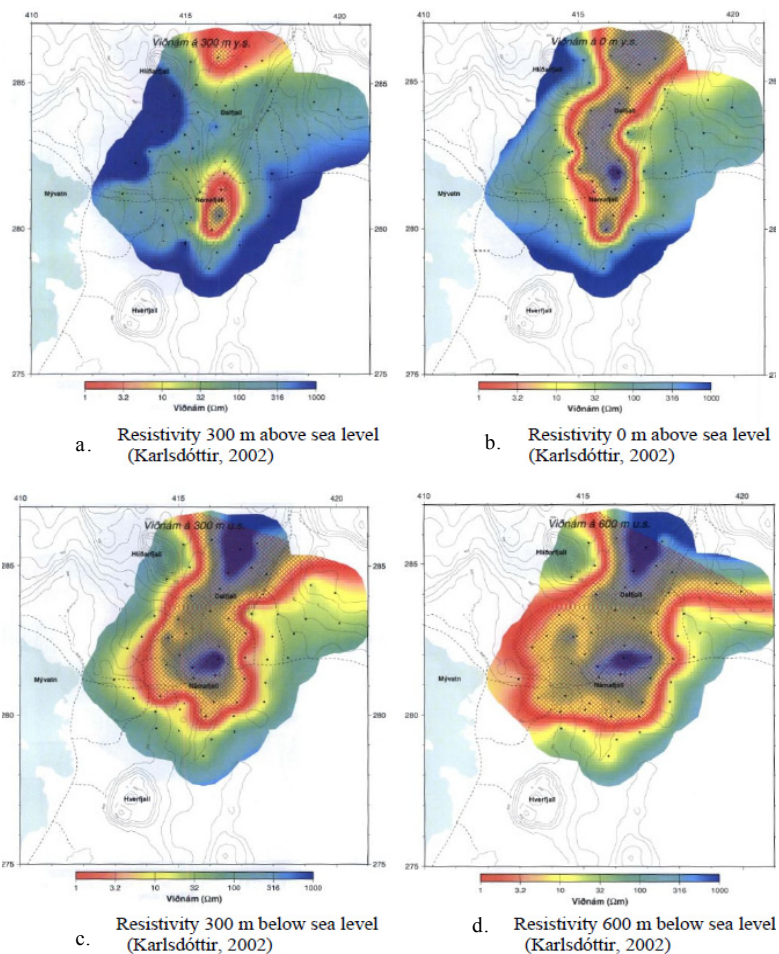


FIGURE 7: Resistivity structure of Námafjall

The geothermal system in Námafjall appears to be distinct. Nevertheless, connection to the geothermal system at Krafla was observed along the NNE-SSW trending, active rift zone, which extends from the highland south of Námafjall north to the coast, crossing the Krafla caldera and Gjástykki geothermal area (Figure 7).

2.4 Geochemical review

Fluid chemistry in the Námafjall geothermal field has been extensively studied by various authors (Ármannsson, 1993, 2005; Ármannsson et al. 1987, 1989; Arnórsson, 1995; Arnórsson et al. 1978, 1983; Giroud, 2008; Gudmundsson and Arnórsson, 2002, 2005; Hauksson and Benjamínsson, 1989, 1995, 1997 and 2000; Kristmannsdóttir, 1979; Ólafsson and Kristmannsdóttir, 1989; Ushakov, 2000).

Fluid samples taken from surface manifestations (fumaroles and mud pools) in the period 1952-1993, and several gas samples were used to indicate reservoir temperatures greater than 300°C, observed east of Námafjall ridge at Hverarönd. Highest reservoir temperatures occur east of the Krummaskard fault, with values close to 280°C, gradually decreasing westwards. At Bjarnaflag, west of the Námafjall ridge where most wells are drilled, the gas geothermometers predict temperatures of 240-260°C (Figure 8). In wells drilled at Námafjall prior to the 1975-84 volcanic episode (well nos. 1-9) temperatures follow the boiling point curve with depth. In wells drilled after the 1975-84 volcanic episode, the temperature at the top of the reservoir is sub-boiling. These low temperatures are considered to be the consequence of cold shallow groundwater incursion along fractures that were activated during the 1975-84 volcanic episode. The maximum recorded temperature as presented by Gudmundsson and Arnórsson (2002) is 320°C, although geothermometry and most recent logs

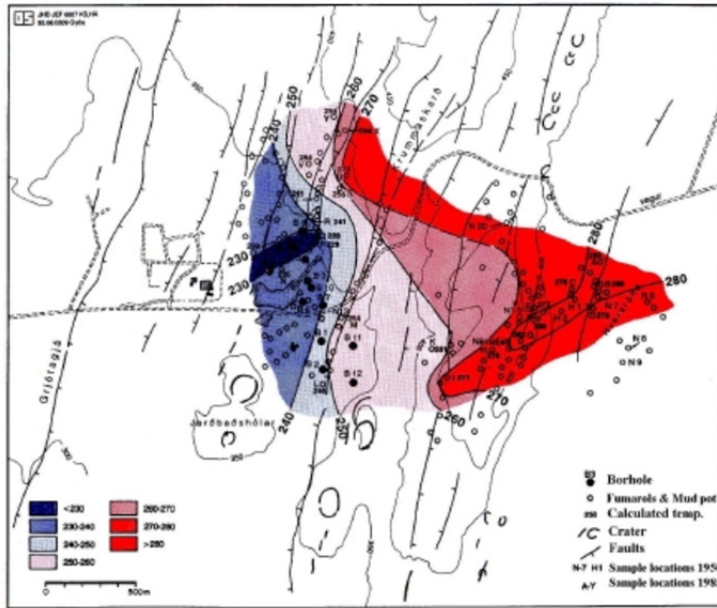


FIGURE 8: Reservoir temperature contours based on geothermometry (Ármansson, 1993)

indicates that aquifers producing into the wells have lower temperatures than this maximum (see Appendix I).

Fumarolic activity at Námafjall increased during the early part of the 1975-84 volcanic episode yet no changes in the gas content of well discharge and fumarole steam was observed (Arnórsson and Gunnlaugsson, 1985). The increase in the fumarolic activity is likely caused by increased boiling by heat flux to an already two-phase aquifer fluid. The apparent lack of increase in the gas content of the fluid in the Námafjall system during this volcanic episode indicates that the magma intruded from the chambers below Krafla had already been largely degassed.

The Námafjall waters are described as of meteoric origin (Arnórsson et al., 1983), slightly alkaline with rather low dissolved solids and composition largely fixed by temperature and salinity (Arnórsson et al., 1978; Kristmanns-dóttir, 1979) with low chloride and sulphate. The most important anions of the geothermal fluid are Cl^- and SO_4^{2-} , the most important cation Na^+ , but silica (SiO_2) is the most abundant dissolved solid. The gas content of individual well discharges is variable and the steam is relatively rich in H_2 , considered to be due to the relatively high fraction of equilibrium steam in the reservoir and its solubility (Arnórsson, 1995). Chemical analysis of the water and steam from wells BN-04, BJ-11 and BJ-12 in the years 1997 and 1998 was carried out (Figure 9, Gudmundsson and Arnórsson, 2002), and

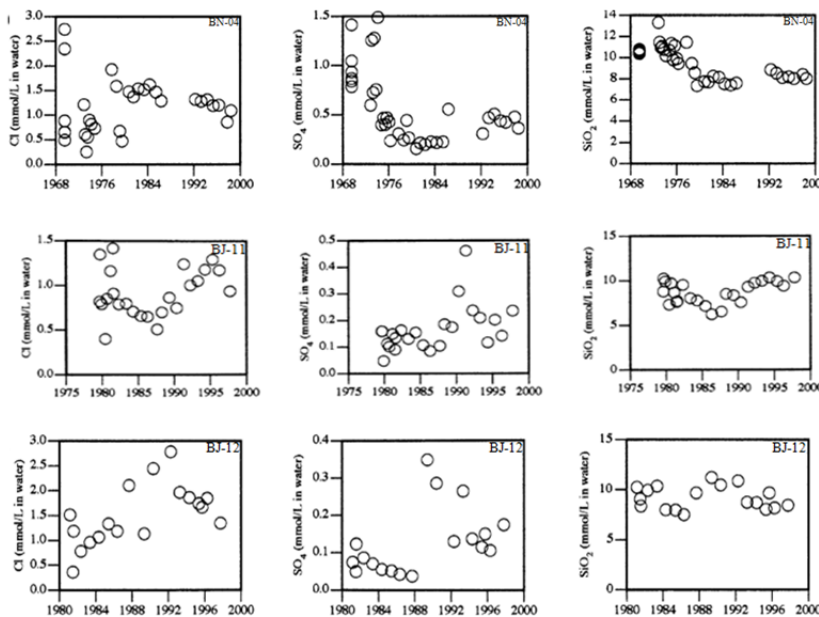


FIGURE 9: Changes during the production period in the concentrations of Cl, SO_4 and SiO_2 at 10 bar-a (180°C) in wells BN-04, BJ-11 and BJ-12; from Gudmundsson and Arnórsson (2002)

from this and a study by Sigurdsson (1993), Gudmundsson and Arnórsson (2002) concluded that the volcanic rifting event occurring in 1977 was followed by an enhanced recharge of cold water into the reservoir, possibly because the tectonic movements caused an opening of fractures/fissures that allowed surface groundwater to enter the reservoir. After 1988, the groundwater incursion seems to have decreased. For more descriptions, see Gudmundsson and Arnórsson (2002; 2005) and Sigurdsson (1993).

2.5 Reservoir characteristics

Numerical modelling in reservoir engineering is one of the tools that aid the characterization and optimal use of geothermal resources in addition to the other geosciences. Detailed numerical models (distributed-parameter models) of geothermal reservoirs have become a standard tool used as an input to the development and exploitation strategy in the geothermal industry (O’Sullivan et al., 2001). The reservoir at Námafjall is two-phase with highest recorded downhole temperature of 320°C, in well BJ-11. Limited discharge enthalpy data are available for the first ten wells but for wells BJ-11 and BJ-12 it was about 2300 kJ/kg when these wells were initially discharged in 1982. Following the volcanic-rifting event in 1977, cooling took place in the uppermost 600 m of the Námafjall reservoir due to extensive inflow of groundwater from shallow levels, presumably along new fractures, as noted earlier. Since then, the enthalpy has declined and was 1700–1850 kJ/kg in 1997 (Ármannsson et al., 1987; Hauksson and Benjamínsson, 1997; Sigurdsson, 1993).

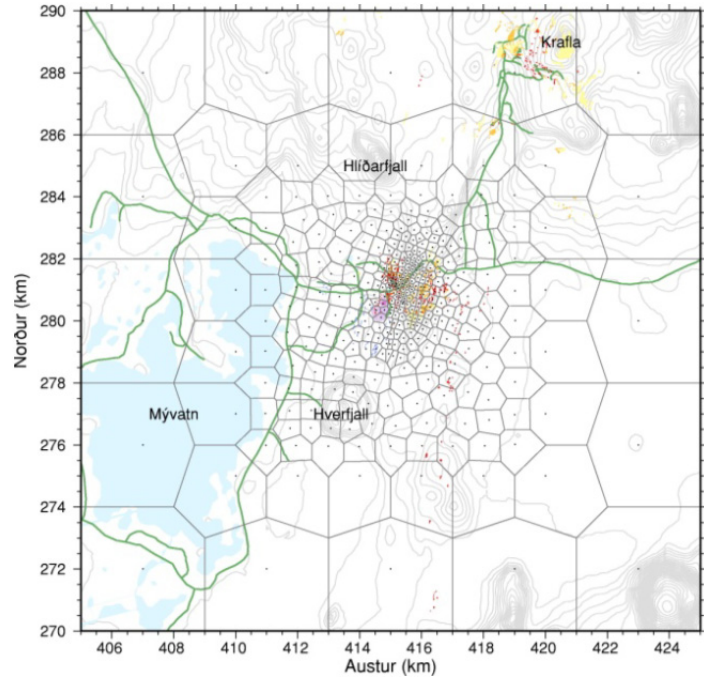


FIGURE 10: The basic grid of the Námafjall model

Different authors have presented numerical simulation models for the geothermal reservoir at Námafjall (Gudmundsson et al., 2010; Hjartarson et al., 2005; Rivera Ayala, 2010; Sigurdsson, 1993). Detailed results from these studies are described in the publications but Figure 10 gives an overview of the grid models as presented by Gudmundsson et al. (2010). Sigurdsson (1993) presents a numerical simulation model for the geothermal reservoir at Námafjall describing the reservoir as three separate layers. Permeability and porosity values were adjusted to match flow data from wells BJ-11 and BJ-12; other wells were not included. The model gave satisfactory results for estimating the minimum generating capacity of the field and was used to predict the effect on the geothermal reservoir if a 20 MWe power plant were operated in the field for 30 years, with results that the reservoir can easily sustain such production. Rivera Ayala (2010) presents a detailed numerical model of the Námafjall geothermal field, with coupled reservoir wellbore simulation. Three exploitation scenarios are considered, 40 MWe, 60 MWe and 90 MWe, and conclusions are that it is possible to maintain a 90 MWe case for 30 years. Estimates of the total recharge into the reservoir, calculated by the recharge through the top, bottom and side boundaries (i.e. through the different cap rock and base rock of the system) as well as from the mass sources located at the bottom for all the stages of the simulation: natural state in year 1963, history match up to year 2007 and the 3 forecast scenarios up to year 2045 are also presented (Figure 11).

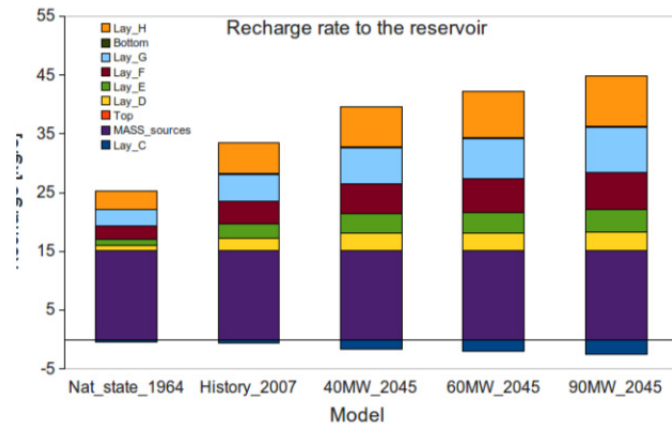


FIGURE 11: Mass recharge into the reservoir; from Rivera Ayala (2010)

3. METHODOLOGY

Sampling, sample treatment/preservation and chemical analysis of fluids from wellheads of geothermal boreholes require specific techniques in addition to normal procedures used for surface and non-thermal waters. These techniques ensure attaining representative and uncontaminated samples (considering the high temperatures of geothermal fluids and the effects of cooling or exposing the samples to the atmosphere) and are a first in the steps required to determine aquifer fluid composition. The subsequent steps require that initial aquifer fluid chemical compositions be calculated based on a model for boiling and potential causes of the measured discharge enthalpy (in the case of ‘excess’ enthalpy wells). The procedures are in principle similar to the details discussed by different authors (e.g. Angcoy, 2010; Arnórsson et al., 2007, 2010; Karingithi et al., 2010 and Scott, 2011). This chapter, furthermore, focuses on the methods taken to complete the techniques/steps and pays attention on the mathematical foundation for calculating initial aquifer fluid chemical compositions. The theoretical basis for different quantitative measures used to describe aquifer fluids is explained.

3.1 Sampling and analysis

The primary data for this study are obtained from chemical analysis of water and steam discharges from seven wells in the Námafjall high-temperature field. The well samples were collected and analysed by Kemia Ltd and Orkustofnun (National Energy Authority - NEA) for the pre-2003 samples and by Iceland Geosurvey (ÍSOR) for the post-2003 samples (Table 2).

A chromium steel Webre separator was used to collect water and steam samples from the two-phase fluid pipeline close to the wellhead of each well. A cold water jacketed coil of stainless steel was attached to the separator by teflon-coated steel tubing. Before sampling, some of the sample was pumped through the sampling/filtration apparatus to clean the sampling line and remove any contaminants. Steam samples were collected into gas sampling bulbs, which had been evacuated in the laboratory and contained 20 to 50 ml of freshly prepared 50 % w/v KOH or 5M NaOH solution. The strong base is used to capture the major non-condensable gases (CO₂ and H₂S) while residual gases (H₂, CH₄, N₂ and O₂) occupy the head space. Samples for analysis of all components except for pH, CO₂, H₂S and SiO₂ were filtered on site to prevent interaction with any suspended matter through 0.2 to 0.45 µm cellulose acetate membranes into low density polyethylene bottles using a polypropylene filter holder. For the determination of major cations, the samples were acidified with concentrated Suprapur nitric acid, 0.5 ml into 100 ml of sample. A 100 ml sample was collected for sulphate analyses. To this sample 2 ml of 0.1 M zinc acetate solution was added to remove H₂S as ZnS. The ZnS precipitate was filtered from the sample. Two amber glass bottles, 60 and 250 ml, with special caps that prevent entrapment of air under the cap, were used to collect samples for the determination of pH and CO₂. Samples for determination of Cl and F were not treated, except for filtration.

The non-condensable gases in the headspace of the gas sampling bulb were analysed by gas chromatography. CO₂ concentration and pH in the liquid phase were determined in the laboratory immediately upon return from the field (within 2–3 days) by potentiometric titration and a calibrated pH electrode respectively. H₂S was determined titrimetrically using mercuric acetate and dithizone (Ármannsson and Ólafsson, 2006; 2007; Arnórsson et al., 2000). For the Kemia Ltd samples, the major aqueous components (SiO₂, Na, K, Mg, Ca), along with Fe, Al and B, were analysed by ICP-AES. The NEA/ÍSOR samples were analysed by various methods: atomic absorption spectrometry (Na, K, Mg, Ca, Fe and Al); spectrophotometry (SiO₂ and B); ion chromatography (Cl, SO₄); ion selective electrode for F and gravimetry for TDS. It can be summarised that the analyses of water samples are grouped into onsite/immediate analysis (pH, CO₂, H₂S), and laboratory analysis of major elements and some minor elements by Kemia Ltd and NEA/ÍSOR. Approximately 250 samples have been collected and analysed from the Námafjall wells, dating back to 1969. However, a few samples (25) have been selected for the requirements of this study (Table 2).

TABLE 2: Measured discharge enthalpies, sampling pressures and analysis of elements in the collected water and steam samples

Well No.	Sample No.	Date	h ^{dt} (kJ/kg)	Sp ^b (bar-g)	pH/°C	Liquid components (mg/kg)																Gas (volume %)							Total steam (mg/kg)			Condensate (mg/kg)		
						CO ₂	H ₂ S	B	SiO ₂	Na	K	Mg	Ca	F	Cl	SO ₄	Al	Fe	TDS	Gas / T (20°C)	CO ₂	H ₂ S	H ₂	O ₂	CH ₄	N ₂	CO ₂	H ₂ S	Na	pH/°C	CO ₂	H ₂ S	Na	
BN-04	4036	Jun-99	983 ^a	3.70	9.55/21.3	35.2	109.5	0.95	547	185	20.0	0.010	4.76	0.79	41.3	37.0	0.69	0.080	920	0.97	87.4	1.3	4.9	6.3	2404	959				4.44/26	423	422	0.48	
	1014	May-86	1019 ^a	5.20	9.44/26.1	48.9	89.1	0.75	470	151	21.9		3.30	0.67	47.0	21.8			1008	1.50	32.4	13.8	37.4	10.0	6.3				4.30/23	541	566	0.78		
	1012	Mar-79	1033 ^a	8.10	9.12/23.0	69.2	125.0		515	149	23.8		2.54	0.72	23.6	22.9			1097	3.80	32.9	13.3	46.7	0.3	6.8									
BN-09	4034*	Jun-07	1014 ^a	11.8	9.03/23.2	37.1	122.7	0.75	432	139	17.9	0.090	2.60	0.64	37.1	39.0	0.83	0.008	837	1.75	90.5	0.1	3.9	5.6	2180	1273								
	4008*	Apr-04	1060 ^b	13.5	8.96/21.9	29.7	126.6	0.77	545	138	18.0	0.010	2.44	0.72	36.4	71.0	0.92	0.006	979	1.72	91.1	0.3	3.5	5.1	2431	1329								
BI-11	4033	May-03	1620	19.0	8.50/20.2	2.1	115.4	2.10	604	101	17.0	0.010	0.50	0.69	38.4	24.0	2.00	0.010	834	1.44	95.9	0.1	1.2	2.8	3757	1374								
	4059	Jul-98	1850	23.5	8.10/25.0	31.4	95.1	2.67	576	118	16.2	0.001	0.39	0.60	37.4	14.0		0.030	848	1.37	97.1	0.2	0.9	1.8	2751	1298								
	4035	Jul-97	1850	23.1	7.97/25.7	29.4	95.0	1.93	560	87.0	14.5	0.010	0.26	0.76	37.7	13.9		0.010	800	1.44	96.9	0.2	0.8	2.1	2554	1326								
	4013	May-95	1867	14.5	8.83/25.8	24.2	86.3	1.22	563	121	18.5	0.030	0.27	0.88	39.2	18.0		0.010	894	1.12	96.1	0.2	0.8	2.9	1779	1213								
	4024	May-94	1867	19.0	8.42/20.8	28.6	89.5		566	94.0	14.8	0.050	0.53	0.93	41.8	10.0		0.010	808	1.31	94.6	0.3	0.7	4.4	1896	1295								
	4022	May-93	1981	19.9	8.19/20.7	82.9	51.3		542	115	15.4	0.050	0.26	0.77	37.8	18.0		0.010	1056	1.50	97.8	0.2	1.3	0.7	1453	1538				4.35/24	260	733	0.32	
	1022	Jun-85	2293	14.7	8.72/24.5	20.6	114.1	5.17	426	104	16.4		0.45	0.77	22.8	9.9	1.42		836	1.06	20.1	21.2	57.3	0.3	1.1				4.51/21	217	905	1.70		
	1024	May-83	2309	16.2	8.60/21.0	19.6	110.4		440	97.4	15.1	0.008	0.68	0.69	22.8	11.2			660	1.96	16.7	19.8	62.3	0.2	1.0				4.45/26	130	738	2.36		
	1050	Aug-81	2355	18.0	8.20/26.0	50.7	95.9		412	92.4	14.9	0.004	0.79	0.65	25.0	11.3			820	1.20	21.1	25.4	52.2	1.1	0.3				5.52/25	257	364	54.0		
	1024	Jun-80	2355	11.0	8.75/25.0	24.7	78.6		436	95.0	13.9	0.016	0.93	0.56	29.8	10.5			636	1.04	16.3	15.8	66.7	0.2	1.0									
BI-12	4034	May-03	1813	16.0	8.19/20.2	7.4	109.6	3.40	582	127	22.0	0.010	0.60	0.52	100	13.0	0.60	0.010	883	2.00	97.8	0.2	0.8	1.2	3864	1925								
	4013	May-90	2127	17.8	7.6/26.0	34.5	143.0		572	153	21.2	0.043	0.51	0.62	79.1	25.0			1216	2.22	95.3	0.8	1.1	2.8	2570	1663								
	4010	May-89	2138	15.9	7.89/20.0	53.0	133.0		623	144	21.2	0.180	0.47	0.62	36.8	31.0		0.100	1021	2.14	96.6	0.6	0.7	2.1	2034	1774								
BI-13	1033	Sep-87	2203	19.6	8.43/19.0	42.0	135.0		521	147	20.2	0.060	0.65	0.58	66.8	3.0			1025	2.17	25.4	18.8	54.6	0.2	1.0				4.42/19	344	687	0.25		
	1021	May-83	2402	17.0	9.43/25.0	25.8	98.5		535	135	18.2	0.005	0.22	0.88	24.5	7.2			1032	1.92	23.3	18.3	57.2	0.1	0.2				4.42/21	348	771	0.90		
	1038	Jul-81	2380	20.2	8.32/24.0	30.0	189.0		478	135	18.5	0.003	0.14	0.81	10.8	4.0			911	2.96	18.8	20.0	60.2	0.1	0.8				4.38/24	544	512	0.35		
	1005	Mar-81	2321	18.0	8.5/22.0	27.9	147.0		552	143	18.2	0.018	0.38	0.87	48.2	6.2			990	0.38	18.1	16.8	64.2	0.1	0.8				4.16/22	175	768	0.32		
	0351*	Sep-06	2021	15.2	9.18/23.1	5.7	53.3	0.21	766	114	22.4	0.005	1.11	0.80	78.8	25.9	2.18	0.019	1170	0.52	91.4	0.2	8.2	8.2	560	526								
BI-14	0311*	Jul-08	1807	15.9	9.05/21.7	4.2	104.0	1.00	776	240	49.6	0.004	1.15	1.03	260	19.5	1.53	0.009	1610	0.98	83.9				570	1330								
	0343*	Aug-08	1169 ^a	10.0	8.88/19.6	161	1.2	0.80	426	160	17.5	0.001	1.29	1.39	50.6	26.9	1.36	0.003	868	2.58	87.3				1765	2320								

^a liquid enthalpy well samples, ^b Sampling pressure (bar-g), ^{dt} discharge enthalpy (kJ/kg), *sampled and analysed by ISOR, otherwise by Kemia Ltd and NEA.

3.2 Data handling

Samples from individual wells have been collected at different pressures. The sampling pressure for individual wells generally lies between 4 and 24 bar-a (Table 2). Analytical results are, therefore, not directly comparable because component concentrations, both in water and steam, depend on the pressure of separation. To obtain a common reference point to evaluate component concentrations in both water and steam in the production period of the selected wells, the sample concentrations were calculated at 10 bar-a vapour pressure with the aid of the WATCH-program (Arnórsson et al., 1982), version 2.1 (Bjarnason, 1994), using the measured discharge enthalpy value to account for steam formation between sampling and reference pressures. The rationale for selecting a reference pressure of 10 bar-a vapour pressure, according to Arnórsson et al., 1990 is that 1) many samples were collected at a pressure close to this one so the effect of any imprecision in the measurement of discharge enthalpy on the calculated component concentration in water and steam at the reference pressure is minimized; and 2) the enthalpy of steam in the range 10–55 bar-a (equivalent to 180–270°C for steam-saturated water) is close to being constant. As a result, vaporization of water during pressure drop from 270 to 180°C is insignificantly affected by the steam to water ratio (enthalpy) of the flowing fluid, whereas this is not the case above 270°C (most of the Námafjall wells have aquifer temperatures below this temperature), and particularly not so below 180°C (Figure 12 adapted from Gudmundsson and Arnórsson, 2002).

The concentrations of the components selected for this study, calculated at 10 bar-a vapour pressure

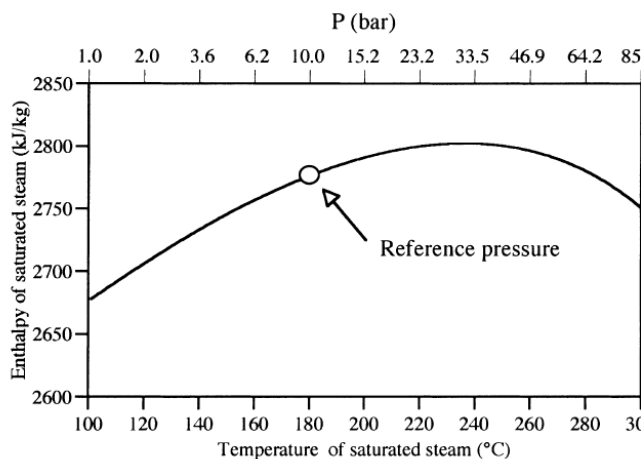


FIGURE 12: Relationship between p/T and enthalpy of saturated steam in the range 100-300°C. The circle represents the p/T (10 bar-a/180°C) selected reference point for calculation of fluid concentration in water and steam phases from collected samples

(liquid phase - pH, TDS, SiO₂, Na, K, Cl, and SO₄, and steam phase - CO₂, H₂S, and H₂) are shown plotted against time for the wells at Námafjall (Appendix II). At p/T conditions 10 bar-a/180°C, the lowest pH is 7.66 (BJ-12) and highest pH 8.16 (BN-04). Some of the selected constituents (e.g. SiO₂, Na, K, CO₂, H₂ and H₂S) are used as geothermometers thus changes in their concentrations or ratios reflect temperature changes, either due to colder or hotter recharge into producing aquifers, partial re-equilibration in the depressurization zone around the producing wells where cooling occurs by extensive boiling, or changes in the yield from different aquifers. Additionally, a graphical depiction of some of the major fluid characteristics / constituent concentrations through five number summaries by box plots – minimum and maximum,

lower and upper quartiles and the median - are illustrated (Figure 13), to display the differences between the data without making any assumptions of the underlying statistical distribution (non-parametric) hence display the degrees of dispersion, skewness and outliers.

3.3 Aquifer fluid modelling

3.3.1 'Excess' enthalpy and phase segregation

When a well intersects a two-phase aquifer (i.e. both liquid and vapour present) intensive depressurization boiling starts in the aquifer-well system during discharge. In case the pressure drop produced by discharging the well is sufficiently large, boiling can also start in the aquifer even if the aquifer fluid was initially sub-boiling. During the intensive boiling, vapour may not only form by

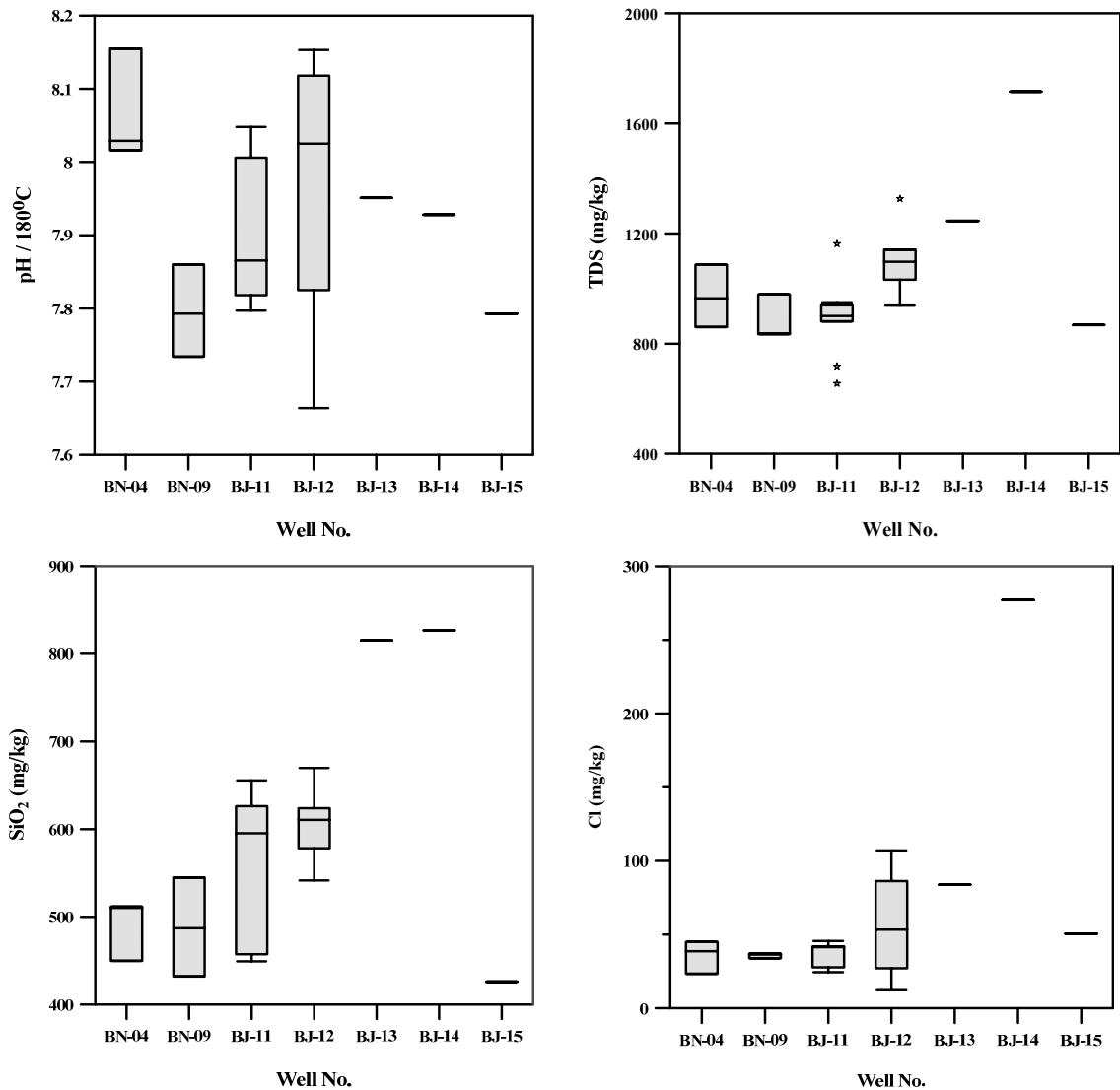


FIGURE 13: Fluid characteristics and concentration of Námajfall wells at 10 bar-a

depressurization boiling, but also by conductive heat transfer from the rock to the fluid: depressurization boiling lowers the fluid temperature, creates a temperature gradient between fluid and aquifer rock and favours conductive heat transfer from rock to fluid. Addition of heat to the two-phase fluid will not affect its temperature, but will enhance boiling, i.e. steam formation. The boiling point of an aqueous solution is affected by its salinity and gas content. Increasing salinity raises the boiling point (Bischoff and Rosenbauer, 1989), whereas dissolved gases lower it. Boiling of a rising geothermal liquid starts at a depth where the sum of the water vapour pressure and all dissolved gas partial pressures become equal to the hydrostatic pressure. Partial pressures of individual gases in the geothermal systems may be determined by their supply to the geothermal fluid or fixed by specific temperature-dependent mineral-gas equilibria (Arnórsson et al., 2007; Gudmundsson and Arnórsson, 2005; Karingithi et al., 2010).

Liquid and vapour may segregate in two-phase aquifers, leading to an increase in the vapour to liquid ratio of well discharges. Phase segregation results from the different flow properties of liquid/vapour, and from the effects of capillary pressure and relative permeability (Horne et al., 2000; Pruess, 2002; Li and Horne, 2004a and b). The mass flow rate of each phase is affected by the relative permeability, the pressure gradient, density and viscosity. Adhesive forces between mineral grain surfaces and fluid, which are the cause of capillary pressure, are stronger for liquid than for vapour. In this way, the mobility of liquid is reduced relative to that for vapour. The effect of capillary pressure becomes stronger in rocks of small pores and fractures, i.e. when permeability is low.

Due to boiling and phase segregation in two-phase aquifers, the discharge enthalpy of wells producing from liquid-dominated geothermal reservoirs is often higher than the enthalpy of the initial aquifer fluid, and it is not uncommon that wells drilled into such systems discharge steam only. Wells with discharge enthalpies higher than that of steam-saturated water at the aquifer temperature have been referred to as “excess enthalpy wells” (Angcoy, 2010; Arnórsson et al., 2007; 2010; Karingithi et al., 2010; Scott, 2011). Some of the excess enthalpy may be due to the presence of vapour in the initial aquifer fluid. However, the effects of conductive heat transfer, phase segregation, or both, generally seem to be more important. To calculate the chemical composition of the initial aquifer liquid and vapour, the relative contributions of the different processes to the excess discharge enthalpy and the initial vapour fraction of the aquifer fluid need to be evaluated.

Wells BN-04, BN-09 and BJ-15 in Námafjall field are considered to have liquid enthalpy (Table 2 and Figure 14), i.e. the enthalpy of the discharge is the same (within the limit of measurement error) to that of steam saturated liquid at the aquifer temperature, thus for liquid enthalpy wells, it is a reasonable assumption to take the total well discharge composition to represent the initial aquifer fluid. The other wells (BJ-11, BJ-12, BJ-13 and BJ-14) display variable degrees of ‘excess’ enthalpy although the discharge enthalpy has decreased with time in the wells for which data are available for more than 15 years (Figure 14). For excess enthalpy wells, a model needs to be selected that explains the cause of the elevated well enthalpy by considering the effects of depressurization boiling, possible phase segregation in the depressurization zones around wells, conductive heat transfer from the aquifer rock to the flowing fluid that enhances boiling as well as loss of gaseous steam from the fluid flowing into wells, likely during horizontal flow.

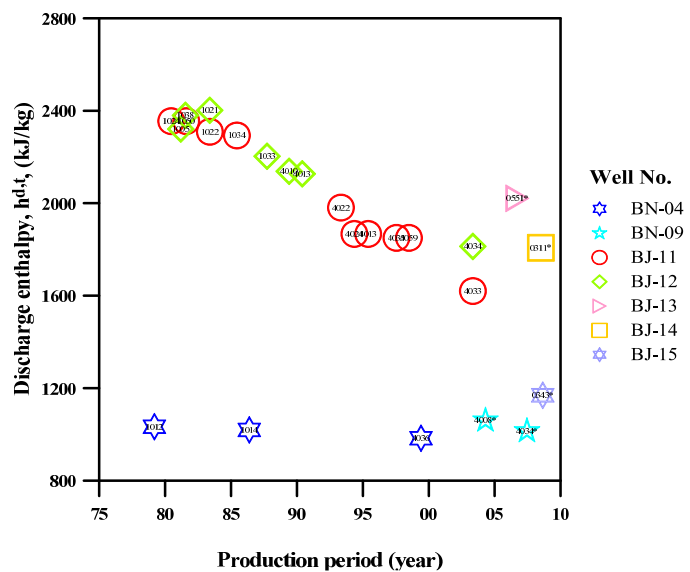


FIGURE 14: Discharge enthalpy of wells in Námafjall field; numbers in the symbols indicate the sample

Glover et al. (1981) used the chemistry of well discharges in a simple way to distinguish between excess well enthalpy caused by phase segregation from that caused by conductive heat transfer from aquifer rock to fluid. For phase segregation, the concentration of a conservative component that only occupies the liquid is expected to decrease in the total discharge with increasing discharge enthalpy and approach zero as the discharge enthalpy approaches that of saturated steam. For many wet-steam wells, discharge enthalpy may not vary sufficiently with time to make the method of Glover et al. (1981) applicable. In a specific well-field, one may use many wells with a range of discharge enthalpies to determine whether conductive heat transfer or phase segregation dominates the excess enthalpy. If conservative components like Cl vary much across the well field, they may not be a good choice, but if aquifer temperatures are about constant, SiO₂ is useful because its concentration is determined almost solely by temperature through its equilibrium with quartz (Figure 15). The observed correlation for SiO₂ in the total discharge for the excess enthalpy wells at Námafjall suggests that phase segregation in the producing aquifers is largely the cause of excess well discharge enthalpy.

3.3.2 Aquifer fluid temperature

Many chemical and isotopic geothermometers are used to estimate the aquifer temperatures beyond the zone of secondary processes like boiling, cooling and mixing on the basic assumptions that the sampled fluids are representative of the undisturbed aquifers where local equilibrium conditions are achieved. Actual downhole measurements may or may not agree with geothermometers. For fields of

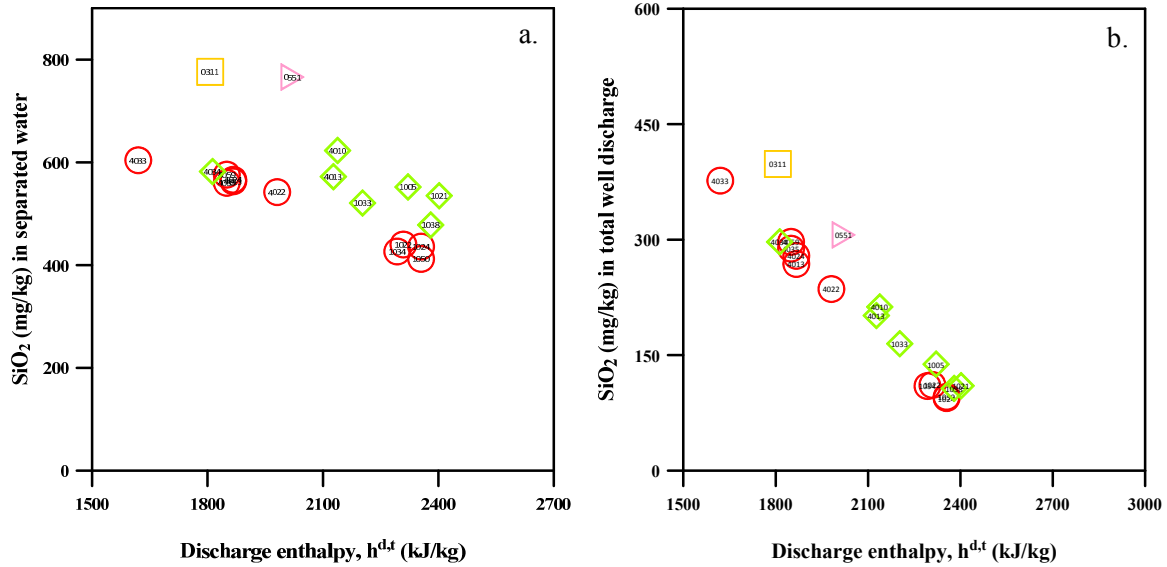


FIGURE 15: Variation in silica content in (a) separated waters, and (b) total discharge of the excess enthalpy wells. The total discharge silica content approaches zero as the discharge enthalpy value approaches that of saturated steam: an indication that excess enthalpy of well discharges is at least largely caused by phase segregation, symbology as in Figure 14

heterogeneous permeability, the fluids reaching the surface are inevitably a mixture from the different aquifers as deduced from tracer tests and geochemical monitoring. By these scenarios, selecting a representative reference temperature is at best an approximation.

Since some of the wells in Námafjall have excess discharge enthalpy, the cause of the increase in the flowing fluid enthalpy needs to be taken into account when calculating individual component concentrations in the initial aquifer fluid from analytical data on samples of liquid water and vapour collected at the wellhead. To select the aquifer reference temperature, T^f , solute (quartz and Na/K) geothermometers calculated from the well discharge components are used and comparison with well temperature logs considered. The equations used for calculation of aquifer temperature are as indicated in Table 3 and the calculated geothermometer temperatures presented in Table 4. The temperature logs of the main aquifers generally compare well with the calculated geothermometers for each well's sample(s), considering that some of the wells seem to have more than one producing aquifer (see Appendix I for temperature logs). The calibration used for the quartz geothermometer is that presented by Gudmundsson and Arnórsson (2002) based on the calibration of Fournier and Potter (1982). The Na/K geothermometer results are independent of the process producing 'excess' well discharge enthalpy because it is based on component ratio (i.e. Na^+/K^+). Quartz temperatures have been related to the Na/K temperature (Figure 16). It is seen that the quartz and Na/K geothermometers yield approximately similar results although quartz temperatures are systematically higher on average. The average difference between T_{qtz} and $T_{\text{Na/K}}$ is 19°C with a standard deviation of 11°C .

TABLE 3: Geothermometer equations valid in the range $0\text{-}350^\circ\text{C}$ at P_{sat} .

Geothermometer	Equation ($T^\circ\text{C}$)
T_{qtz}	$-132.2 + 0.036206 \cdot X + 55.865 \times 10^{-6} \cdot X^2 - 2.699 \times 10^{-8} \cdot X^3 + 128.277 \cdot \log X$
$T_{\text{Na/K}}$	$733.6 - 770.551 \cdot Y + 378.189 \cdot Y^2 - 95.753 \cdot Y^3 + 9.544 \cdot Y^4$

X is SiO_2 in mg/kg. T_{qtz} represents the temperature calculated from unionized silica (as SiO_2) concentration in water initially in equilibrium with quartz after adiabatic boiling to 180°C (10 bar-a vapour pressure) according to Gudmundsson and Arnórsson (2002) based on the calibration of Fournier and Potter (1982). Y represents the logarithm of the molal Na/K concentration ratio at equilibrium with pure low-albite and pure microcline according to Arnórsson and Stefánsson (1999) and Arnórsson (2000)

TABLE 4: Geothermometer temperatures (°C) and aquifer temperature logs for Námafjall wells

Well No.	Sample No.	Date	SP (bar-g)	h ^{d,t} (kJ/kg)	Geothermometer Temperatures (°C)			Aquifer depth (m)	Aquifer Temp (°C)
					T _{Na/K}	T _{qtz}	T _{av.}		
BN-04	4036	Jun-99	3.70	983 ^a	209	245	227	300 1000	160-220 200-260
	1014	May-86	5.20	1019 ^a	238	233	236		
	1012	Mar-79	8.10	1033 ^a	248	245	246		
BN-09	4034*	Jun-07	11.8	1014 ^a	226	232	229	500-800	200-235
	4008*	Apr-04	13.5	1060 ^a	227	255	241		
BJ-11	4033	May-03	19.0	1620	254	269	262	600 1300	150-170 200-240
	4059	Jul-98	23.5	1850	232	268	250		
	4035	Jul-97	23.1	1850	253	265	259		
	4013	May-95	14.5	1867	243	259	251		
	4024	May-94	19.0	1867	247	263	255		
	4022	May-93	19.9	1981	230	260	245		
	1034	Jun-85	14.7	2293	247	235	241		
	1022	May-83	16.2	2309	245	239	242		
	1050	Aug-81	18.0	2355	249	235	242		
	1024	Jun-80	11.0	2355	239	233	236		
BJ-12	4034	May-03	16.0	1813	257	264	261	700 1100	150 150-240
	4013	May-90	17.8	2127	233	264	249		
	4010	May-89	15.9	2138	239	272	255		
	1033	Sep-87	19.6	2203	232	257	244		
	1021	May-83	17.0	2402	230	259	245		
	1038	Jul-81	20.2	2380	232	250	241		
1005	Mar-81	18.0	2321	225	262	243			
BJ-13	0551*	Sep-06	15.2	2021	273	293	283	500 2000	260 320
BJ-14	0311*	Jul-08	15.9	1807	279	295	287	800 1700	250-270 230-280
								800 1700	210-290 300-320
BJ-15	0343*	Aug-08	10.0	1169 ^a	210	229	220	800 1700	210-290 300-320

^a liquid enthalpy well samples, *sampled and analysed by ÍSOR otherwise by Kemia Ltd and NEA, T_{av.} is average of T_{qtz} and T_{Na/K}.

Due to fluid discharged from a well being a composite of different aquifers/feed zones, it is a simplification to select a single temperature value and calculate aqueous speciation and mineral saturation at that temperature. Measured downhole temperatures of producing aquifers in wells at Námafjall have a good comparison with the calculated geothermometers for all but one well (BJ-15).

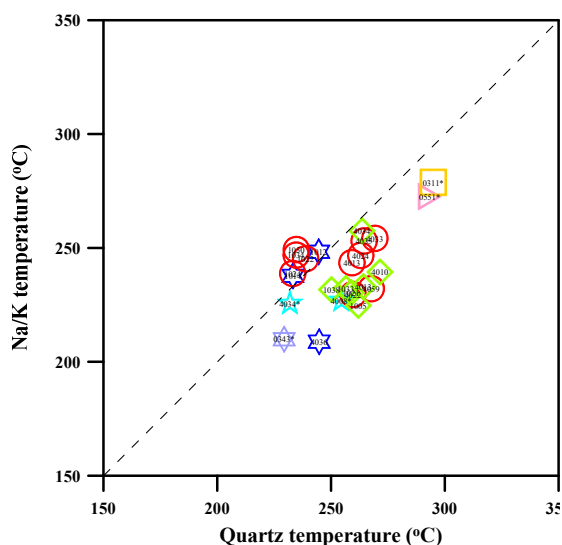


FIGURE 16: Relationship between geothermometer temperatures in Námafjall wells; symbology as in Figure 14

The correlation between the Na/K and quartz geothermometers is representative when considering all errors, including contribution of fluid from two or more aquifers to individual wells, as indicated by well logs. T^f for the Námafjall wells is therefore selected as T_{qtz} but calculations for aquifer gas composition shall also be made considering T_{av.} in the fourth chapter for comparison purposes. The selection of T^f has some effect on how much individual data points lie above the equilibrium curves as shall be seen. It is known that the Na-K geothermometer typically yields significantly lower temperatures than the quartz geothermometers for wet-steam wells in Iceland. The reason is likely the faulty calibration of the former geothermometer or partial re-equilibration in the depressurization zone around discharging wells (Gudmundsson and Arnórsson, 2002). It is for this reason that the aquifer temperature is selected as T_{qtz}.

3.3.3 Phase segregation pressure

Fluid in geothermal reservoirs/systems consists of liquid and vapour, or a mixture of the two. At overall chemical equilibrium, the Gibbs phase rule dictates that two independent variables are necessary to completely describe the system. These variables are temperature and pressure. The phase rule is given by:

$$F = C - \phi + 2 \quad [3.1]$$

where F , C and ϕ are degrees of freedom, components in the system and phases in thermodynamic equilibrium with each other, respectively. In the production zone of a geothermal reservoir, the independent variables necessary to completely define the system are temperature, Cl and sometime CO_2 . In geothermal systems, pressure has little influence and Cl and CO_2 are typically source rather than equilibrium controlled.

Upon entering the production zone of a discharging well, the pressure of the aquifer fluid is greatly reduced and intensive depressurization boiling will start in the aquifer when the well is discharged. In a liquid-dominated aquifer, this pressure drop may be insufficient to initiate boiling in the aquifer itself, and the first boiling takes place in the well. In case the pressure drop produced by discharging the well is sufficiently large, boiling can also start in the aquifer even if the aquifer fluid was initially sub-boiling. As already indicated, phase segregation may occur at some point as the two-phase fluid flows through the geothermal reservoir towards the production zone of the well due to increased relative permeability of the vapour phase. The steam and water flow defined in terms of a modified expression of Darcy's law for each phase are represented by:

$$M_i = k_{ri} \cdot \frac{k_a}{\mu_i} \cdot A \cdot \left(\frac{\Delta P}{L} \right) \quad [3.2]$$

Where M_i , μ_i and k_{ri} are the mass flow, dynamic viscosity and relative permeability of phase i , k_a is the intrinsic permeability, A the cross-sectional area and $\Delta P/L$ the pressure gradient. The low viscosity of the vapour phase in comparison to the liquid phase permits it to ascend faster in response to buoyant forces. Throughout most of the pressure range of interest in geothermal systems (from 1 bar-a to ~100 bar-a) the liquid phase dynamic viscosity is 5 to 10 times that of the vapour phase and the two phases are exposed to different pressure gradients. In addition, capillary forces cause retention of water in the rock matrix, due to the hydrophilic nature of most mineral surfaces and the surface tension of liquid water (Chen et al., 2004; Horne et al., 2000; Ingebritsen et al., 2010; Pruess, 2002). The strength of these effects varies based on temperature, the degree of liquid saturation, the geometry of the pore space and the connectivity of a pore network considering the interface between fluid and rock.

Relative permeabilities have been determined for porous media and in fractures in experimental settings, and are described in terms of liquid saturation and volume fraction of liquid, rather than the mass fraction. Liquid saturation is related to vapour mass fraction by consideration of the density of each phase at a given vapour saturation pressure, (if pressure selected is at the phase segregation pressure, P^e):

$$S^{e,l} = 1 - \frac{X^{e,v} \frac{1}{\rho^{e,v}}}{X^{e,v} \cdot \frac{1}{\rho^{e,v}} + (1 - X^{e,v}) \cdot \frac{1}{\rho^{e,l}}} \quad [3.3]$$

where $S^{e,l}$ represents liquid saturation, $X^{e,v}$ the vapour mass fraction, and $\rho^{e,v}$ and $\rho^{e,l}$ the densities of the vapour and liquid phases respectively, determined at a given vapour saturation pressure (in this study, the pressure is taken as the phase segregation pressure, P^e). Due to the low vapour density compared to liquid density, even a small vapour mass fraction significantly reduces the liquid saturation.

To model steam-water relative permeabilities, two models as represented by the Corey type (Corey, 1957) and the x-type curves for both phases (Figure 17) are used. The curves show the relationship

3.3.4 Thermodynamics of the phase segregation model

In studying high-temperature geothermal reservoirs around the world, various researchers (e.g. Angcoy, 2010; Arnórsson et al., 1990, 2007, 2010; Arnórsson and Stefánsson, 2005; Karingithi et al., 2010; Remoroza, 2010; Scott, 2011) have modelled aquifer fluid compositions by applying the phase segregation model to wellhead data. Arnórsson et al. (2007) and Arnórsson et al. (2010) present meticulous procedures to compute the chemical composition of aquifer fluids from the analyses obtained at the wellhead using different reasonable sets of assumptions.

Having selected T^f ($^{\circ}\text{C}$) and P^e (bar-a), modelling of the initial aquifer fluid by phase segregation follows the symbology by Arnórsson et al. (2007) and Arnórsson et al. (2010) as outlined in the publications and is given by parameters and equations in Table 5. In the equations that follow, M is the mass flow (kg/s), h specific enthalpy (kJ/kg), m concentration (moles/kg), V relative mass of initial aquifer fluid that has boiled relative to the well discharge, D distribution coefficient of the gaseous species between vapour and liquid phases, and X the steam fraction. The subscripts represent a component (i -either component, r -non-volatile, s -volatile), the first superscript represents the location of the fluid (d -discharge, f -initial aquifer, e -phase segregation point or zone i.e. between aquifer and wellhead) and the second superscript the fluid phase (l -liquid, v -vapour, t -total two phase).

TABLE 5: Conservation equations and equations to calculate individual component concentrations of the initial aquifer fluid by the phase segregation model. From Arnórsson et al. (2010)

Parameter	Equation
a. Mass flow	$M^{d,t} = M^{f,t} - M^{e,l}$
b. Specific enthalpy	$h^{d,t} \cdot M^{d,t} = h^{f,t} \cdot M^{f,t} - h^{e,l} \cdot M^{e,l}$
c. Non-volatile component	$m_r^{d,t} \cdot M^{d,t} = m_r^{f,t} \cdot M^{f,t} - m_r^{e,l} \cdot M^{e,l}$
d. Volatile component	$m_s^{d,t} \cdot M^{d,t} = m_s^{f,t} \cdot M^{f,t}$
e. Component concentration in aquifer liquid	$m_r^{f,l} = \frac{m_r^{d,t}}{1 - X^{f,v}} \cdot \left[V^{f,t} \left(1 - \frac{1}{1 - X^{e,v}} \right) + \frac{1}{1 - X^{e,v}} \right]^{-1}$
f. Component concentration in aquifer vapor	$m_s^{f,v} = \frac{m_s^{d,t}}{V^{f,t}} \cdot \left[X^{f,v} \left(1 - \frac{1}{D_s^f} \right) + \frac{1}{D_s^f} \right]^{-1}$

One of the assumptions taken into consideration in dealing with the phase segregation model is that chemical reactions in the depressurization zones do not change fluid component concentrations, neither by mineral dissolution/precipitation, nor by dissolution of casing material and wellhead equipment. This appears to be a reasonable approximation for components present in high concentrations in the fluid. On the other hand, minor reactive components, such as Ca, Al and Fe may change their concentrations considerably in the fluid between undisturbed aquifer and wellhead. Additional assumptions describing the nature of the initial reservoir fluid include selection of the pressure at which phase segregation occurs, P^e , a single “reference” temperature, T^f , (also referred to as temperature of initial aquifer fluid) at which composition and speciation is calculated, as well as the presence (or lack thereof) of a vapour phase, $X^{f,v}$, in the initial reservoir fluid. Due to the significant uncertainty associated with many of these assumptions, the approach chosen for this study is to calculate aquifer fluid compositions taking into account the assumptions listed.

Aquifers penetrated by wells drilled into high-temperature, liquid-dominated geothermal systems are often at P (bar-a)/T (°C) conditions insufficient to initiate boiling in the contained geothermal fluid. If the pressure drop caused by discharging such wells is not sufficient to initiate boiling in the aquifer itself, the depth level of first boiling is within the well and it is therefore a reasonable approximation to treat the aquifer and well as an isolated system, in which case boiling is adiabatic. In the context of thermodynamics, a system is isolated when no transfer of heat or mass occurs across its boundaries. Hence, considering the well and aquifer as an isolated system implies that the discharge enthalpy and chemical composition of the well discharge are the same as those of the aquifer fluid.

Under isolated system conditions, conservation of fluid mass and specific enthalpy between the aquifer and the point of discharge can be expressed by

$$M^{f,t} = M^{d,t} = M^{d,v} + M^{d,l} \quad [3.4]$$

and

$$h^{f,t} = h^{d,t} = h^{d,v} \cdot X^{d,v} + h^{d,l} (1 - X^{d,v}), \quad [3.5]$$

respectively, while conservation of mass for chemical components is described by:

$$m_i^{f,t} = m_i^{d,t} = m_i^{d,v} \cdot X^{d,v} + m_i^{d,l} (1 - X^{d,v}) \quad [3.6]$$

If $X^{d,v}$ is the steam (vapour mass) fraction at sampling (discharge) conditions, then $(1 - X^{d,v})$ in Equations 3.5 and 3.6 represent the liquid mass fraction. Since $X^{d,v}$ is the vapour mass fraction at sampling conditions (well discharge), its value can be obtained from the specific enthalpies of the liquid aquifer at the assumed aquifer temperature and of the saturated liquid and vapour at sampling pressures by rearranging Equation 3.5:

$$X^{d,v} = \frac{h^{d,t} - h^{d,l}}{h^{d,v} - h^{d,l}} \quad [3.7]$$

Values for $h^{d,l}$ and $h^{d,v}$ can be obtained from Steam Tables and a value for $h^{d,t}$ can either be obtained from measurement of the discharge enthalpy or, in the case of sub-boiling aquifer, from evaluation of the aquifer temperature, T^f . In a sub-boiling aquifer, the enthalpy of the aquifer fluid, $h^{f,t}$, is simply that of liquid water, $h^{f,l}$, at the aquifer temperature.

Under the assumption of phase segregation, considering the version that the vapour fraction in the initial aquifer is zero i.e. $X^{f,v} = 0$, and selecting a phase segregation temperature, T^e , mass of the boiled liquid is retained in the formation ($M^{e,l}$), and the above conservation of mass and energy Equations are modified by a term accounting for this “outflow” stream to give

$$M^{d,t} = M^{f,t} - M^{e,l} \quad [3.8]$$

$$h^{d,t} \cdot M^{d,t} = h^{f,t} \cdot M^{f,t} - h^{e,l} \cdot M^{e,l} \quad [3.9]$$

Taking Equation 3.8 comparative to $M^{d,t}$, we get the relative mass equation

$$1 = V^{f,t} - V^{e,l} \quad [3.10]$$

where $V^{f,t}$ and $V^{e,l}$ are defined as the relative mass of the total two-phase fluid inflowing into the production zone of a well and the mass of boiled and degassed liquid retained in the formation, in that $V^{f,t} = M^{f,t}/M^{d,t}$ and $V^{e,l} = M^{e,l}/M^{d,t}$ respectively, in relation to the mass flow of the well discharge.

If we divide Equation 3.9 by $M^{d,t}$, substitute $V^{f,t} - 1$ for $V^{e,l}$ and isolate $V^{f,t}$, an alternate expression for $V^{f,t}$ is found in terms of enthalpy as:

$$V^{f,t} = \frac{h^{d,t} - h^{e,l}}{h^{f,t} - h^{e,l}} \quad [3.11]$$

Assuming a steam fraction of zero in the aquifer, ($h^{f,t} = h^{f,l}$), $h^{f,l}$ and $h^{e,l}$ can be obtained from Steam Tables once T^e (relating to P^e) and T^f are selected, thus $V^{f,t}$ is easily obtained. $V^{f,t}$ changes under the assumption of different phase segregation conditions (>10 bar-a) and initial aquifer temperatures as seen from Equation 3.11. To demonstrate the changes in $V^{f,t}$ the following conditions have been selected for an initial saturated fluid: aquifer temperature 280 and 300°C corresponding to aquifer pressure of ~64 and 86 bars-a, and varying discharge enthalpies from 1400-2700 kJ/kg (Figure 19). For the aquifer fluid with the P/T conditions described above, the ratio of inflowing initial aquifer fluid to the discharge mass has a small uncertainty as $V^{f,t}$ is fairly low (the $V^{f,t}$ changes are <2) and not highly affected by change in the selected T^f .

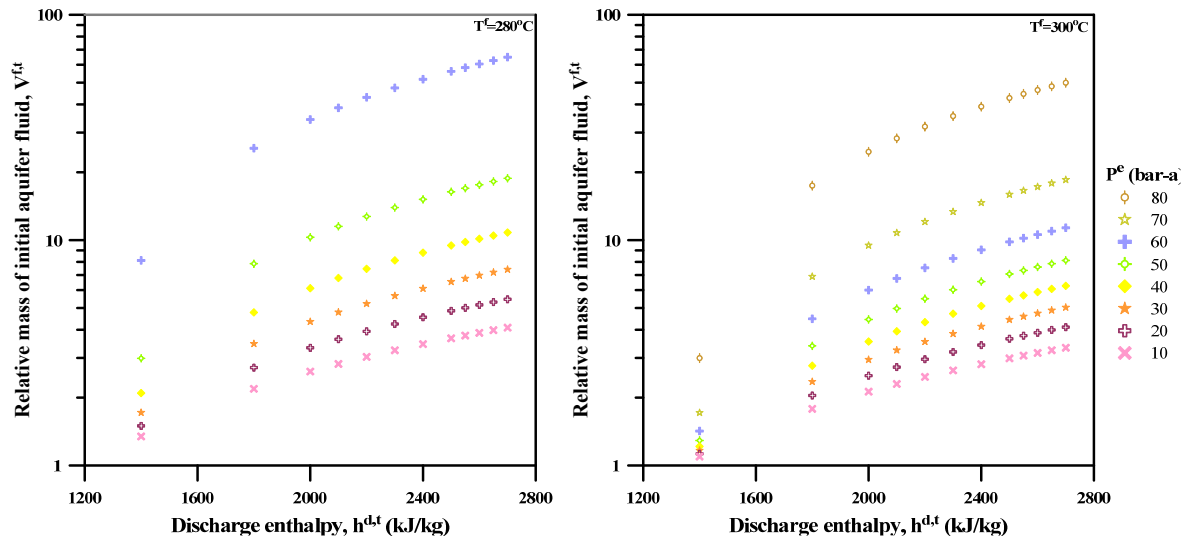


FIGURE 19: Relative $V^{f,t}$ of initial inflowing aquifer fluid as a function of $h^{d,t}$ (kJ/kg), given different P^e (10 to 80 bar-a) and T^f (300 and 280°C)

Scott (2011) indicates that calculated $V^{f,t}$ values increase rapidly at higher discharge enthalpies ($h^{d,t} > 2400$ kJ/kg) and when phase segregation pressures close to the initial aquifer pressure are assumed. At phase segregation pressures closer to the initial aquifer fluid temperature, less vapour has been generated by boiling. In order to account for a given observed ‘excess’ discharge enthalpy, the increase in the vapour/liquid mass ratio upon phase segregation must be greater for assumed phase segregation pressures closer to the initial aquifer fluid pressure, thus the reason for considering larger $V^{f,t}$ values calculated assuming higher phase segregation pressures. Aquifer compositions are hereby calculated at multiple assumed phase segregation pressures and initial aquifer fluid temperature, but a pressure where the liquid phase is to some extent immobile is taken to be the most logical assumption, as it seems that phase segregation most likely occurs across a pressure interval rather than a single pressure and in this light; the relationship between the most logical assumed phase segregation pressure and the considered residual liquid saturation is not straightforward. For volcanic rock reservoirs, it is likely that this interval is well approximated by the selected phase segregation pressure. In hyaloclastites and vesicular tops of basalt lavas, phase segregation may be expected to occur at higher liquid saturations than in fractures where fluid flows must be concentrated.

Sensitivity analysis

Assessing the chemical composition of the initial aquifer fluid from wellhead data from Námafjall field is the principal objective of this study. A sensitivity analysis is given, describing how selection of

P^e and T^f affects the calculated concentrations of chemical components (volatile and non-volatile) in an initial aquifer fluid. For a non-volatile component, its total mass at discharge is equal to the mass contained in the initial aquifer fluid minus the mass in the retained liquid at the point of phase segregation, expressed in terms of relative mass as:

$$m_r^{d,t} = m_r^{f,t} \cdot V^{f,t} - m_r^{e,l} \cdot V^{e,l} \quad [3.12]$$

Assuming that no loss of the non-volatile component, r , occurs between the aquifer and the point of phase segregation, i.e. $m_r^{f,t} = m_r^{e,t}$, $m_r^{e,l}$ can be written as:

$$m_r^{e,l} = m_r^{f,t} \left(\frac{1}{1 - X^{e,v}} \right) \quad [3.13]$$

Where $X^{e,v}$ is the vapour mass fraction of flowing fluid after depressurization boiling to phase segregation pressure, P^e but before retention of liquid in the aquifer and is given by:

$$X^{e,v} = \frac{h^{f,l} - h^{e,l}}{h^{e,v} - h^{e,l}} \quad [3.14]$$

On selecting the initial aquifer and phase segregation P/T conditions, the terms described above can be combined in a single relationship (after substituting $V^{f,t} - 1$ for $V^{e,l}$) to calculate the concentration of a non-volatile in the initial aquifer fluid from measurements taken at the point of discharge, and using Equation e in Table 5:

$$m_r^{f,l} = m_r^{f,t} = \frac{m_r^{d,t}}{1 - X^{f,v}} \cdot \left[V^{f,t} \left(1 - \frac{1}{1 - X^{e,v}} \right) + \frac{1}{1 - X^{e,v}} \right]^{-1} \quad [3.15]$$

The sensitivity of the model outcomes to assumed phase segregation and initial aquifer conditions for non-volatile components using Equation 3.15, are shown in Figure 20. From this figure, it is seen that the selected phase segregation pressure does not significantly affect the calculated concentration of a non-volatile component in the initial aquifer fluid, especially across the middle of the pressure range where phase segregation is most likely to occur and for wells with discharge enthalpies below 2000 kJ/kg. $m_r^{f,t}$ is, however, significantly affected if only at higher T^f , $h^{f,t}$ and P^e close to initial aquifer conditions and thus the calculated concentration differences increase highly. The phase segregation model assumes that most of the gases present in the initial reservoir fluid are discharged from the well, with exception of CO_2 and H_2S that are slightly soluble in the liquid and thus not completely discharged. Thus:

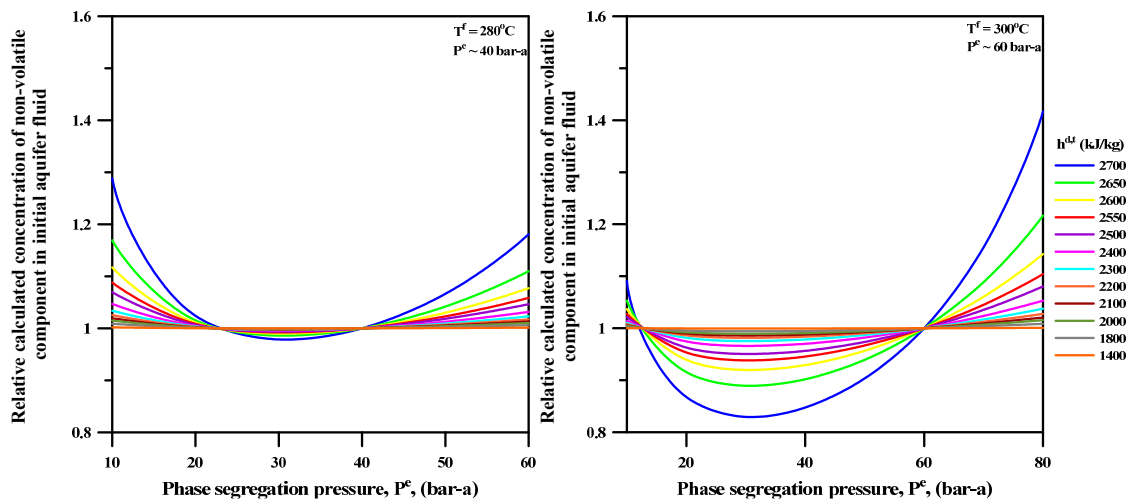


FIGURE 20: Relative calculated concentration of a non-volatile component ($m_r^{f,t}$) in initial aquifer fluid at selected phase segregation pressures and calculated concentration at P^e when volume fraction of flowing vapor is ~80% (i.e. $S^{e,l} \sim 0.2$), for different $h^{d,t}$ (kJ/kg) and T^f ($^{\circ}C$). Aquifer fluid was assumed to have liquid enthalpy

$$m_s^{d,t} \cdot M^{d,t} = m_s^{f,t} \cdot M^{f,t} \quad [3.16]$$

As $h^{f,t} = h^{f,l}$ and $m_s^{f,t} = m_s^{f,l}$ because $X^{f,v}$ is selected here as zero, in addition to assuming that the concentration of gaseous components in the retained liquid is negligible, the calculated aquifer concentration is simply inversely proportional to $V^{f,t}$, expressed by:

$$m_s^{f,t} = \frac{m_s^{d,t}}{V^{f,t}} \quad [3.17]$$

The calculated concentrations of gaseous components are markedly more sensitive to the selected P^e and T^f , because the assumed phase segregation pressure greatly impacts the composition and relative mass of the retained liquid. Assuming that the retained liquid represents an ‘outflow’ stream, Equation 3.12 is modified to

$$m_s^{d,t} = m_s^{f,t} \cdot V^{f,t} - m_s^{e,l} \cdot V^{e,l}, \quad [3.18]$$

where $m_s^{e,l}$ is the concentration of a volatile species in the retained liquid. Assuming its total concentration in the two phase fluid at the point P^e , prior to phase segregation is equal to its total concentration in the initial aquifer fluid ($m_s^{f,t} = m_s^{e,t}$), $m_s^{e,l}$ can be approximated by the formulation:

$$m_s^{e,l} = \frac{m_s^{f,t}}{[X^{e,v}(D_s^e - 1) + 1]} \quad [3.19]$$

D_s^e is the distribution coefficient of a gaseous species between vapour and liquid, calculated at the phase segregation pressure. The coefficient D_s is a function of gas solubility and fluid pressure, and is defined by

In Equation 3.20, $K_{H,s}$ is the Henry’s Law coefficient (moles/(kg.bar)) for a certain gas species and P_{tot} (bars-a) is the vapour pressure of water, P_{H_2O} , plus the sum of partial pressures of all gaseous components. Since the partial pressures of non-condensable gas species contribute little relative to

$$D_s = \frac{m_s^v}{m_s^l} \cong \frac{55.508}{P_{tot} \cdot K_{H,s}} \xi \quad [3.20]$$

vapour pressure, $P_{tot} = P_{H_2O}$. ξ is a degassing factor (assumed to be unity, representing equilibrium degassing) and 55.508 is the factor for converting 1 kg of H_2O into moles of H_2O . Sources for Henry’s gas constants and additional information regarding the gas law are as shown in Table 6.

After combining Equations 3.17 and 3.18 and substituting $V^{f,t} - 1$ for $V^{e,l}$, one can obtain an equation for the concentration of a volatile component in the initial aquifer fluid from discharge measurements, selection of phase segregation and initial aquifer conditions represented by:

$$m_s^{f,t} = m_s^{d,t} \cdot \left[V^{f,t} \left(1 - \frac{1}{[X^{e,v}(D_s^e - 1) + 1]} \right) + \frac{1}{[X^{e,v}(D_s^e - 1) + 1]} \right]^{-1} \quad [3.21]$$

An analysis similar to Equation 3.15 was performed using Equation 3.21 to examine the effect of

TABLE 6: Henry’s law constants and equations. Equations are valid in the range of 0-350°C at saturation pressure^a

Reaction	Log K (T in K)
$K_H: H_2S_g = H_2S_{aq}$	$\log K_{H_2S} = 24.229 + 837819/T^2 - 490.63/T - 9.836 \times 10^{-2}T - 900.43/T^{0.5} + 5.500 \times 10^{-5}T^2 + 17.610 \log T$
$K_H: H_{2,g} = H_{2,aq}$	$\log K_{H_2} = 10.650 + 768091/T^2 - 7651.7/T - 4.61 \times 10^{-2}T + 94.908/T^{0.5} + 3.336 \times 10^{-5}T^2 + 3.452 \log T$
$K_H: CO_{2,g} = CO_{2,aq}$	$\log K_{CO_2} = 17.135 + 726530/T^2 + 65.396/T - 6.964 \times 10^{-2}T - 731.5/T^{0.5} + 3.912 \times 10^{-5}T^2 + 13.190 \log T$

^a sources of thermodynamic data are as outlined by Arnórsson et al. (2010) and Karingithi et al. (2010).

assumed phase segregation pressure on calculated initial aquifer fluid gas (H_2S , H_2 and CO_2) concentration (Figure 21). From this figure, a conclusion that the calculated concentration of a gaseous component is quite sensitive to the assumed phase segregation pressure but not so for the selected T^f is made. Equations 3.19 and 3.21 assume that the volatile components are found in the liquid phase as a single species, whose solubility is described by the Henry's law constant. However, CO_2 and H_2S can exist as dissociated weak acids; thus, the magnitude of pH change between the initial aquifer fluid and the phase segregation pressure affects the distribution of these components.

Modelled initial aquifer fluid compositions

In practice WATCH 2.1 (Arnórsson et al., 1982 and Bjarnason, 1994) was used to infer the initial aquifer fluids. WATCH 2.1 is suited to handle geochemical data from wet-steam wells. The program reads the chemical analyses of water and gas samples collected at the wellhead then computes for the chemical composition at the selected reference temperature including pH, aqueous speciation, partial pressure of gases, redox potentials and activity products of mineral dissolution reactions. No mineral precipitation or dissolution is assumed as the fluid is modelled from the aquifer to the surface.

To model liquid enthalpy wells the analytical data were input into WATCH 2.1, excluding the measured discharge enthalpy then iterated the selected reference temperature until the total silica concentration in the liquid aquifer was consistent with T^f . The 1st step in modelling the excess enthalpy wells was done by inputting both analytical data and measured discharge enthalpy then choosing a reference temperature, in this case, T^e (equivalent to the selected segregation pressure, P^e). The output of WATCH 2.1 by this 1st step is picked up to become the input file of the 2nd step. When executing the 2nd step, no enthalpy will be input as it is calculated from the reference temperature, then iterating the input until the total silica concentration in the liquid aquifer is consistent with T^f . The modelled liquid enthalpy aquifers feeding the Námafjall wells as described by the above procedures are summarized in Table 7.

For comparison with Figures 20 and 21, the aquifer fluid concentrations of silica and the main gases (CO_2 , H_2S and H_2) at different assumed phase segregation pressures are calculated and shown for a few representative well discharges in Figures 22 and 23, respectively. Figure 22 shows the modelled initial aquifer SiO_2 concentration, in mg/kg, of the excess enthalpy wells, considering various selected phase segregation pressures. The computed gas concentrations in the deep liquid in log units as a function of phase segregation pressures are illustrated in Figure 23.

From Figure 23 it is evident that the calculated concentration of a gaseous component in the initial aquifer fluid is quite sensitive to the assumed phase segregation pressure, even at relatively low excess discharge enthalpies. The selected phase segregation pressure described in Section 3.3.3 are considered to be reasonable in light of consideration of the liquid saturation after boiling from T^f (given by pressure P^f) to P^e . It should be noted that the selected phase segregation pressure corresponds to residual liquid saturation of 0.2 which is an extreme limit for liquid immobility (see Section 3.3.3). In this case the pressures lower than the indicated P^e would be unlikely to select and the calculated values not representative in light of this discussion. Liquid saturation at the phase segregation pressure is fairly consistent; approximately the residual liquid saturation as shown by Corey curves (Figure 17). A slight extent of phase segregation may be expected to take place before the residual liquid saturation has been reached during depressurization boiling. In that case, the selected phase segregation pressure may overestimate the initial aquifer fluid gas concentrations.

TABLE 7: Composition of initial aquifer fluid for Námalfall wells

Well No.	Sample No.	Date	SP (bar-g)	h ^{dt} (kJ/kg)	T _{qz} (°C)	P ^c (bar-a)	pH ^b	Dissolved solids (mg/kg)											Dissolved gases (mmol/kg)					
								B	SiO ₂	Na	K	Mg	Ca	F	Cl	SO ₄	Al	Fe	CO ₂	H ₂ S	H ₂	CH ₄	N ₂	
BN-04	4036	Jun-99	3.70	983 ^a	245		6.98	0.76	435	147.5	15.9	0.008	3.79	0.63	32.9	29.5	0.55	0.064	11.77	8.31	7.26	0.404	0.518	
	1014	May-86	5.20	1019 ^a	233		7.19	0.63	396	127.1	18.4	0.000	2.78	0.56	39.6	18.4			5.64	5.52	3.72	0.986	0.620	
	1012	Mar-79	8.10	1033 ^a	245		6.97	0.00	435	125.7	20.1	0.000	2.14	0.61	19.9	19.3			11.36	8.99	11.64	1.681		
BN-09	4034*	Jun-07	11.8	1014 ^a	232		7.04	0.68	391	125.8	16.2	0.081	2.35	0.58	33.6	35.3	0.75	0.007	5.48	6.83	6.34	0.271	0.388	
	4008*	Apr-04	13.5	1060 ^a	255		7.05	0.67	469	118.7	15.5	0.009	2.10	0.62	31.3	61.1	0.79	0.005	8.30	8.66	9.19	0.351	0.510	
BJ-11	4033	May-03	19.0	1620	269	35.9	7.12	1.79	517	86.4	14.5	0.008	0.43	0.59	32.9	20.5	1.71	0.009	8.00	5.94	4.77	0.059	0.138	
	4059	Jul-98	23.5	1850	268	35.3	7.22	2.35	508	104.0	14.3	0.001	0.34	0.53	33.0	12.3		0.026	5.47	5.21	4.16	0.038	0.076	
	4035	Jul-97	23.1	1850	265	33.5	7.19	1.71	497	77.2	12.9	0.009	0.23	0.68	33.5	12.3		0.009	4.95	5.15	4.27	0.035	0.092	
	4013	May-95	14.5	1867	259	30.6	7.29	1.04	480	103.1	15.8	0.008	0.23	0.75	33.4	15.3		0.009	3.46	4.98	3.22	0.027	0.096	
	4024	May-94	19.0	1867	263	32.9	7.25		493	81.8	12.9	0.044	0.46	0.81	36.4	8.7		0.009	3.64	5.07	3.70	0.027	0.170	
	4022	May-93	19.9	1981	260	31.2	7.23		479	101.5	13.6	0.044	0.23	0.68	33.4	15.9		0.009	2.75	5.57	4.20	0.056	0.030	
	1034	Jun-85	14.7	2293	235	21.5	7.54	4.70	387	94.6	14.9	0.000	0.41	0.70	20.8	9.0	1.29		0.97	4.09	1.22	0.006	0.023	
	1022	May-83	16.2	2309	239	22.8	7.33		400	88.6	13.8	0.008	0.62	0.63	20.7	10.2			1.20	4.94	2.61	0.008	0.041	
	1050	Aug-81	18.0	2355	235	21.5	7.47		385	86.4	13.9	0.004	0.73	0.61	23.4	10.6			0.87	4.22	1.25	0.007		
	1024	Jun-80	11.0	2355	233	21.1	7.63		381	82.9	12.1	0.014	0.81	0.49	26.0	9.2			0.82	2.32	1.33	0.004	0.020	
BJ-12	4034	May-03	16.0	1813	264	33.5	6.98	2.89	495	107.9	18.7	0.008	0.51	0.44	85.3	11.1	0.51	0.009	7.37	6.92	6.07	0.049	0.074	
	4013	May-90	17.8	2127	264	34.1	7.22		491	131.4	18.2	0.037	0.44	0.53	67.9	21.5			4.68	6.33	5.96	0.068	0.173	
	4010	May-89	15.9	2138	272	38.4	7.32		514	118.8	17.5	0.149	0.39	0.51	30.4	25.6	0.083		4.13	7.38	6.44	0.046	0.139	
BJ-15	1033	Sep-87	19.6	2203	257	29.5	7.46		462	130.4	17.9	0.053	0.58	0.51	59.2	2.6			2.58	5.62	3.29	0.012	0.060	
	1021	May-83	17.0	2402	259	30.6	7.58		460	116.0	15.7	0.005	0.19	0.76	21.0	6.2			2.29	6.13	3.07	0.011	0.053	
	1038	Jul-81	20.2	2380	250	27.5	7.54		434	122.5	16.8	0.003	0.12	0.74	9.8	3.6			2.67	6.14	4.16	0.007	0.055	
1005	Mar-81	18.0	2321	262	31.2	7.77		476	123.2	15.7	0.016	0.33	0.75	41.5	5.3			0.66	4.68	0.75	0.001	0.009		
BJ-13	0551*	Sep-06	15.2	2021	293	52.5	7.74	0.16	589	87.7	17.2	0.004	0.85	0.62	60.6	19.9	1.68	0.015	1.49	3.04	1.92	0.004	0.170	
BJ-14	0311*	Jul-08	15.9	1807	295	50.0	7.56	0.77	595	184.2	38.1	0.003	0.88	0.79	200	15.0	1.17	0.007	1.81	8.11	4.18	0.064	0.721	
BJ-15	0343*	Aug-08	10.0	1169 ^a	229	6.80	6.80	0.72	382	143.7	15.7	0.001	1.16	1.25	45.4	24.2	1.22	0.003	7.38	7.01	9.67	0.396	0.987	

^a liquid enthalpy well samples, ^b pH at aquifer temperature T_{qz}, *sampled and analysed by ISOR, otherwise by Kemra Ltd and NEA.

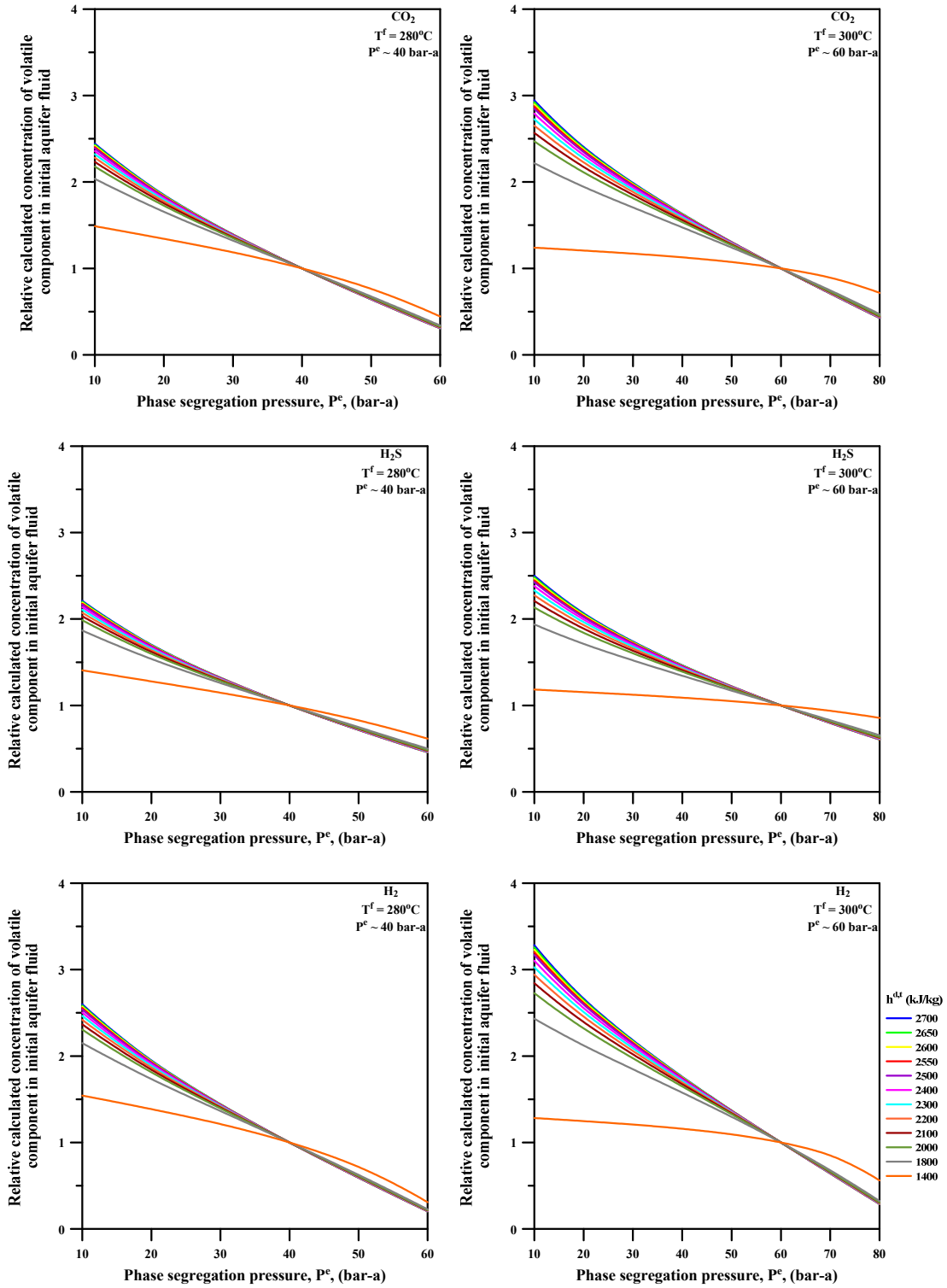


FIGURE 21: Relative calculated concentration of volatile components ($m_s^{f,t}$) in initial aquifer fluid at selected phase segregation pressures and calculated concentration at P^e when volume fraction of flowing vapor is $\sim 80\%$ (i.e. $S^{e,l} \sim 0.2$), for different $h^{d,t}$ (kJ/kg) and T^f ($^\circ\text{C}$). Aquifer fluid was assumed to have liquid enthalpy

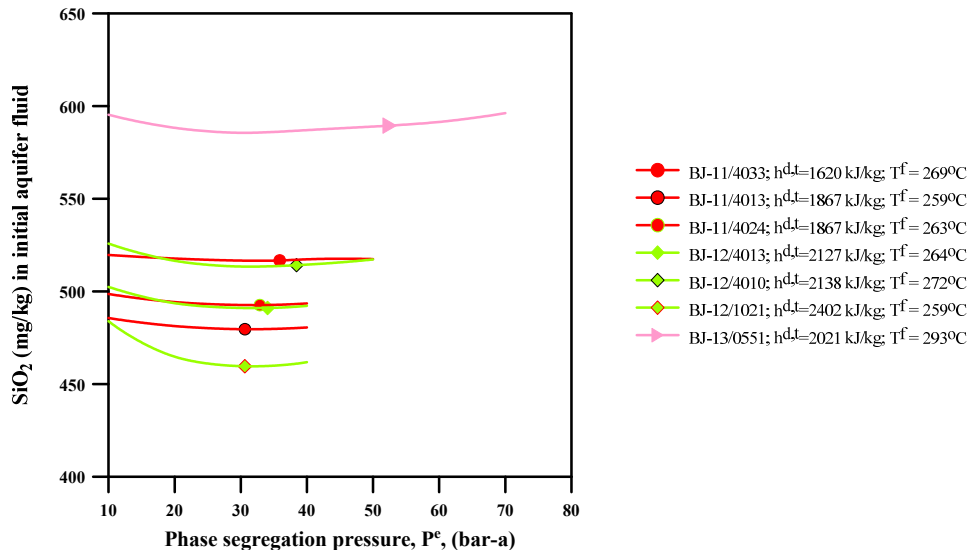


FIGURE 22: Calculated SiO_2 concentration of excess enthalpy wells, in the initial aquifer fluid, as a function of phase segregation pressure, assuming no aquifer vapour fraction. Markers designate the selected phase segregation pressures as indicated in Table 7

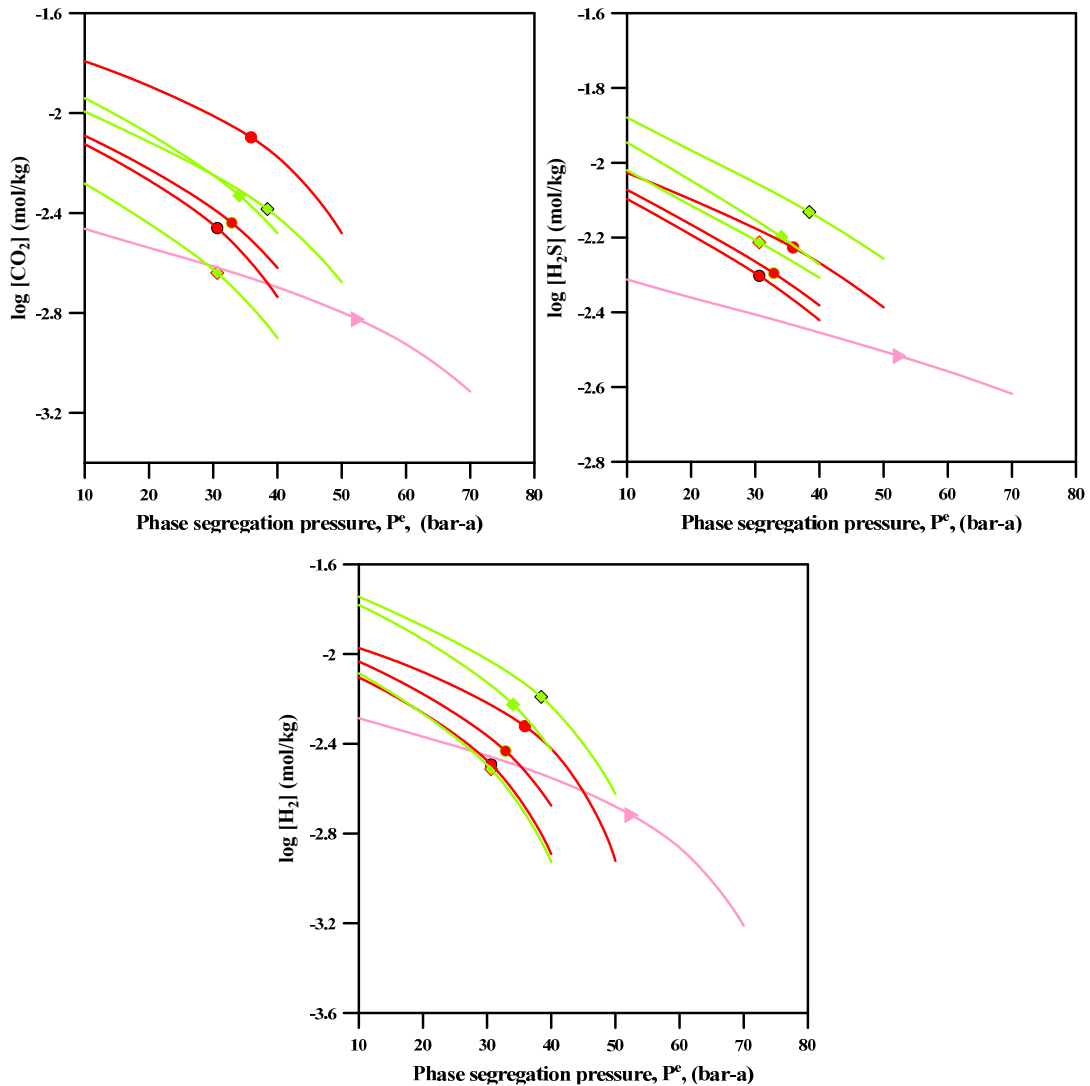


FIGURE 23: Calculated concentration of volatiles (CO_2 , H_2S and H_2) in the initial aquifer of excess enthalpy wells, as a function of phase segregation pressure, assuming no aquifer vapour fraction; symbology as in Figure 22

3.4 Equilibrium vapour fraction

In reservoirs where temperatures follow the boiling point curve with depth, some vapour may be present in the initial aquifer fluid. Vapour fraction obtained by chemical methods is termed equilibrium vapour fraction to distinguish from the physical vapour fraction. Published methods to calculate equilibrium vapour fractions vary based on the chemical reactions for which equilibria are assumed, either specific gas-gas (e.g. D'Amore and Celati, 1983, D'Amore and Truesdell, 1985) or mineral-gas (e.g. Arnórsson et al., 1990, Arnórsson et al., 2007) equilibria. The former methodology utilizes redox reactions for which systematic disequilibrium has been observed in Icelandic geothermal fluids (Stefánsson and Arnórsson, 2002). This method, in addition, assumes the total discharge chemical composition to be representative of the aquifer fluid, which is not true for well discharges that have undergone phase segregation. The primary advantage of mineral-gas equilibria to estimate initial vapour fractions is that chemical equilibrium between hydrothermal mineral assemblages and reactive gas concentrations in the aquifer liquid is generally assumed to be closely approached (Arnórsson and Gunnlaugsson, 1985).

The physical vapour fraction, $X^{f,v}$, in the initial aquifer fluid i.e. the fluid beyond the depressurization zone around wells, is given by an enthalpy conservation equation

$$X^{f,v} = \frac{h^{f,t} - h^{f,l}}{h^{f,v} - h^{f,l}} \quad [3.22]$$

where $X^{f,v}$ is the vapour fraction relative to the total aquifer fluid ($M^{f,v}/M^{f,t}$). $X^{f,v}$ can be derived from the individual H_2S and H_2 content of well discharges i.e. $X_{H_2S}^{f,v}$ and $X_{H_2}^{f,v}$ respectively, or a combination of the two ($X_{H_2S-H_2}^{f,v}$), by assuming chemical equilibrium between these gases in the aquifer liquid and specific hydrothermal mineral assemblages. CO_2 is often source rather than equilibrium controlled and therefore not used for calculation of equilibrium vapour fractions. H_2S and H_2 partition into the vapour phase as determined by Henry's constants and the total vapour pressure. $X^{f,v}$ calculated using H_2S only tends to be high due to high H_2S in total aquifer fluid. When $X_{H_2S}^{f,v}$ is higher than $X_{H_2}^{f,v}$ then the calculated $X_{H_2S-H_2}^{f,v}$ tends to be low and vice versa.

The basic equation that relates the vapour fraction in the initial aquifer fluid to the H_2S or H_2 concentration in the aquifer liquid and the total fluid is given by

$$m_s^{f,t} = m_s^{f,l} [X_s^{f,v} (D_s^f - 1) + 1] = m_s^{f,l} \left[\left(\frac{h^{f,t} - h^{f,l}}{h^{f,v} - h^{f,l}} \right) (D_s^f - 1) + 1 \right] \quad [3.23]$$

Subscript s stands for a volatile component, H_2S or H_2 , and m_s represents concentration (moles/kg) of the subscribed gases. The superscripts have the same meaning as given before. D_s^f is the distribution coefficient for gas s between vapour and liquid of the initial aquifer fluid at its temperature (T^f) and is given by Equation 3.20, of which K_H for the volatile components are calculated by equations given in Table 6.

Inserting Equation 3.23 into the volatile species conservation equation f given in Table 5 results in

$$\frac{M^{d,t}}{M^{f,t}} = \frac{m_s^{f,l}}{m_s^{d,t}} [X_s^{f,v} (D_s^f - 1) + 1] \quad [3.24]$$

Considering two gases, H_2S and H_2 , whose $m_s^{f,l}$ are fixed by equilibrium with mineral buffers (pyrite-pyrrhotite-prehnite-epidote), writing their equations like Equation 3.24 and solving them together for common $X^{f,v}$:

$$X_{H_2S-H_2}^{f,v} = \frac{A_{H_2S} - A_{H_2}}{\frac{55.51}{P_{tot}} \left[\frac{A_{H_2}}{K_{H_2S}} - \frac{A_{H_2S}}{K_{H_2}} \right] + A_{H_2S} - A_{H_2}} \quad [3.25]$$

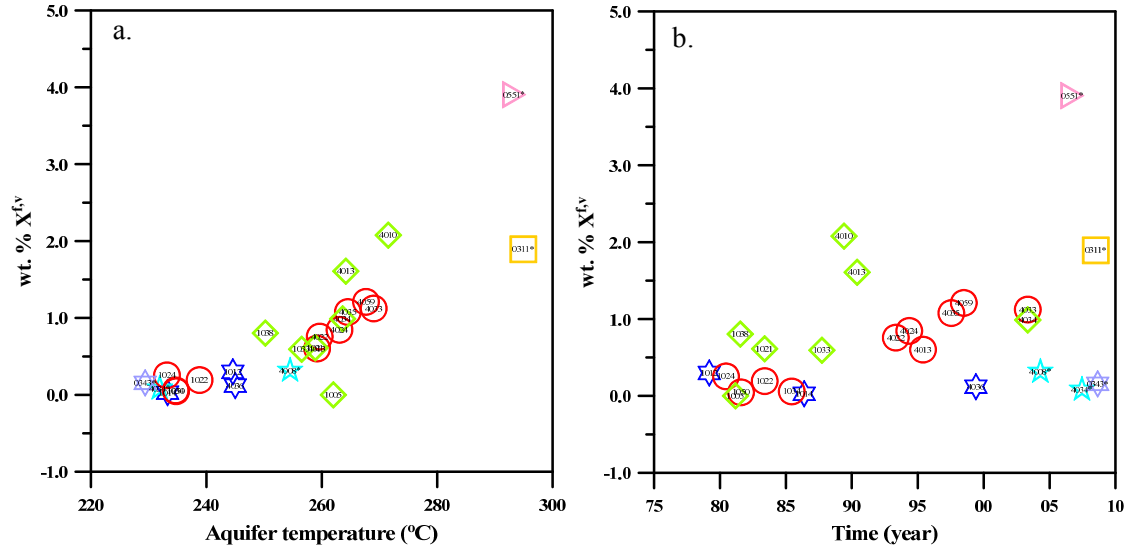


FIGURE 24: Calculated equilibrium vapour fractions ($X_{H_2S-H_2}^{f,v}$) for Námafjall wells as a function of: (a) aquifer temperature, and (b) time; symbology as in Figure 14

where $A_{H_2S} = m_{H_2S}^{d,t} / m_{H_2S}^{f,l}$ and $A_{H_2} = m_{H_2}^{d,t} / m_{H_2}^{f,l}$; $m_{H_2S}^{d,t}$ and $m_{H_2}^{d,t}$ are measured; $m_{H_2S}^{f,l}$ and $m_{H_2}^{f,l}$ are taken to be known functions of temperature, T^f ($^{\circ}C$), as are K_{H_2S} and K_{H_2} (Henry's law coefficients for H_2S and H_2 respectively). After deriving an equilibrium vapour fraction, $X^{f,v}$ (Table 8 and Figure 24) the total aquifer fluid enthalpy ($h^{f,t}$) is no longer equal to $h^{f,l}$, but can be solved using the relationship given by Equation 3.22. Albeit liquid enthalpy exhibited by some of the wells, $X^{f,v}$ values for these wells were also calculated, and a phase segregation pressure chosen in the same way as calculated for the 'excess' enthalpy wells.

From Figure 24a, it is evident that the calculated equilibrium vapour fractions are dependent on the initial aquifer fluid temperature and in turn to the assumed phase segregation pressure. Taking the wells with long production period, the equilibrium vapour fraction seems to be increasing over time (Table 8), but the increase is relatively small e.g. for well BJ-11 a wt. % $X_{H_2S-H_2}^{f,v}$ increase from 0.05 to 1.21 has been observed in the time period of about 20 years. An overestimation of the initial aquifer temperature by $\pm 10^{\circ}C$ would result in a relatively small overestimation or

TABLE 8: Calculated equilibrium vapour fractions for Námafjall wells

Well No.	Sample No	$h^{d,t}$ (kJ/kg)	T_{qtz} ($^{\circ}C$)	wt. % $X_{H_2}^{f,v}$	wt. % $X_{H_2S-H_2}^{f,v}$
BN-04	4036	983 ^a	245	1.85	0.12
	1014	1019 ^a	233	0.90	0.03
	1012	1033 ^a	245	3.05	0.30
BN-09	4034*	1014 ^a	232	1.61	0.08
	4008*	1060 ^a	255	2.37	0.31
BJ-11	4033	1620	269	1.07	1.12
	4059	1850	268	0.90	1.21
	4035	1850	265	0.95	1.08
	4013	1867	259	0.68	0.60
	4024	1867	263	0.79	0.85
	4022	1981	260	0.95	0.76
	1034	2293	235	0.22	0.06
	1022	2309	239	0.59	0.19
	1050	2355	235	0.23	0.05
	1024	2355	233	0.25	0.25
BJ-12	4034	1813	264	1.46	0.99
	4013	2127	264	1.43	1.61
	4010	2138	272	1.53	2.08
	1033	2203	257	0.71	0.59
	1021	2402	259	0.64	0.61
	1038	2380	250	0.98	0.80
1005	2321	262	-0.03	0.00	
BJ-13	0551*	2021	293	-0.02	3.90
BJ-14	0311*	1807	295	0.64	1.89
BJ-15	0343*	1169 ^a	229	2.51	0.16
Average:				1.05	0.79

^a liquid enthalpy well samples, *sampled and analysed by ÍSOR, otherwise by Kemia Ltd and NEA.

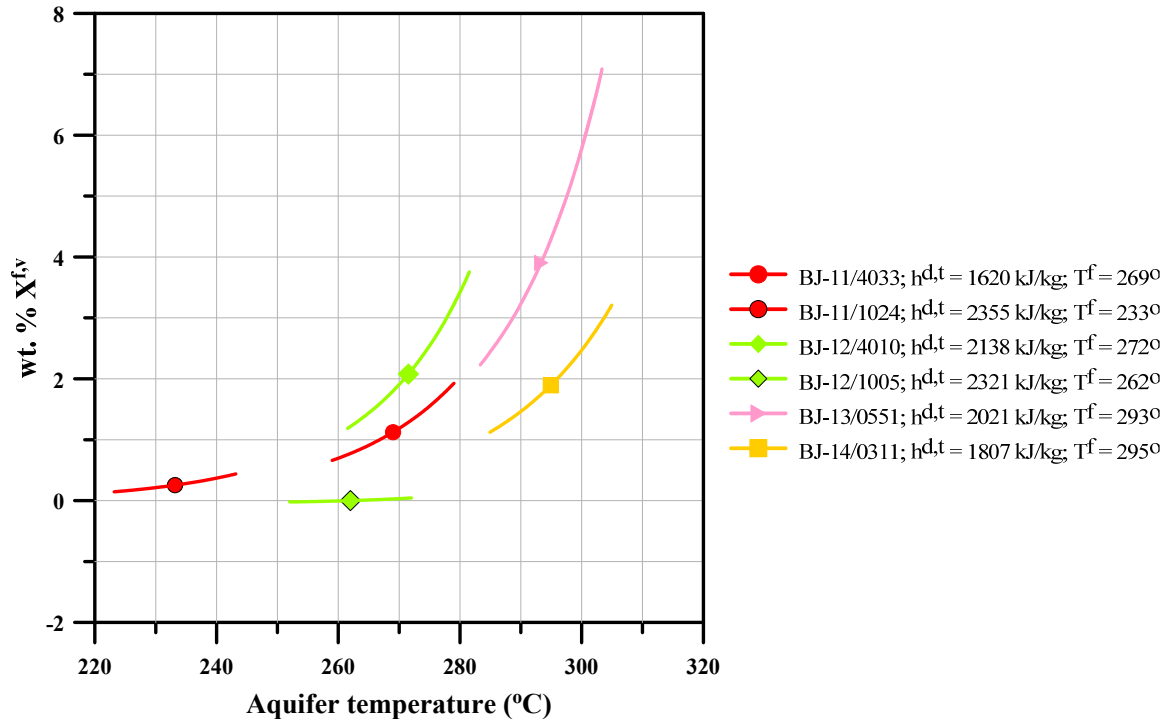


FIGURE 25: Calculated equilibrium vapour fractions, $X_{\text{H}_2\text{S}-\text{H}_2}^{\text{f},\text{v}}$ for representative Námafjall well discharges as a function of selected initial aquifer fluid temperature

underestimation of the equilibrium vapour fraction, $X^{\text{f},\text{v}}$ i.e. about $\pm 0.02 X_{\text{H}_2\text{S}-\text{H}_2}^{\text{f},\text{v}}$ units for the highest selected aquifer temperatures (Figure 25), but much less for the lower aquifer temperatures. This shows that there is substantial uncertainty in calculated equilibrium vapour fractions, and that the calculated equilibrium vapour fractions for ‘excess’ enthalpy well discharges should be interpreted as order-of-magnitude, rather than absolute, indicators. To model the aquifer fluid composition taking into consideration the equilibrium vapour fraction, for the liquid enthalpy wells, the calculated $h^{\text{f},\text{t}}$ was input in the WATCH program together with the analytical data, and then iterated the selected reference temperature until the total silica concentration in the liquid aquifer was consistent with T^{f} . For the ‘excess’ enthalpy wells, the $h^{\text{f},\text{t}}$ value obtained by using Equation 3.22 was inserted into WATCH during the 2nd step of the procedure for modelling ‘excess’ enthalpy wells. Consequently, the concentrations of all components will be calculated by WATCH, both in the liquid and vapour phases of the initial aquifer at the assumed reference temperature (T^{f}), for the liquid and excess enthalpy wells. Modeled initial aquifer fluid compositions considering the derived equilibrium vapour fractions $X_{\text{H}_2\text{S}-\text{H}_2}^{\text{f},\text{v}}$ are shown in Table 9. Since ‘excess’ enthalpy is attributed to phase segregation, a derived $X^{\text{f},\text{v}}$ is meaningful if the corresponding $V^{\text{e},\text{l}}$ value is positive. Using Equations 3.10 and 3.11, $V^{\text{f},\text{t}}$ and thus $V^{\text{e},\text{l}}$ values are calculated for each sample and presented in Table 9.

TABLE 9: Composition of initial aquifer liquid taking into account the presence of equilibrium vapor fraction in the initial aquifer fluid

Well No.	Sample No.	Date	SP (bar-g)	h ^{u,t} (kJ/kg)	T _{qtz} (°C)	P ^e (bar-a)	X ^{f,v}	wt. %	pH ^b	Dissolved solids (mg/kg)											Dissolved gases (mmol/kg)		
										B	SiO ₂	Na	K	Mg	Ca	F	Cl	SO ₄	Al	Fe	CO ₂	CH ₄	N ₂
BN-04	4036	Jun-99	3.70	983 ^a	245	25.0	0.12	-0.79	7.04	0.76	435	147	15.9	0.008	3.79	0.63	32.9	29.5	0.55	0.064	10.01	0.15	0.22
	1014	May-86	5.20	1019 ^a	233	20.6	0.03	0.14	7.24	0.63	396	127	18.4	0.000	2.78	0.56	39.6	18.4			5.05	0.39	0.28
	1012	Mar-79	8.10	1033 ^a	245	25.0	0.30	-0.31	7.05	0.00	435	126	20.1	0.000	2.14	0.61	19.9	19.3			9.12	0.51	
BN-09	4034*	Jun-07	11.8	1014 ^a	232	20.6	0.08	0.16	7.08	0.68	391	126	16.2	0.081	2.35	0.58	33.6	35.3	0.75	0.007	4.94	0.12	0.19
	4008*	Apr-04	13.5	1060 ^a	255	28.5	0.31	-0.45	7.10	0.67	469	119	15.5	0.009	2.10	0.62	31.3	61.1	0.79	0.005	7.12	0.14	0.24
BJ-11	4033	May-03	19.0	1620	269	35.9	1.12	2.98	7.27	1.79	517	86.4	14.5	0.008	0.43	0.59	32.9	20.5	1.71	0.009	4.79	0.009	0.025
	4059	Jul-98	23.5	1850	268	35.3	1.21	4.66	7.35	2.35	508	104	14.3	0.001	0.34	0.53	33.0	12.3		0.026	3.32	0.006	0.014
	4035	Jul-97	23.1	1850	265	33.5	1.08	4.91	7.32	1.71	497	77.2	12.9	0.009	0.23	0.68	33.5	12.3		0.009	3.11	0.006	0.017
	4013	May-95	14.5	1867	259	30.6	0.60	5.72	7.39	1.04	480	103	15.8	0.008	0.23	0.75	33.4	15.3		0.009	2.39	0.004	0.020
	4024	May-94	19.0	1867	263	32.9	0.85	5.35	7.36	4.93	81.8	12.9	0.044	0.46	0.81	36.4	8.7		0.009	2.35	0.004	0.032	
	4022	May-93	19.9	1981	260	31.2	0.76	6.57	7.32	4.79	102	13.6	0.044	0.23	0.68	33.4	15.9		0.009	1.87	0.009	0.006	
	1034	Jun-85	14.7	2293	235	21.5	0.06	14.5	7.54	4.7	387	94.6	14.9	0.000	0.41	0.70	20.8	9.0	1.29		0.97	0.006	0.023
	1022	May-83	16.2	2309	239	22.8	0.19	13.2	7.35	400	88.6	13.8	0.008	0.62	0.63	20.7	10.2			1.07	0.003	0.018	
	1050	Aug-81	18.0	2355	235	21.5	0.05	15.2	7.47	385	86.4	13.9	0.004	0.73	0.61	23.4	10.6			0.87	0.007		
	1024	Jun-80	11.0	2355	233	21.1	0.25	15.1	7.68	381	82.9	12.1	0.014	0.81	0.49	26.0	9.2			0.69	0.001	0.004	
BJ-12	4034	May-03	16.0	1813	264	33.5	0.99	4.89	7.11	2.89	495	108	18.7	0.008	0.51	0.44	85.3	11.1	0.51	0.009	4.53	0.008	0.014
	4013	May-90	17.8	2127	264	34.1	1.61	6.76	7.39	491	131	18.2	0.037	0.44	0.53	67.9	21.5			2.45	0.007	0.021	
	4010	May-89	15.9	2138	272	38.4	2.08	6.08	7.46	514	119	17.5	0.149	0.39	0.51	30.4	25.6		0.083	2.19	0.005	0.018	
BJ-13	1033	Sep-87	19.6	2203	257	29.5	0.59	8.7	7.53	462	130	17.9	0.053	0.58	0.51	59.2	2.6			1.99	0.003	0.015	
	1021	May-83	17.0	2402	259	30.6	0.61	10.0	7.65	460	116	15.7	0.005	0.19	0.76	21.0	6.2			1.78	0.002	0.013	
	1038	Jul-81	20.2	2380	250	27.5	0.80	11.1	7.66	434	123	16.8	0.003	0.12	0.74	9.8	3.6			1.81	0.001	0.008	
1005	Mar-81	18.0	2321	262	31.2	0.00	9.3	7.77	476	123	15.7	0.016	0.33	0.75	41.5	5.3			0.66	0.001	0.009		
BJ-13	0551*	Sep-06	15.2	2021	293	52.5	3.90	3.37	7.83	0.16	589	87.7	17.2	0.004	0.85	0.62	60.6	19.9	1.68	0.015	0.80	0.001	0.023
BJ-14	0311*	Jul-08	15.9	1807	295	50.0	1.89	2.45	7.63	0.77	595	184	38.1	0.003	0.88	0.79	200	15.0	1.17	0.007	1.16	0.011	0.159
BJ-15	0343*	Aug-08	10.0	1169 ^a	229	19.8	0.16	2.15	6.92	0.72	382	144	15.7	0.001	1.16	1.25	45.4	24.2	1.22	0.003	5.15	0.07	0.21

^a liquid enthalpy well samples, ^b pH at aquifer temperature T_{qtz}. *sampled and analysed by ISOR, otherwise by Kernia Ltd and NEA.

4. MINERAL-GAS-LIQUID EQUILIBRIA

Appraisal of the chemical evolution of hydrothermal fluids and of the extent to which the fluids have approached equilibrium according to certain chemical reactions is based on the concept of local equilibrium within the larger open geothermal system, analytical data on the composition of well discharges, modelling of aquifer fluid compositions and thermodynamic data on gases, aqueous species and minerals. An emphasis on the underlying assumptions and simplifications before interpreting the equilibrium state of the aquifer fluid at Námafjall is that: the samples collected at the wellhead are taken to represent the deep aquifers feeding the well and no dissolution or precipitation reactions occur between the initial aquifer fluids and wellhead, and that the selection of T^f , is reasonable. In addition, aqueous speciation distribution of the aquifer fluid uses thermodynamic databases that carry uncertainties. Assuming the concept of local equilibrium within the larger open geothermal system allows the application of thermodynamic principles to assess how closely local equilibrium conditions are approached based on the geochemical data of the modelled aquifers.

4.1 Alteration mineralogy and thermodynamic data

Alteration mineralogy in the high-temperature geothermal systems in Iceland has been summarized by Arnórsson (1995). All Icelandic geothermal fields show a zonation with depth reflecting the temperature stability range of the minerals within the system. Calcite is stable but disappears at temperatures above $\sim 280^\circ\text{C}$ and pyrite is stable over the whole range of temperature. Chalcedony is stable up to $\sim 180^\circ\text{C}$ but above that temperature quartz is the dominant silica polymorph. Prehnite appears above 200°C and epidote at slightly higher temperature (Hreggvidsdóttir, 1987; Lonker et al., 1993). Albite is common, especially at temperatures above 150°C , whereas K-feldspar (adularia) is scarce, due to the low K content of the host rocks. Hydrothermal sheet silicates are represented by smectite interstratified with chlorite above 200°C , and above $230\text{-}240^\circ\text{C}$ discrete chlorite is formed. Garnet, represented by the grossular-andradite solid solution is widely present in high saline fluids (Lonker et al., 1993; Giroud, 2008). Magnetite is mostly present as a primary mineral but is generally unstable in high-temperature geothermal systems.

Gudmundsson and Arnórsson (2005), Isabirye (1994) and Kristmannsdóttir (1978) have studied the alteration minerals in the Námafjall geothermal system and indicate the occurrence of albite, calcite, chlorite, epidote, K-feldspar (adularia), prehnite, pyrite, pyrrhotite, quartz and wairakite. Garnet has been reported as a mineral formed by contact metamorphism. Its presence is considered to be the consequence of extensive boiling of the aquifer water in response to intrusion of magma forming small intrusive bodies within the geothermal system. Námafjall waters are under-saturated with respect to anhydrite and Gudmundsson and Arnórsson (2005) conclude that the stability of anhydrite is considered to be linked with that of epidote. Frauke et al., 2008 studied CO_2 fixation by calcite in the Icelandic high-temperature fields and concluded that vast amounts of CO_2 and thus calcite is distributed in the upper 1km of the three fields considered.

The thermodynamic database selected for this study plays an essential role for both the speciation calculations performed by WATCH 2.1 and to interpret the saturation state of the aquifer with respect to different mineral-fluid reactions that could potentially control the composition of aquifer fluids. The saturation state of the aquifer liquid is assessed for hydrothermal alteration minerals, and several potential mineral pair and assemblages evaluated for their potential to control selected activity ratios and gas species concentrations in the initial aquifer fluid. The thermodynamic data base used for speciation calculations is that depicted in Arnórsson et al. (1982) with slight modifications. The reactions considered and equations describing the temperature dependence of their equilibrium constants are shown in Tables 10 and 11, for the mineral pairs or assemblages and the individual alteration minerals, respectively.

Equilibrium constants for the reactions given in Tables 10 and 11 are based on thermodynamic data ($\Delta G_f^\circ, S^\circ, V^\circ, C_p^\circ$) of the minerals from Holland and Powell (1998) except for pyrite, pyrrhotite and calcite. Data on the sulfide minerals were taken from Robie and Hemingway (1995) and calcite

TABLE 10. Temperature equations for equilibrium constants for individual mineral dissolution reactions. Valid in the range 0-350°C at P_{sat} . Unit activity was selected for all minerals and liquid water ^a

Mineral	Symbol	Dissolution reaction	Log K (T in K)
1.	Andradite and	$Ca_3Fe_2Si_3O_{12} + 4H^+ + 8H_2O_{(l)} = 3Ca^{+2} + 2Fe(OH)_4^- + 3H_4SiO_4^0$	$+940.225 - 15419.3/T + 0.58092T - 2.971X10^{-4}T^2 - 421.727\log T$
2.	Anhydrite* anh	$CaSO_4 = Ca^{+2} + SO_4^{2-}$	$+78.414 - 3247.2/T - 9.03X10^{-7}T^2 - 28.723\log T$
3.	Calcite cal	$CaCO_3 + 2H^+ = Ca^{+2} + H_2O_{(l)} + CO_{2(aq)}$	$-68.271 + 4385.24/T - 7.525x10^{-3}T + 25.856\log T$
4.	Clinozoisite czo	$Ca_2Al_3Si_3O_{12}(OH) + 12H_2O_{(l)} = 2Ca^{+2} + 3Al(OH)_4^- + 3H_4SiO_4^0 + OH^-$	$+36.052 - 6854.78/T + 0.13236T - 1.3749X10^{-4}T^2 + 33.508\log T$
5.	Epidote epi	$Al_2FeSi_3O_{12}(OH) + 12H_2O_{(l)} = 2Ca^{+2} + Fe(OH)_4^- + 2Al(OH)_4^- + 3H_4SiO_4^0 + OH^-$	$+893.547 - 27077.4/T + 0.154124T - 3.022x10^{-4}T^2 - 398.38\log T$
6.	Grossular gro	$Ca_3Al_2Si_3O_{12} + 4H^+ + 8H_2O_{(l)} = 3Ca^{+2} + 2Al(OH)_4^- + 3H_4SiO_4^0$	$-571.662 + 17623.7/T - 0.14343T - 203.808\log T$
7.	Magnetite mag	$Fe_3O_4 + 4H_2O_{(l)} = Fe^{+2} + 2Fe(OH)_4^-$	$+949.951 - 24258.2/T + 0.51474T - 2.402x10^{-4}T^2 - 417.136\log T$
8.	Prehnite pre	$Ca_2Al_2Si_3O_{10}(OH)_2 + 10H_2O_{(l)} = 2Ca^{+2} + 2Al(OH)_4^- + 3H_4SiO_4^0 + OH^-$	$+833.95 - 25642.8/T + 0.5035T - 2.941x10^{-4}T^2 - 369.297\log T$
9.	Pyrite pyr	$FeS_2 + 2H^+ + H_{2(aq)} = Fe^{+2} + 2H_2S^0_{(l)}$	$-1.397 - 461.3/T - 9.128x10^{-4}T + 1.626\log T$
10.	Pyrrhotite pyrr	$FeS + 2H^+ = Fe^{+2} + H_2S_{(aq)}$	$-3.043 + 1579.06/T - 1.987x10^{-3}T + 0.12\log T$
11.	Quartz qtz	$SiO_2 + 2H_2O_{(l)} = H_4SiO_4^0$	$-34.188 + 197.47/T - 5.851x10^{-6}T^2 + 12.245\log T$
12.	Wollastonite wol	$CaSiO_3 + H_2O_{(l)} + 2H^+ = Ca^{+2} + H_4SiO_4^0$	$-127.096 + 8151.38/T - 2.981x10^{-2}T + 49.282\log T$

^a sources of thermodynamic data are as outlined by Armórrsson and Stefánsson (1999) and Karingithi et al. (2010), * from Gudmundsson and Armórrsson (2005).

TABLE 11: Mineral pair and mineral assemblage reactions that may control activity ratios and gas concentrations in solution, and equations describing temperature dependence of equilibrium constant. Equations are valid in the range of 0-350°C at saturation pressure. Unit activity was selected for all minerals and liquid water^a

Reaction	Log K (T in K)
1. $\text{Ca}^{+2}/(\text{H}^+)^2$: $\frac{3}{2}\text{pre} + 2\text{H}^+ = \text{czo} + \frac{3}{2}\text{qtz} + 2\text{H}_2\text{O}_1 + \text{Ca}^{+2}$	$\log[\text{Ca}^{+2}/(\text{H}^+)^2] = 2.643 + 335608/\text{T}^2 + 1550.1/\text{T} + 6.563 \times 10^{-4}\text{T} - 6.123 \times 10^{-6}\text{T}^2 + 0.870 \log\text{T}$
2. $\text{Ca}^{+2}/(\text{H}^+)^2$: $\text{wol} + 2\text{H}^+ = \text{qtz} + \text{H}_2\text{O}_1 + \text{Ca}^{+2}$	$\log[\text{Ca}^{+2}/(\text{H}^+)^2] = 3.047 + 302461/\text{T}^2 + 3088.8/\text{T} - 4.542 \times 10^{-3}\text{T} - 2.571 \times 10^{-6}\text{T}^2 + 0.748 \log\text{T}$
3. $\text{Fe}(\text{OH})_4^-/\text{OH}^-$: $\text{epi} + \text{OH}^- + 2\text{H}_2\text{O}_1 = \text{pre} + \text{Fe}(\text{OH})_4^-$	$\log[\text{Fe}(\text{OH})_4^-/\text{OH}^-] = -2.786 + 132357/\text{T}^2 - 1144.9/\text{T} + 2.26 \times 10^{-4}\text{T} + 8.115 \times 10^{-6}\text{T}^2 - 0.933 \log\text{T}$
4. $\text{Fe}(\text{OH})_4^-/\text{OH}^-$: $\text{epi} + \text{wol} + \text{OH}^- + \text{H}_2\text{O}_1 = \text{qtz} + \text{gro} + \text{Fe}(\text{OH})_4^-$	$\log[\text{Fe}(\text{OH})_4^-/\text{OH}^-] = -2.935 + 177922/\text{T}^2 - 1210.84/\text{T} + 4.109 \times 10^{-4}\text{T} + 8.970 \times 10^{-6}\text{T}^2 - 0.978 \log\text{T}$
5. $\text{Fe}(\text{OH})_4^-/\text{OH}^-$: $\frac{1}{2}\text{hem} + \frac{3}{5}\text{H}_2\text{O}_1 + \text{OH}^- = \text{Fe}(\text{OH})_4^-$	$\log[\text{Fe}(\text{OH})_4^-/\text{OH}^-] = -2.675 + 127537/\text{T}^2 - 1494.6/\text{T} + 2.0402 \times 10^{-3}\text{T} + 7.393 \times 10^{-6}\text{T}^2 - 0.817 \log\text{T}$
6. $\text{Fe}(\text{OH})_4^-/\text{OH}^-$: $\frac{1}{2}\text{mag} + \frac{3}{5}\text{H}_2\text{O}_1 + \text{OH}^- = \text{Fe}(\text{OH})_4^- + \frac{1}{6}\text{H}_{2,\text{aq}}$	$\log[\text{Fe}(\text{OH})_4^-/\text{OH}^-] = -1.452 + 21398.6/\text{T}^2 - 671.80/\text{T} - 8.861 \times 10^{-5}\text{T} + 5.453 \times 10^{-6}\text{T}^2 - 0.486 \log\text{T}$
7. $\text{H}_2\text{S}_{\text{aq}}/(\text{H}_{2,\text{aq}})^3$: $\frac{1}{2}\text{pyr} + \frac{1}{3}\text{H}_{2,\text{aq}} + \frac{2}{3}\text{H}_2\text{O}_1 = \frac{1}{6}\text{mag} + \text{H}_2\text{S}_{\text{aq}}$	$\log\left[\frac{\text{H}_2\text{S}_{\text{aq}}}{(\text{H}_{2,\text{aq}})^3}\right] = 12.225 + 500528/\text{T}^2 - 7771.49/\text{T} - 3.8468 \times 10^{-2}\text{T} + 2.424 \times 10^{-5}\text{T}^2 + 4.546 \log\text{T}$
8. $\text{H}_2\text{S}_{\text{aq}}/\text{H}_{2,\text{aq}}$: $\text{pyr} + \text{H}_{2,\text{aq}} = \text{pyrr} + \text{H}_2\text{S}_{\text{aq}}$	$\log[\text{H}_2\text{S}_{\text{aq}}/\text{H}_{2,\text{aq}}] = 0.549 - 124186/\text{T}^2 - 972.2/\text{T} + 3.6744 \times 10^{-3}\text{T} - 3.227 \times 10^{-6}\text{T}^2 + 0.383 \log\text{T}$
9. H_2S : $\frac{1}{3}\text{pyr} + \frac{2}{3}\text{pyrr} + \frac{2}{3}\text{pre} + \frac{2}{3}\text{H}_2\text{O}_1 = \frac{2}{3}\text{epi} + \text{H}_2\text{S}_{\text{aq}}$	$\log[\text{H}_2\text{S}] = 13.608 + 592324/\text{T}^2 - 9346.7/\text{T} - 4.3552 \times 10^{-2}\text{T} + 2.9164 \times 10^{-5}\text{T}^2 + 5.139 \log\text{T}$
10. H_2S : $\frac{1}{4}\text{pyr} + \frac{1}{2}\text{pyrr} + \text{H}_2\text{O}_1 = \frac{1}{4}\text{mag} + \text{H}_2\text{S}_{\text{aq}}$	$\log[\text{H}_2\text{S}] = 13.589 + 590215/\text{T}^2 - 9024.5/\text{T} - 4.4882 \times 10^{-2}\text{T} + 2.978 \times 10^{-5}\text{T}^2 + 5.068 \log\text{T}$
11. H_2 : $\frac{4}{3}\text{pyrr} + \frac{2}{3}\text{pre} + \frac{2}{3}\text{H}_2\text{O}_1 = \frac{2}{3}\text{epi} + \frac{2}{3}\text{pyr} + \text{H}_{2,\text{aq}}$	$\log[\text{H}_2] = -1.640 - 124524/\text{T}^2 - 777.19/\text{T} - 5.501 \times 10^{-4}\text{T} + 7.756 \times 10^{-6}\text{T}^2 - 0.565 \log\text{T}$
12. H_2 : $\frac{2}{3}\text{pyrr} + \text{H}_2\text{O}_1 = \frac{3}{4}\text{pyr} + \frac{1}{4}\text{mag} + \text{H}_{2,\text{aq}}$	$\log[\text{H}_2] = -1.654 - 95456.8/\text{T}^2 - 621.84/\text{T} - 1.257 \times 10^{-3}\text{T} + 7.569 \times 10^{-6}\text{T}^2 - 0.600 \log\text{T}$
13. CO_2 : $\text{czo} + \text{cal} + \frac{3}{2}\text{qtz} + \text{H}_2\text{O}_1 = \frac{3}{2}\text{pre} + \text{CO}_{2,\text{aq}}$	$\log[\text{CO}_2] = -0.890 + 7251.5/\text{T}^2 - 1710.6/\text{T} + 4.188 \times 10^{-3}\text{T} + 2.683 \times 10^{-6}\text{T}^2 - 0.064 \log\text{T}$

^a sources of thermodynamic data are as outlined by Arnórsson et al. (2010) and Karingithi et al. (2010).

solubility constants from Arnórsson et al. (1982). The thermodynamic properties of the aqueous species and liquid water entering the reactions were taken from various sources; data on $\text{H}_4\text{SiO}_4^\circ$ are from Gunnarsson and Arnórsson (2000), those on H_2O_l , Ca^{+2} , Fe^{+2} , and OH^- are from SUPCRT92 (Johnson et al., 1992) using the slop98.dat data set and those on $\text{Fe}(\text{OH})_4^-$ and $\text{Al}(\text{OH})_4^-$ are from Diakonov et al. (1999) and Pokrovskii and Helgeson (1995), respectively. The properties for $\text{CO}_{2,\text{aq}}$, $\text{H}_2\text{S}_{\text{aq}}$ and $\text{H}_{2,\text{aq}}$ were retrieved from the gas solubility constants in pure water as given by Fernandez-Prini et al. (2003) and the thermodynamic properties as given in Robie and Hemingway (1995) assuming ideal behaviour. Henry's Law coefficients, K_s (moles per kg-bar), as a function of temperature for the different gases are as presented in Table 6. The Henry's Law coefficients were also used to calculate the distribution coefficients, D_s , and equilibrium vapour fractions, $X^{f,v}$, in the initial aquifer fluids as discussed in the previous chapter.

A few points reiterated here concerning the sources of thermodynamic data as noted in Tables 10 and 11 are that: the equations assume unit activity (a_i) of all minerals and liquid water. However, when the log K curves are plotted, the equations are modified to account for the activities of end-members of minerals that form solid solutions (i.e. epidote, garnet, and prehnite). Activities of end members in solid solution used here are analogous to those used by Giroud (2008), retrieved from their analyzed composition assuming ideal behaviour. The composition of epidote, expressed as X_{ps} , the mole fraction of pistacite ($\text{Ca}_2\text{Fe}_3\text{Si}_3\text{O}_{12}\text{OH}$), is in the range 0.18-0.32 (Bird and Spieler, 2004) and 0.24-0.41 (Sveinbjörnsdóttir, 1992), respectively. This gives an average epidote end-member ($\text{Ca}_2\text{FeAl}_2\text{Si}_3\text{O}_{12}\text{OH}$), activity of 0.7 and a corresponding clinozoisite activity of 0.3. In prehnite ($\text{Ca}_2\text{Al}(\text{Al}, \text{Fe})\text{Si}_3\text{O}_{10}(\text{OH})_2$), Al-Fe substitution occurs on one site and the activity, assuming ideal behaviour, is proportional to the ratio of Fe to one Al. The selected activity for prehnite is equal to 0.9 (Hreggvidsdóttir, 1987). For garnet (grossular-andradite, $\text{Ca}_3(\text{Al}, \text{Fe})\text{Si}_3\text{O}_{12}$), from the average X_{Al} in grossular and X_{Fe} in andradite, activities of 0.2 and 0.3 are obtained for the grossular and andradite end members, respectively, assuming ideal solid-solution (Lonker et al., 1993). Water and the other minerals are considered to be pure (calcite, magnetite, pyrite, pyrrhotite, quartz, and wollastonite), their activities are taken as 1. For instance, considering Equation 13 in Table 11:

$$\log K = \frac{3}{2} \log a_{\text{pre}} + \log[\text{CO}_{2,\text{aq}}] - \log a_{\text{czo}} - \log a_{\text{cal}} - \frac{3}{2} \log a_{\text{qtz}} - \log[\text{H}_2\text{O}_l] \quad [4.1]$$

To determine the equilibrium concentration of aqueous CO_2 in the initial aquifer, Equation 4.1 is reduced to:

$$\log [\text{CO}_{2,\text{aq}}] = \log K + \log a_{\text{czo}} - \frac{3}{2} \log a_{\text{pre}} \quad [4.2]$$

The equilibrium constants for the dissolution reactions listed in Table 10 have been used to evaluate the state of equilibrium of the hydrothermal solutions with respect to individual minerals. In the next sections, focus on the individual minerals that comprise the most likely assemblages that buffer the concentrations of the reactive gases (CO_2 , H_2S and H_2) in Námafjall: calcite, epidote-clinozoisite, wollastonite, pyrrhotite, pyrite and magnetite are undertaken. The temperature equations of the equilibrium constants of the dissolution reactions in Table 10 were cited from various authors as indicated.

4.2 Mineral-gas equilibria

Various mineral assemblages control equilibrium of reactive gases in aquifers. Equilibrium concentrations of gases predicted by different possible mineral buffers fall within a narrow range, even within the range of uncertainty inherent in the process of fluid sampling and analysis, and are considered one of the difficulties in making the determination of which mineral assemblages are involved. In addition, different mineral assemblages have been identified to control reactive gas concentrations in geothermal fields of different geological settings (e.g. Angcoy, 2010; Giroud, 2008; Karingithi et al., 2010; Scott, 2011). Epidote and prehnite or pyrite, pyrrhotite and magnetite assemblages have been suspected to control reactive gas concentrations in Icelandic geothermal field

containing dilute geothermal fluids, of which Námafjall is considered to be. However, for the Icelandic geothermal fields with saline aquifer fluids, a mineral assemblage of grossular-quartz-calcite-clinozoisite-wollastonite has been found to control reactive gas concentrations (Arnórsson et al., 2010; Giroud, 2008; Scott 2011). A prominent feature of the mineral assemblage-gas diagrams is that the equilibrium constants for the reactions that could potentially control H_2S and H_2 , i.e. those which either include prehnite or magnetite in addition to the sulphide minerals (reactions nos. 9 and 10 for H_2S and nos. 11 and 12 for H_2 , Table 11), are very similar for the selected mineral compositions in the temperature range of the aquifer fluids, 200-300°C (<0.28 log K units).

4.2.1 H_2S and H_2

The concentration of H_2S and H_2 in the initial aquifer fluid of Námafjall wells in relation to equilibrium with selected mineral assemblages is depicted in Figures 26 and 27, respectively. The data points for both gases lie above the respective mineral-gas equilibrium curves. This indicates that the

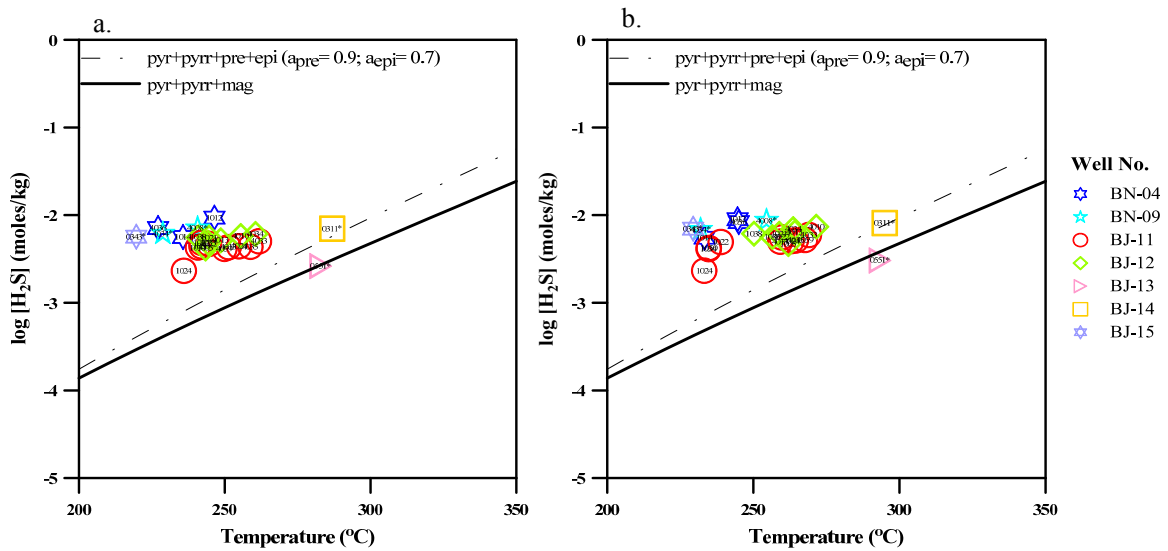


FIGURE 26: Potential mineral buffers controlling H_2S gas concentrations in the initial aquifer fluid of Námafjall wells using (a) the average of $T_{Na/K}$ and T_{Qtz} to represent T^f , and (b) T_{Qtz} only; numbers in the symbols indicate the sample number

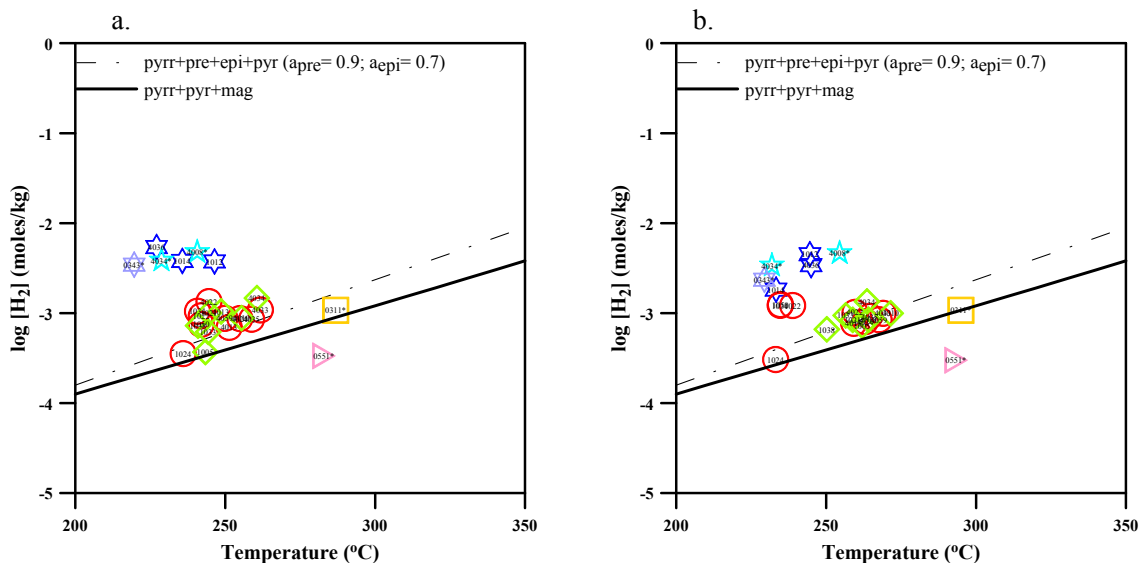


FIGURE 27: Potential mineral buffers controlling H_2 gas concentrations in the initial aquifer fluid of Námafjall wells using (a) the average of $T_{Na/K}$ and T_{Qtz} to represent T^f , and (b) T_{Qtz} only; symbology as in Figure 26

initial aquifer fluid contains some vapour. Alternatively, the calculated aquifer fluid H_2S and H_2 concentrations are truly in excess of equilibrium. Shallower aquifer are higher in H_2S and H_2 and also seen in the other gases CO_2 and N_2 , indicating that gaseous steam from deeper aquifers has condensed in the shallower ones signifying that they are, at least partly, steam-heated. The selection of T^f has some effect on how much individual data points lie above the equilibrium curves.

It is known that the Na-K geothermometer typically yields significantly lower temperatures than the quartz geothermometers for wet steam wells in Iceland. The reason is likely the faulty calibration of the former geothermometer or partial re-equilibration in the depressurization zone around discharging wells (Gudmundsson and Arnórsson, 2002). Thus the use of the two selected T^f to compare the use of selected aquifer temperature to the effect of calculated gas concentrations in the initial aquifer fluid.

4.2.2 CO_2

Figure 28 shows the calculated total aquifer fluid concentrations of carbon dioxide ($CO_{2,aq}$) as a function of temperature. Also shown are equilibrium constants of the mineral assemblage that would potentially fix $CO_{2,aq}$ if equilibrium was attained i.e. czo+cal+qtz+pre (Equation 13 in Table 11). The liquid enthalpy well sample points fall close to the equilibrium curves while only a few sample points for the ‘excess’ enthalpy wells plot close to the equilibrium curve, if the clinozoisite activity of 0.1 is considered, with most of the samples plotting below the equilibrium curve. This is the same trend that has been seen in other dilute liquid geothermal fields in Iceland e.g. Scott (2011). The ‘excess’ enthalpy samples collected from wells with a long production period (BJ-11 and BJ-12) define a clear trend with temperature showing a steeper slope from the equilibrium slope but tending towards equilibration. The ‘excess’ enthalpy samples (for wells BJ-11 and BJ-12) collected in the time period of approximately 6 years after drilling plot further away from the equilibrium curve while the most recent sample points are closer to the equilibrium state. With time, it can be expected that the well samples would reach equilibrium if the current trend is to be considered (Figure 28).

Equilibrium between epidote, prehnite, quartz and solution fixes aqueous $Ca^{+2}/[H^+]^2$ activity ratios (as will be seen later in the discussion of calcite saturation). From the reaction $CaCO_{3,calcite} + 2H^+ = Ca^{+2} + CO_{2,aq} + H_2O_l$, it is seen that a specific CO_2 partial pressure is required to stabilize calcite, if $Ca^{+2}/[H^+]^2$ activity ratio is fixed. Assuming equilibrium vapour fraction lowers the overall concentration of CO_2 in the computed aquifer fluid although the same trend remains i.e. higher CO_2

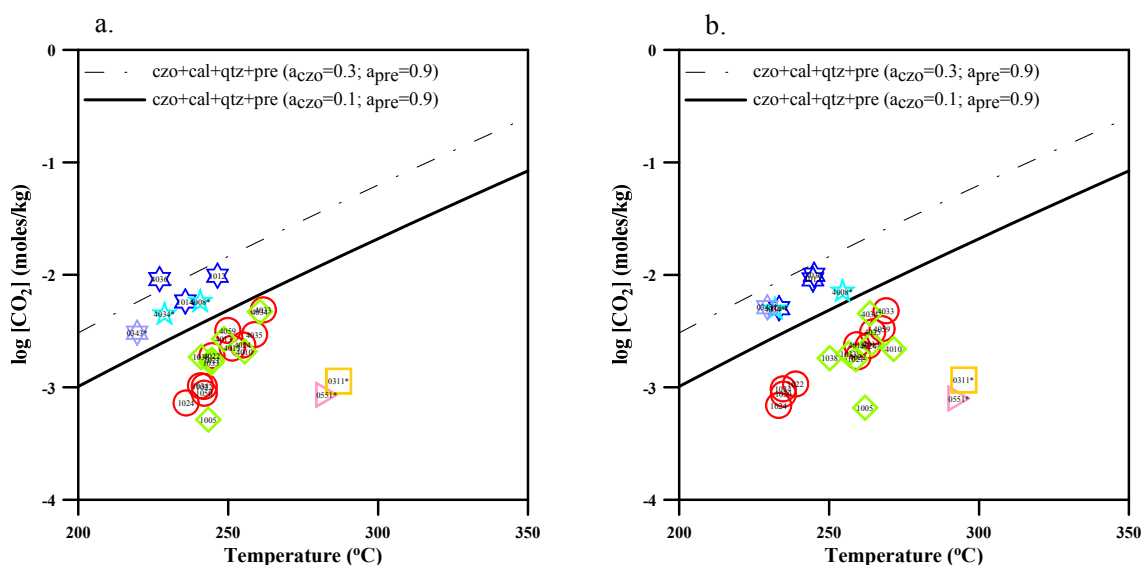


FIGURE 28: Potential mineral buffers controlling CO_2 gas concentrations in the initial aquifer fluid of Námafjall wells using (a) the average of $T_{Na/K}$ and T_{Qtz} to represent T^f , and (b) T_{Qtz} only; symbology as in Figure 26

in the liquid enthalpy wells as compared to the excess enthalpy wells. CO_2 is affected by supply from source (magma) but also by condensation of steam in relatively shallow sub-boiling aquifers (liquid enthalpy wells). Considering the higher concentration of dissolved acidic gases like CO_2 (which is also shown by the H_2S and H_2 concentration) in the shallower aquifer wells than the deeper aquifers, it can be suggested that the fluids feeding the aquifers in the liquid enthalpy wells are steam heated waters with the excess enthalpy wells showing degassed aquifer fluid.

4.3 Mineral-solute equilibria

If the aqueous concentrations of H_2S , H_2 and CO_2 are controlled by equilibria with particular mineral assemblages, then the individual minerals in these assemblages should be in equilibrium with the solution. Dissolution reactions of the hydrothermal minerals considered and their corresponding log K-temperature equations are listed in Table 10. For each reaction, departure from equilibrium is expressed as saturation index. The saturation index (SI) is defined as

$$\text{SI} = \log \left(\frac{Q}{K} \right) \quad [4.3]$$

where Q represents activity product of a mineral dissolution reaction and K the equilibrium constant. The activity product (Q) for a mineral or a mineral assemblage is given by

$$Q = \prod_i a_i^{v_i} \quad [4.4]$$

Where Q is the product of all species activities, a_i , each raised to the power of its stoichiometric coefficient, v_i , which is negative for reactants and positive for products. The activities of aqueous species were obtained with the aid of the WATCH 2.1 program. The activity of water was assumed to be unity. Mineral solid solutions are taken to be ideal. Thus, the activity of end-members of solid solutions were taken to be proportional to their mole fraction raised to the power of the number of exchangeable sites in the crystal lattice, i.e. $a_i = X_i^n$, where X is the mole fraction, a_i the activity of the subscribed species and n the number of exchangeable sites.

Effect of pH on equilibrium state of aquifer fluid

The measured pH of samples affects the calculated initial aquifer pH. For all samples used for this study, pH was measured sometime after the sample was collected and after silica in solution in excess of amorphous silica solubility had polymerized. Precise and immediate onsite measurement of pH of water samples is important for reliable assessment of the state of mineral-solute equilibria in the aquifer and not only for minerals with pH-dependent solubility (e.g. calcite and wollastonite) but also for any mineral-gas equilibria involving $\text{CO}_{2,\text{aq}}$ and $\text{H}_2\text{S}_{\text{aq}}$ because the aquifer water pH affects the relative concentrations of the carbonate and sulphide-bearing species.

Measurement of pH sometime after collection appears to be the common practice worldwide, and such measurement may give faulty pH value because silica polymerization may change the water pH depending on what the initial pH was before onset of polymerization (Karingithi et al., 2010). Arnórsson (2000) indicates that the dissociation constant of aqueous silica (silicic acid) changes very much with temperature below 100°C . Silica polymerization changes the pH of water samples by removing the monomeric silica (weak acid) from solution therefore increases pH and by forming oligomers that decrease pH because oligomers are stronger acids than monomers (Tossell and Sahai, 2000). Silica polymerization, at least when pH value is above 9, will cause an increase of the sample value due to the fact that removal of silica monomers dominate the pH change over oligomer formation and at this high pH a significant fraction of the dissolved silica is ionized.

The measured pH of the samples is very significant during the WATCH speciation calculations. WATCH initially calculates and sums up the concentrations of all conjugate anions of all acids and OH-bearing species at the temperature at which the pH was measured. This sum (A^-) is taken to be constant at all temperatures. The pH at any other temperature is retrieved by iteration until the derived pH satisfies both the value of A^- and all the dissociation constants for the acids and the OH-bearing species.

4.3.1 Calcite, wollastonite and anhydrite

Figure 29 indicates the saturation indices of these calcium containing minerals. Calcite and wollastonite are close to equilibrium but anhydrite is significantly under-saturated in the aquifer waters. The calculated SI values for calcite and wollastonite are sensitive to errors in various parameters, both analytical and thermodynamic.

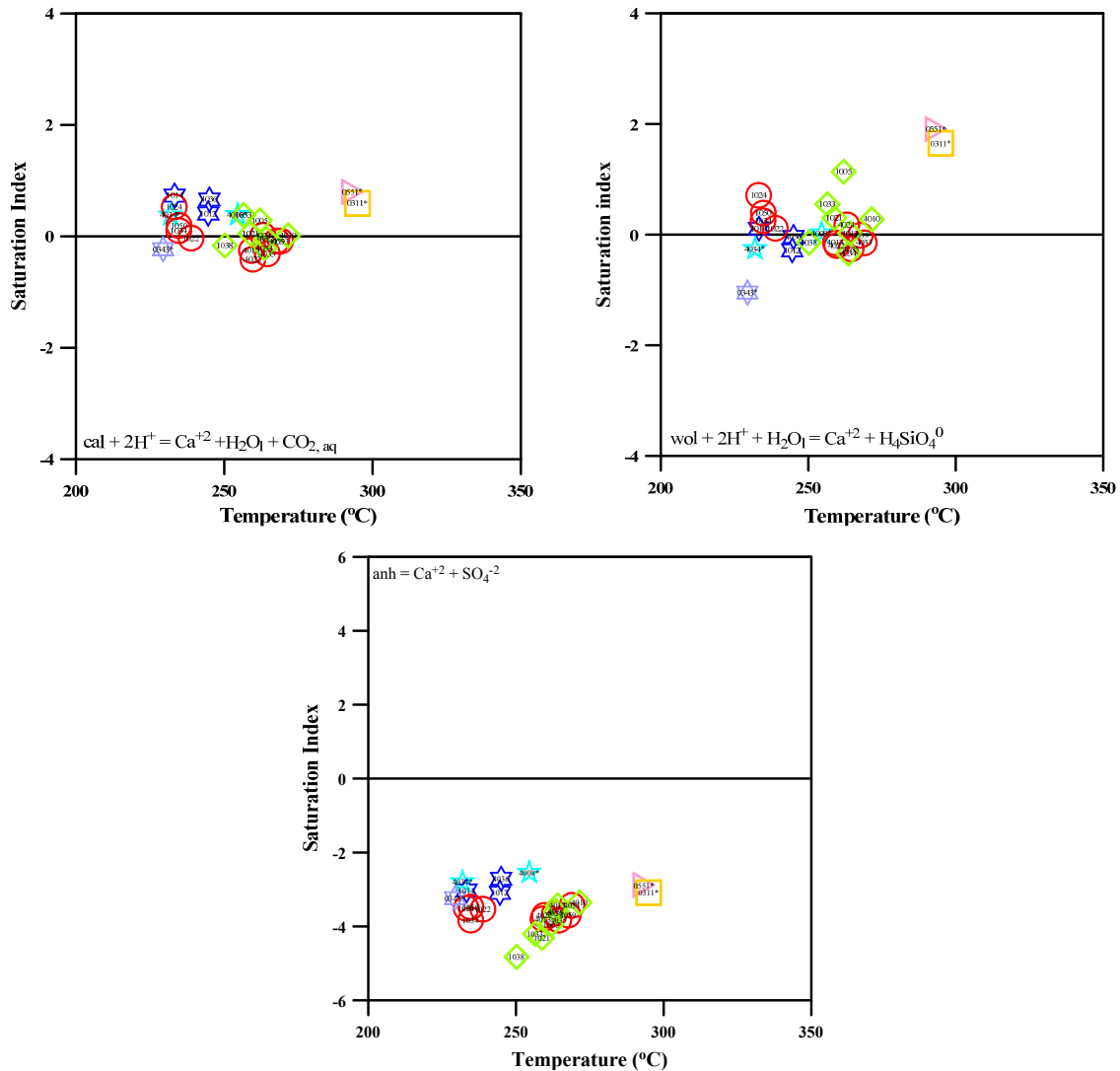
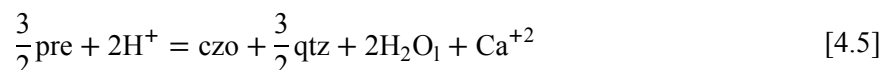


FIGURE 29: Saturation state of Námafjall aquifer waters with respect to calcite, wollastonite and anhydrite assuming liquid aquifer. Symbology as in Figure 26

The most important analytical parameters affecting calcite and wollastonite saturation include measured pH (discussed in section 4.3) and total carbonate carbon in water samples. Higher pH measurements will shift further the calculated SI to more positive values. Figure 30 shows the relationship of pH to calcite and wollastonite saturation in the aquifer fluid. The saturation state of these minerals in the aquifer seems to increase with increasing pH particularly for the ‘excess’ enthalpy well samples. Oversaturation suggests increased Ca^{+2} or CO_2 and/or high pH for the modelled aquifer liquid. From Figure 28, sample points depicting CO_2 in the aquifer fluid of liquid enthalpy wells and the most recent sample points from ‘excess’ enthalpy wells, are close to equilibrium with the mineral assemblage $\text{czo}+\text{cal}+\text{qtz}+\text{pre}$ that controls its aquifer concentrations. Referring to the mineral assemblages, the activity ratio $\text{Ca}^{+2}/[\text{H}^+]^2$ can be fixed by the reaction



or

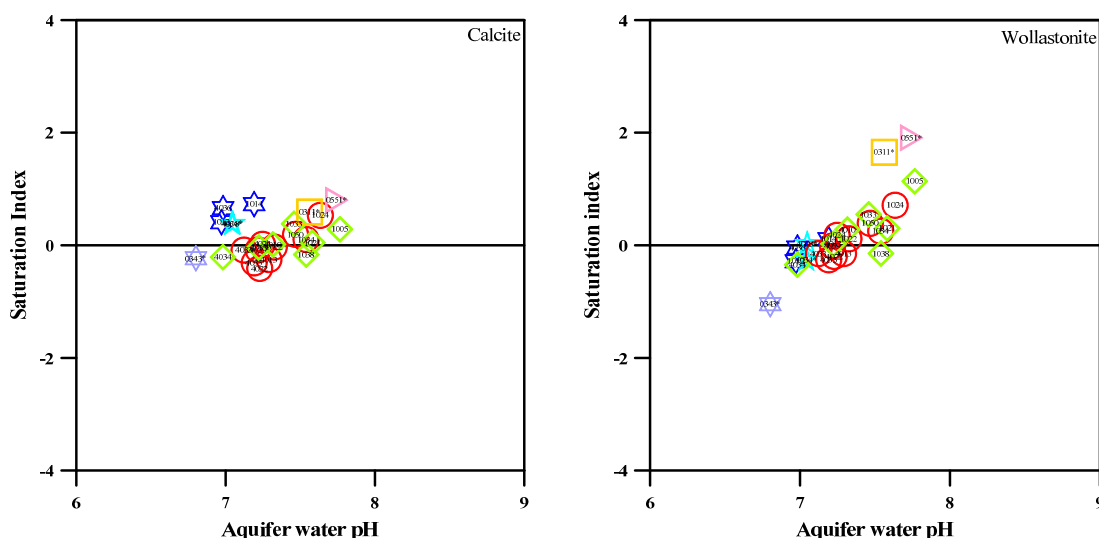
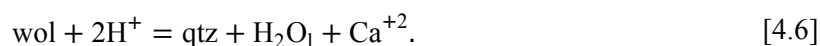


FIGURE 30: Saturation state of Námafjall aquifer waters with respect to calcite and wollastonite as a function of aquifer water pH. Symboly as in Figure 26

The corresponding log K equations modified with the selected activities of end members are shown in Figure 31. From the plot, with respect to the $\text{Ca}^{+2}/[\text{H}^+]^2$ ratio for liquid enthalpy wells, the modelled initial aquifer fluid compositions show a close approach to equilibrium with respect to pre+czo+qtz and wol+qtz assemblages. For the excess enthalpy wells, some points plot closer to the equilibrium curves of pre+czo+qtz and wol+qtz assemblages. These sample points are those that plotted $\text{CO}_{2,\text{aq}}$ closer to the pre+czo+qtz equilibrium curve given $a_{\text{czo}} = 0.1$ in Figure 28. The other sample points of the excess enthalpy wells that displayed significant under-saturation for CO_2 , in Figure 28, with respect to the pre+czo+qtz assemblage are close to equilibrium with or plot slightly above the curve represented by the assemblage wol+qtz in Figure 31. These well samples (from BJ-11 and BJ-12) were collected in a period of approximately 6 years from drilling (see Tables 1 and 2). The CO_2 trend for these wells depicted in Figure 28 shows equilibration in the Námafjall wells with time. The high-temperature wells, BJ-13 and BJ-14, generally show elevated saturation in relation to $\text{Ca}^{+2}/[\text{H}^+]^2$ activity ratios than theoretically predicted, which can be attributed to their high pH or over estimated aquifer temperature.

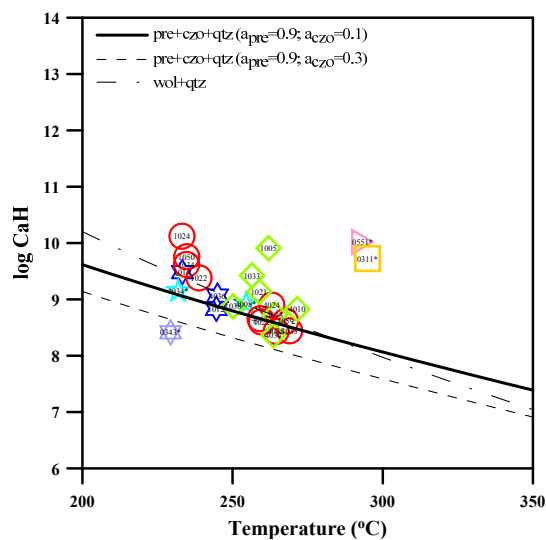


FIGURE 31: $\text{Ca}^{+2}/[\text{H}^+]^2$ activity ratios versus initial aquifer fluid temperatures. Symboly as in Figure 26

4.3.2 Epidote-clinozoisite, grossular, and prehnite

These Ca-Al silicate minerals have pH dependent solubility, with two and four times pH dependence for prehnite and grossular respectively, than for the epidote solid solution, as inferred from their respective dissociation reactions in Table 10. These Ca-Al hydrothermal minerals show approach to equilibrium for most well samples as seen from Figure 32, except for clinozoisite which shows under-

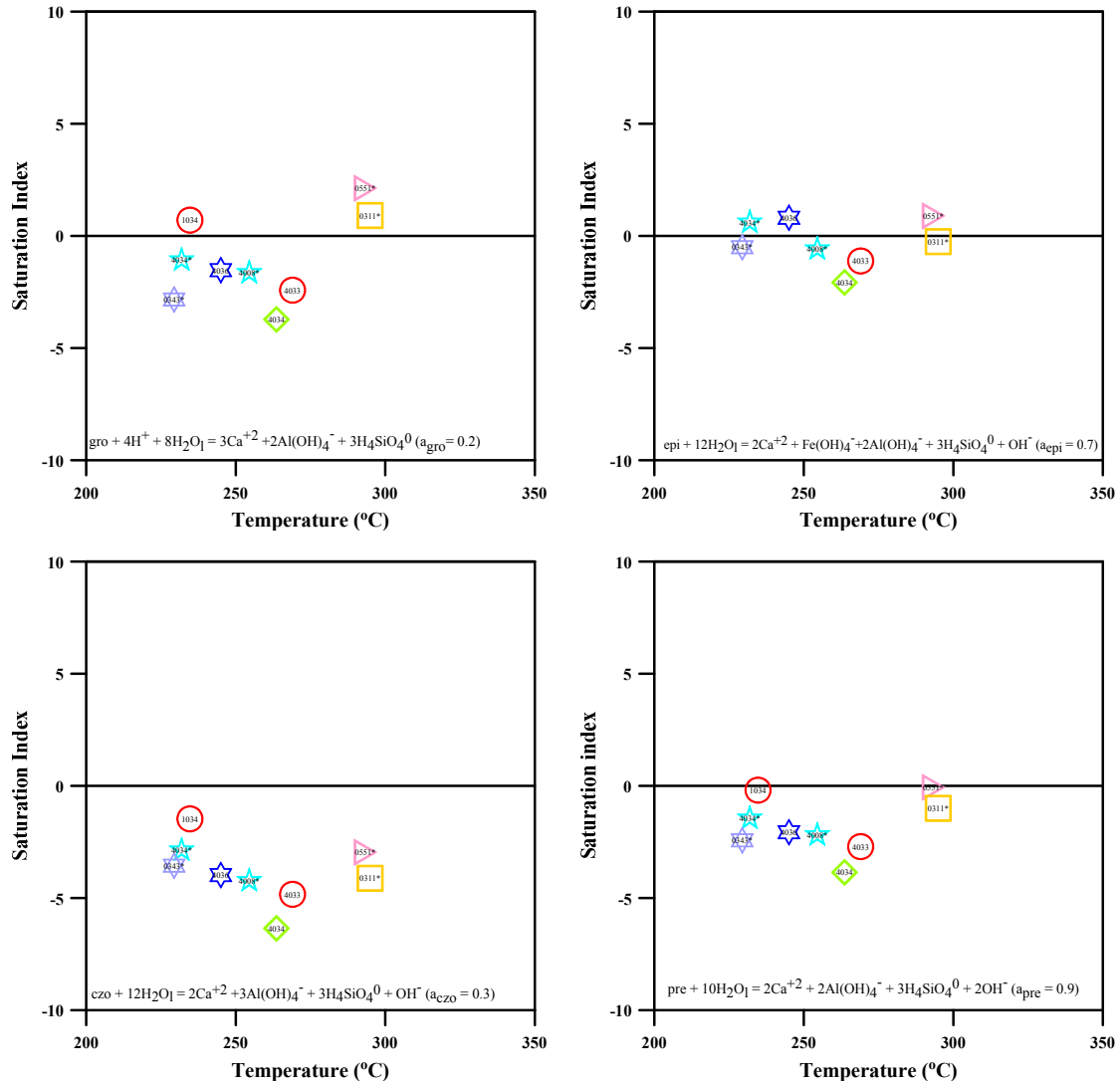


FIGURE 32: Saturation indices of Ca-Al silicate minerals in initial aquifer liquid; symbology as in Figure 26

saturation for all the well samples considered. Since the solubility reactions shown for the minerals are all dependent on pH, they are favourably written in terms of the most dominant species ($Fe(OH)_4^-$ and $Al(OH)_4^-$), and in so doing, the uncertainties of the thermodynamic data of the aqueous species are minimized.

The pH of the initial aquifer water, as calculated by the WATCH programme, is sensitive to various analytical errors (Section 4.3.) and the model adopted to obtain aqueous speciation in the initial aquifer water from analytical data on water and steam samples collected at the wellhead (as detailed in Sections 4.3 and 4.3.1). The calculated pH is particularly sensitive to analyzed carbonate-C and H_2S concentrations in both water and steam samples, as well as the measured pH of the discharged water sample. In turn, the calculated aquifer pH affects the calculated relative abundance of the various aqueous species, including the $Fe(OH)_4^-$ species.

4.3.3 Magnetite, pyrite and pyrrhotite

Figure 33 shows the saturation indices for these Fe-bearing minerals. The SI-values are generally negative decreasing with increasing temperature. This can be attributed to a decrease in the calculated activity of Fe^{+2} but credited more to the faulty thermodynamic data on iron hydrolysis constants.

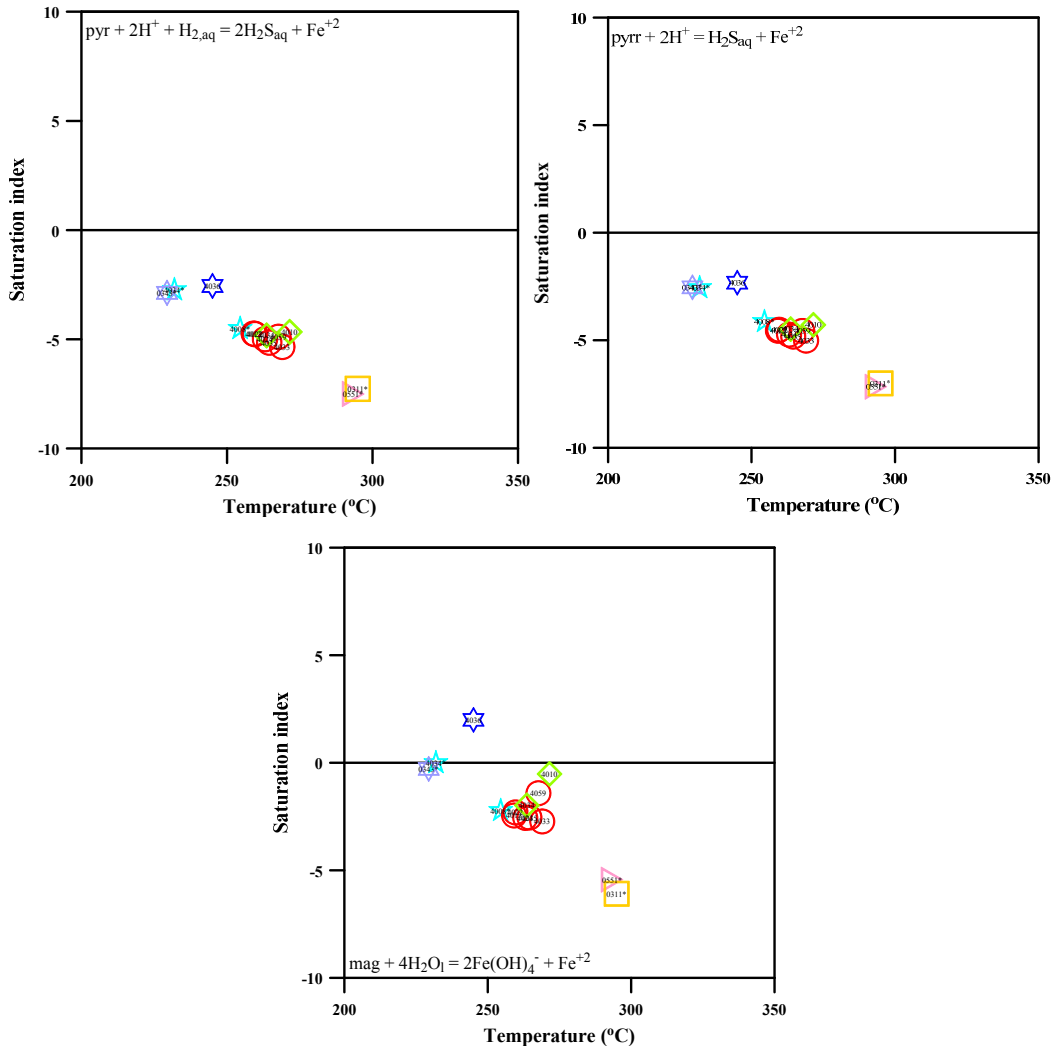


FIGURE 33: Saturation indices of Fe-bearing alteration minerals assuming liquid aquifer; symbology as in Figure 26

Available experimental data on iron speciation constants, for both ferrous and ferric iron below 100°C, are in error leading to over-estimation of the activity of the $\text{Fe}(\text{OH})_4^-$ species but to a corresponding under-estimation of Fe^{+2} activity (Arnórsson et al., 2002). The results of the Arnórsson et al. (2002) study indicate that this is also the case above 200°C. Accordingly, over-estimation of $\text{Fe}(\text{OH})_4^-$ activity is considered to affect the SI-values for epidote. This conclusion is supported by negative SI-values obtained for magnetite and the Fe^{+2} bearing minerals (pyrite and pyrrhotite). Figure 34 shows the $\text{Fe}(\text{OH})_4^-/\text{OH}^-$ activity ratios versus initial aquifer fluid temperatures, with equilibrium concentrations predicted by the epi+pre, epi+wol+qtz+and, magnetite and hematite mineral assemblages. These Fe-bearing minerals are considered to buffer concentration of H_2S and H_2 in initial aquifer fluid.

The potential mineral pairs i.e. pyr+mag and pyr+pyrr, are shown in Figure 35. When considering equilibrium between solution and the mineral pairs mag+pyr and pyr+pyrr, the iron species (Fe^{+2} and $\text{Fe}(\text{OH})_4^-$) are eliminated from the calculation of the activity product values. The calculated Q values now only include H_2S and H_2 as shown by reactions 7 and 8 in Table 11, considering all minerals and liquid water are taken to have unit activity. It is seen that activity products are closer to equilibrium (Figure 35), especially so for the pyr+pyrr pair. The $\text{H}_2\text{S}/\text{H}_2$ ratio observed can be attributed to presence of an equilibrium vapour fraction, and according to this, the pyr+pyrr mineral pair has a better fit for the data. This observation is considered to confirm further that the thermodynamic data on the iron hydrolysis constants are in error.

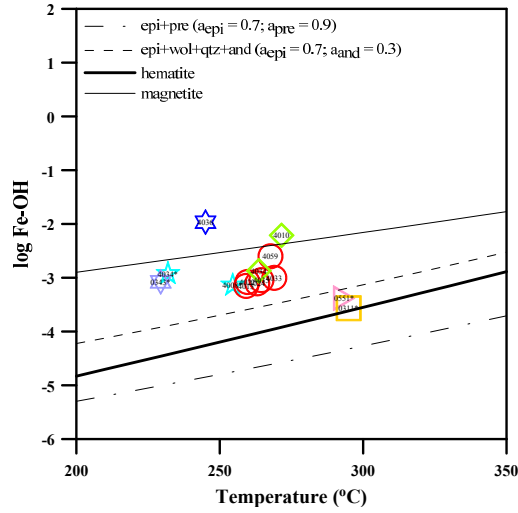


FIGURE 34: $\text{Fe}(\text{OH})_4^- / \text{OH}^-$ activity ratios vs. initial aquifer fluid temperatures, with equilibrium concentrations predicted by the epi+pre, epi+wol+qtz+and, magnetite and hematite mineral assemblages; symbology as in Figure 26

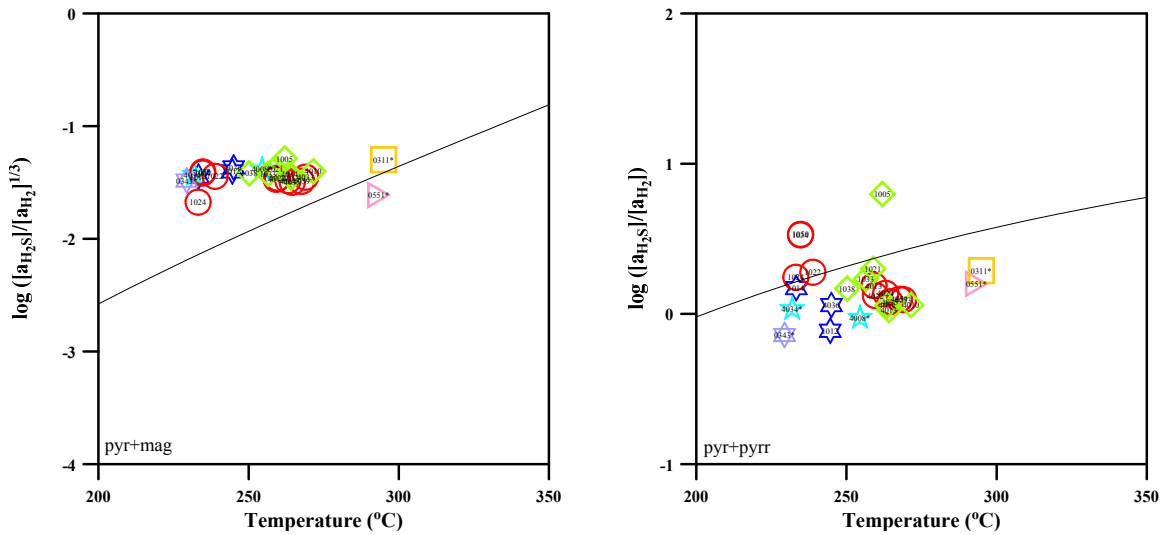


FIGURE 35: Calculated $\text{H}_2\text{S}/\text{H}_2$ activity ratios compared with theoretical equilibrium with pyr+mag and pyr+pyrr. Symbology as in Figure 26

5. SUMMARY AND CONCLUSIONS

This study has focused on the processes controlling the concentrations of chemical components in the aquifer fluids of some of the wells in the Námafjall geothermal field during their production period, for some wells this being more than 20 years (samples studied dated from 1979 to 2008). The overall objective of this thesis was to use these investigations to explicate the physical nature of the hydrothermal system. For this reason, the chemical discussion was preceded by an intensive literature review of the Námafjall area. This review reveals the great advances in understanding the nature of the system that have been made in the past decades. The nature of geothermal development is that this is only possible once a resource has been extensively drilled as is the case of Námafjall field. It is hoped that this study can serve as an example of how geochemistry can be employed for geothermal resource assessment. Calculation of initial aquifer fluid composition is only the first step in assessing the state of equilibrium between particular species in the aqueous phase and minerals. The next step is assessing the state of equilibrium between particular species in the aqueous phase and minerals involved in the calculation of speciation distribution in the aquifer fluid to obtain activity products (Q) for specific mineral-solution reactions leading to the final step of calculating equilibrium constants for these reactions from thermodynamic data.

Wells drilled into liquid dominated geothermal reservoirs sometimes have liquid enthalpy but commonly 'excess' enthalpy. Three of the wells studied have liquid enthalpy while the remaining four wells display various degrees of 'excess' enthalpy, i.e. the enthalpy of well discharges is higher than that of liquid water at the aquifer temperature. Since Námafjall reservoir is liquid-dominated, the excess enthalpy reflects a change in the enthalpy of the flowing fluid between initial aquifer fluid conditions and the wellhead. The processes that can cause such an increase in the enthalpy of the flowing fluid include phase segregation involving partial or complete retention of liquid water in the aquifer due to its adhesion onto mineral grain surfaces by capillary pressure whereas all the vapour flows in the wells of the aquifer fluid, conductive heat transfer from aquifer rock to fluid and presence of vapour in the initial aquifer. The process considered in this study as the main cause of excess enthalpy is phase segregation, either under natural conditions or in producing aquifers where extensive depressurization boiling occurs, although conductive heat flow from aquifer rock cannot be entirely ignored.

The phase segregation model does not take into consideration possible changes in the composition of the flowing fluid between initial aquifer conditions and wellhead by precipitation or dissolution of minerals or reactions with casing material. Such reactions are however likely to occur and they may change significantly the concentrations in the fluid of those components that are present in low concentrations, and are chemically reactive (e.g. Ca, Fe and Al). For this reason, the results of the speciation calculations may indicate significant departure from equilibrium between minerals and the water in the aquifer beyond the depressurization zone, even if such equilibrium was truly closely approached in the initial aquifer fluid. The named reactions, however, have much smaller effects for components that are abundant in the aquifer fluid, such as the reactive gases (CO_2 , H_2S and H_2). Even if equilibrium is upset between solution and individual minerals in assemblages that control the concentrations of components present in high concentrations in the fluid, the well discharge composition will reflect the correct concentrations of such components in the initial aquifer fluid. The selection of a model to calculate the initial aquifer fluid composition is likely a source of errors in calculating the aquifer fluid compositions from wellhead data on excess enthalpy wells.

Selection of a phase segregation pressure at ~80% volume fraction of the flowing vapour was deemed appropriate, in view of the fact that the liquid saturation at this pressure condition was calculated to roughly match the residual liquid saturation in porous and fractured dominated reservoir rock media of 0.2 (i.e. $S^{e,l} \sim 0.2$). Once initial aquifer temperatures (quartz and Na/K geothermometers) and phase segregation pressures were calculated, the chemical composition and speciation of initial aquifer fluids was calculated using the WATCH 2.1 program. The overall approach taken was to calculate initial aquifer fluid chemical compositions assuming a range of different phase segregation pressures. While the calculated concentration of non-volatile components in initial aquifer fluids is not sensitive to the selected phase segregation pressure, the calculated concentration of gaseous components is markedly

more sensitive. For non-volatile components, significant variation in calculated concentrations can only occur if discharge enthalpy is >2000 kJ/kg and phase segregation is selected within the temperature range that gives maximum enthalpy of steam (200-250°C). The calculated concentration of gases in the aquifer fluids varies extensively depending on the choice of phase segregation temperature, with the variation increasing proportionally with the discharge enthalpy of the well thus considerable uncertainty involved when discharge enthalpy approaches that of dry steam.

Having obtained component concentration in the initial aquifer fluid by assuming that the aquifer fluid is represented by liquid alone ($X^{f,v} = 0$), and (2) aquifer is two-phase ($X^{f,v} \neq 0$), the WATCH speciation program was used simultaneously to calculate individual species activities. Most of the wells at Námafjall have higher H_2 aquifer fluid concentrations than expected at equilibrium with the mineral assemblage involving H_2 . The elevated H_2 concentrations indicate the presence of equilibrium vapour fraction in the initial aquifer fluid. The vapour fraction was calculated from a combination of the H_2S and H_2 ($X_{H_2S-H_2}^{f,v}$) and compared with that from H_2 ($X_{H_2}^{f,v}$) content of the aquifer fluid assuming that their concentration in the aquifer liquid was fixed by equilibrium with a specific mineral assemblage (pyrite-pyrrhotite-prehnite-epidote). $X_{H_2S-H_2}^{f,v}$ was calculated as 0-3.9% by weight (0-42% by volume) with a field average of 0.79 % by weight. This vapour fraction has a clear effect on the gas concentrations.

The modelled aquifer fluids were assessed on how closely they have approached equilibrium conditions with respect to various mineral-gas and mineral-solution reactions that may occur in the aquifer. The fluid concentrations of the gases were taken to represent liquid concentrations when calculating the respective mineral-gas equilibrium constants. Aquifer water concentrations of H_2S and H_2 are controlled by close approach to equilibrium with specific mineral assemblage pyrite-pyrrhotite-prehnite-epidote. Different redox reactions that involve gases generally show significant departure from equilibrium conditions largely influenced by the H_2 levels in the fluid. Some of the well discharges (liquid enthalpy wells) show H_2 concentrations are significantly above equilibrium, but the excess enthalpy wells are closer to equilibrium when equilibrium vapour fraction is taken into consideration. The data points for both H_2S/H_2 activity ratio lie somewhat above equilibrium conditions with mineral assemblage involving pyrite-magnetite but are closer to equilibrium when pyrite-pyrrhotite assemblage is involved. Aquifer fluid CO_2 concentrations show larger variation than those of H_2S and H_2 . For the liquid enthalpy wells, CO_2 concentration in the aquifer fluid match generally well with equilibrium with the clinozoisite-calcite-quartz-prehnite mineral assemblage. At the selected activities of clinozoisite and prehnite, data points for CO_2 of the excess enthalpy wells were generally below the equilibrium curve for mineral assemblage including clinozoisite-calcite-quartz-prehnite. There seems to emerge a trend in the CO_2 concentrations, in the aquifer of the 'excess' enthalpy wells with a longer production period, with the values tending towards equilibrium with time. Low CO_2 concentrations in the aquifer fluid could have been the consequence of insufficient supply of CO_2 to the geothermal system from the magma heat source. In that case, CO_2 unlike H_2S and H_2 , would be source- rather than equilibrium-controlled. It can be concluded that the shallower aquifer at Námafjall are higher in gas (H_2S , H_2 , CO_2 and N_2) indicating that gaseous steam from deeper aquifers has condensed in the shallower ones signifying that they are, at least partly, steam-heated.

Considering the uncertainties involved in analysis, model selection and thermodynamic data, the initial aquifer fluids display different saturation states of the hydrothermal minerals considered. Calcite and wollastonite are close to equilibrium while anhydrite is significantly under-saturated. Various Ca-Al bearing minerals seem to closely approach equilibrium. The calcium-proton activity ratio was shown to be controlled by mineral assemblages consisting of prehnite-clinozoisite-quartz and wollastonite-quartz. Over-estimation of $Fe(OH)_4^-$ activity is considered to be the cause of the systematic negative SI-values of Fe^{+2} bearing minerals (magnetite, pyrite and pyrrhotite). The thermodynamic data selected for $Fe(OH)_4^-$ to retrieve equilibrium constants may also contribute to this. It is evident that the cumulative error in the thermodynamic data for the minerals is greater than the departure from equilibrium of aqueous H_2S with the mineral assemblage pyrite-pyrrhotite-prehnite-epidote. Calculation of the equilibrium constant for this reaction assumed pure FeS and FeS_2 . If the FeS is

deficient in iron, the equilibrium curve is shifted to lower values, as does the presence of S^{-2} in FeS_2 . Sulfide mineral analysis is missing for quantitative estimation of the effect of the iron-sulfide mineral composition on the equilibrium constant. In addition, the uncertainties on the thermodynamic data on these mineral, as given by Robie and Hemingway (1995) may produce an error as high as 0.3 log mol/kg on the equilibrium H_2S concentration, in addition to the error produced by the silicate minerals, epidote and prehnite.

REFERENCES

- Ármannsson, H., 2011: *EIA – example from Bjarnaflag in Iceland*. University of Iceland, geothermal resources (JAR218), lecture notes.
- Ármannsson, H., 2005: Monitoring the effect of geothermal effluent from the Krafla and Bjarnarflag power plants on groundwater in the Lake Mývatn area, Iceland, with particular reference to natural. *Proceedings World Geothermal Congress 2005 Antalya, Turkey*, 8 pp.
- Ármannsson, H., 1993: *The geothermal system in Námafjall. Geochemical investigation*. Orkustofnun, Reykjavík, report 93053/JHD-29B, 30 pp.
- Ármannsson, H., Benjamínsson, J., Jeffrey, A.W.A., 1989: Gas changes in the Krafla geothermal system, Iceland. *Chem. Geol.* 76, 175–196.
- Ármannsson, H., Gudmundsson, Á., Steingrímsson, B.S., 1987: Exploration and development of the Krafla geothermal area. *Jökull* 37, 13–30.
- Ármannsson, H. and Ólafsson, M. 2007: Geothermal sampling and analysis. *Presented at the Short Course II on “Surface Exploration for Geothermal Resources”*, organized by UNU-GTP and KenGen, at Lake Naivasha, Kenya, 2-17 November.
- Ármannsson, H. and Ólafsson, M. 2006: *Collection of geothermal fluids for chemical analysis*. ÍSOR, Reykjavík, report ÍSOR-2006/016, 17 pp.
- Árnason, J. G., Bird, D. K., 1992: Formation of zoned epidote in hydrothermal systems. In: *Water-Rock Interaction 7-2*, 1473-1476.
- Árnason, K., Karlsdóttir, R., Eysteinnsson, H., Flóvenz, Ó., and Gudlaugsson, S., 2000: The resistivity structure of high-temperature geothermal systems in Iceland. *Proceedings of the World Geothermal Congress 2000, Kyushu-Tohoku, Japan*, 923-928.
- Angcoy, E.C. Jr., 2010: *Geochemical modelling of the high temperature Mahanagdong geothermal field, Letye, Philippines*. University of Iceland, MSc Thesis, UNU-GTP, Iceland, report 1, 71 pp.
- Arnórsson, S. (ed), 2000: *Isotopic and chemical techniques in geothermal exploration, development and use. Sampling methods, data handling and interpretation*. International Atomic Energy Agency, Vienna, 351 pp.
- Arnórsson, S., 1995: Geothermal systems in Iceland: Structure and conceptual models. 1. High-temperature areas. *Geothermics*, 24, 561-602.
- Arnórsson, S., Angcoy, Jr., E.C., Bjarnason, J.Ö., Giroud, N., Gunnarsson, I., Kaasalainen, H., Karingithi, C., and Stefánsson, A., 2010: Gas chemistry of volcanic geothermal systems. *Proceedings World Geothermal Congress 2010, Bali, Indonesia*.
- Arnórsson, S., Björnsson, S., Muna, Z.W., Bwire-Ojiambo, S., 1990: The use of gas chemistry to evaluate boiling processes and initial steam fractions in geothermal reservoirs with an example from the Olkaria field, Kenya. *Geothermics*, 19, 497–514.
- Arnórsson, S., Fridriksson, Th., Gunnarsson, I., 1998: Gas chemistry of the Krafla geothermal field, Iceland. *Water Rock Interaction, Proc. Int. Symp. Auckland, New Zealand*, 613-616.
- Arnórsson, S. and Gunnlaugsson, E., 1985: New gas geothermometers for geothermal exploration - calibration and application. *Geochim Cosmochim Acta*, 49, 1307-1325.

- Arnórsson, S., Gunnlaugsson, E., and Svavarsson, H., 1983: The chemistry of geothermal waters in Iceland. II. Mineral equilibria and independent variables controlling water compositions. *Geochimica et Cosmochimica Acta*, 47, 547-566.
- Arnórsson, S., Sigurdsson, S., and Grönvold, K., 1978: Aquifer chemistry of four geothermal areas in Iceland. *Geochem. Cosmochim. Acta*, 42, 523-536.
- Arnórsson, S., Sigurdsson, S., and Svavarsson, H., 1982: The chemistry of geothermal waters in Iceland. I. Calculations of aqueous speciation from 0° to 370°C. *Geochim. Cosmochim. Acta*, 46, 1513-1532.
- Arnórsson, S. and Stefánsson, A., 2005: Wet-steam well discharges. II. Assessment of aquifer fluid compositions. *World Geothermal Congress, Antalya, Turkey*.
- Arnórsson, S., and Stefánsson, A., 1999: Assessment of feldspar solubility constants in water in the range 0 to 350 °C at vapour saturation pressures. *Amer. J. Sci.*, 299, 173-209.
- Arnórsson, S., Stefánsson, A., and Bjarnason, J.Ö., 2007: Fluid-fluid interaction in geothermal systems. *Reviews in Mineralogy & Geochemistry*, 65, 229-312.
- Bird, D. K., Spieler, A. R., 2004: Epidote in geothermal systems. *Reviews in Mineralogy & Geochemistry*, 56, 235-300.
- Bischoff, J.L. and Rosenbauer, R.J., 1989: Salinity variations in submarine hydrothermal systems by double diffusive convection. *Journal of Geology*, 7, 613-623.
- Bjarnason, J.Ö., 1994: *The speciation program WATCH, version 2.1*. Orkustofnun, Reykjavík, 7 pp.
- Bödvarsson, G.S., Benson, S.M., Sigurdsson, Ó., Stefánsson, V., Eliasson, E.T., 1984a: The Krafla geothermal field, Iceland. 1. Analysis of well test data. *Water Resour. Res.*, 20, 1515-1530.
- Bödvarsson, G.S., Pruess, K., Stefánsson, V., Eliasson, E.T., 1984b: The Krafla geothermal field Iceland 2. The natural state of the system. *Water Resour. Res.*, 20, 1531-1544.
- Brandsdóttir, B. and Einarsson, P. 1979: Seismic activity associated with September 1977 deflation of the Krafla central volcano in NE Iceland. *J. Volcanol. Geotherm. Res.*, 6, 197-212.
- Chen, C.Y., and Horne, R.N., 2006: Two-phase flow in rough-walled fractures: Experiments and a flow structure model. *Water Resources Research*, 42.
- Chen, C.Y., Horne, R.N., and Fourar, M., 2004: Experimental study of two-phase flow structure effects on relative permeabilities in a fracture. *29th Workshop on Geothermal Reservoir Engineering, Stanford University, Stanford, CA*.
- Corey, A.T., 1957: Measurement of water and air permeabilities in unsaturated soil. *Soil Sci. Soc. Am. Proc.*, 21, 7-10.
- D'Amore, F., and Celati, R., 1983: Methodology for calculating steam quality in geothermal reservoirs. *Geothermics* 12, 129-140
- D'Amore, F., and Truesdell, A.H., 1985: Calculation of geothermal reservoir temperatures and steam fractions from gas compositions. *Geotherm. Res. Council, Trans.*, 9, 305-310
- Darling, G., Ármannsson, H., 1989: Stable isotopic aspects of fluid flow in the Krafla, Námafjall and Theistareykir geothermal systems of northeast Iceland. *Chem., Geol.* 79, 197-213.

- De Zeeuw, E. and Gíslason, G., 1988: *The effect of volcanic activity on the groundwater system in the Námafjall geothermal area, NE-Iceland*. Orkustofnun, Reykjavík, report OS-88042/JHD-07, 39 pp.
- Diakonov, I. I., Schott, J., Martin, F., Harrichourry, J. C., Escalier, J., 1999: Iron(III) solubility and speciation in aqueous solutions. Experimental study and modelling: Part 1. Hematite solubility from 60 to 300 degrees C in NaOH-NaCl solutions and thermodynamic properties of Fe(OH)₄,aq. *Geochim. Cosmochim. Acta*, 63, 2247-2261.
- Fernández-Prini, R., Alvarez, J. L., Harvey, A. H., 2003: Henry's constants and vapour-liquid distribution constants for gaseous solutes in H₂O and D₂O at high temperatures. *Journal of Physical and Chemical Reference Data*, 32-2, 903-916.
- Flóvenz, Ó.G., 2011: *Resistivity, magma and geothermal systems*. University of Iceland, Geothermal Resources (JAR218), lecture notes.
- Flóvenz, Ó.G., Spangenberg, E., Kulenkamp, J., Árnason, K., Karlsdóttir, R., Huenges, E., 2005: The role of electrical interface conduction in geothermal exploration. *Proceedings World Geothermal Congress 2005 Antalya, Turkey*, 24-29.
- Fournier, R.O., and Potter, R.W.II, 1982: A revised and expanded silica (quartz) geothermometers. *Geotherm. Res. Council, Bull.*, 11, 3-9.
- Frauke, W., Fridriksson, Th., and Ármannsson, H., 2008: *CO₂ fixation by calcite in high-temperature geothermal systems in Iceland*. ÍSOR, Reykjavík, report 2008/003, 68 pp.
- Georgsson, L.S., 2010. Geophysical methods used in geothermal exploration. *Presented at "Short Course V on Exploration for Geothermal Resources"*, organized by UNU-GTP, GDC and KenGen, at Lake Bogoria and Lake Naivasha, Kenya, Oct. 29 – Nov. 19, 2010.
- Georgsson, L.S. and Karlsdóttir R., 2009: Resistivity methods - DC and TEM with examples and comparison from the Reykjanes peninsula and Öxarfjörður, Iceland. *Presented at "Short Course on Surface Exploration for Geothermal Resources"*, organized by UNU-GTP and LaGeo, in Ahuachapan and Santa Tecla, El Salvador, 17-30.
- Giggenbach, W.F., 1980: Geothermal gas equilibria. *Geochim. Cosmochim Acta*, 44, 2021-2032.
- Giroud N., 2008: *A chemical study of arsenic, boron and gases in high-temperature geothermal fluids in Iceland*. University of Iceland, Reykjavík, PhD thesis, 128 pp.
- Glover, R.B., Lovelock, B., and Ruaya, J.R., 1981: A novel way of using gas and enthalpy. *New Zealand Geothermal Workshop, Auckland, New Zealand*, 163-169.
- Gudmundsson, Á. 1993: *The alteration formation temperature in the geothermal system in Bjarnarflag*. Orkustofnun, Reykjavík, report OS-93065/JHD-31 B (in Icelandic), 21 pp.
- Gudmundsson, B.T. and Arnórsson, S., 2005: Secondary mineral-fluid equilibria in the Krafla and Namafjall geothermal systems, Iceland. *Appl. Geochem.*, 20, 1607-1625.
- Gudmundsson, B., and Arnórsson, S., 2002: Geochemical monitoring of the Krafla and Námafjall geothermal areas, N-Iceland. *Geothermics*, 31, 195-243.
- Gudmundsson, M.T., Larsen, G., Höskuldsson, Á. and Gylfason, Á.G., 2008: Volcanic hazards in Iceland. *Jökull*, 58, 251-268.

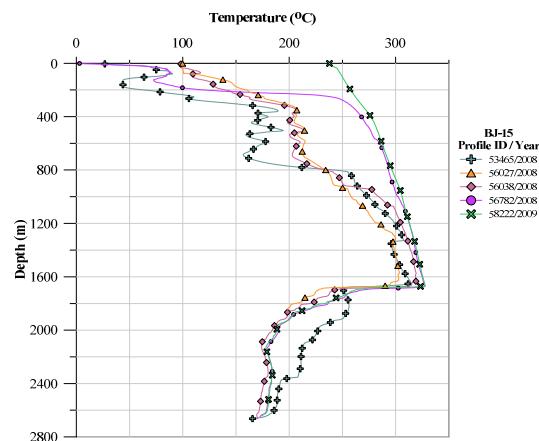
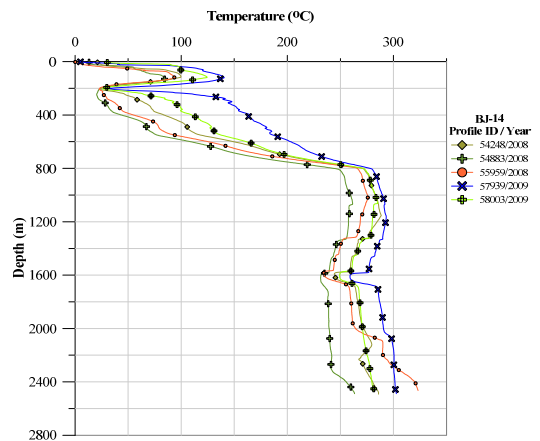
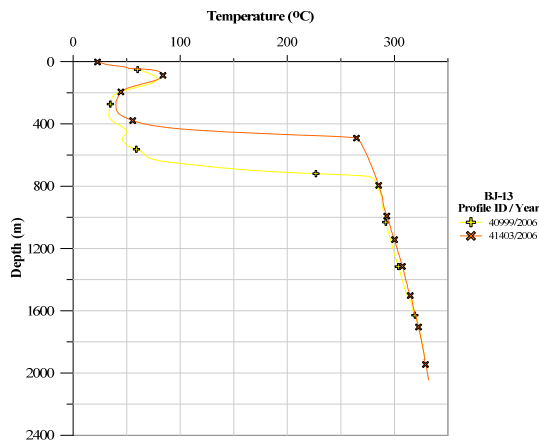
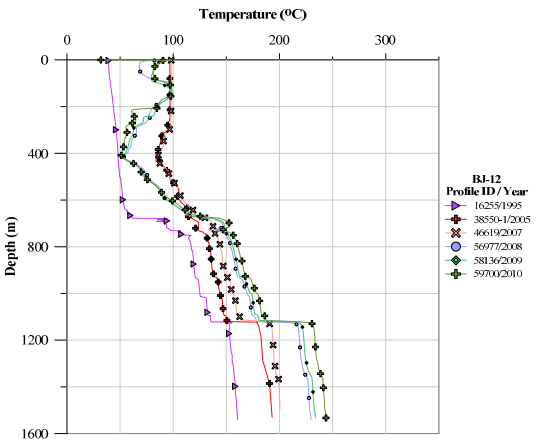
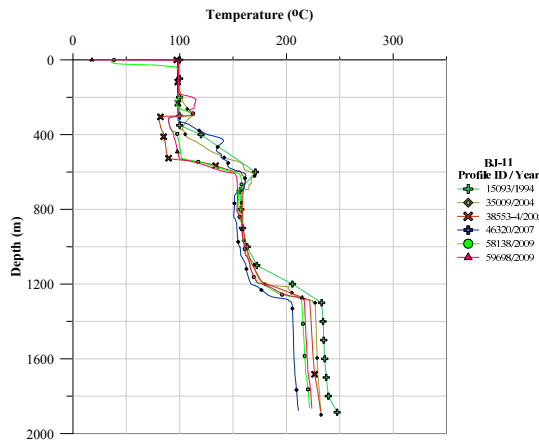
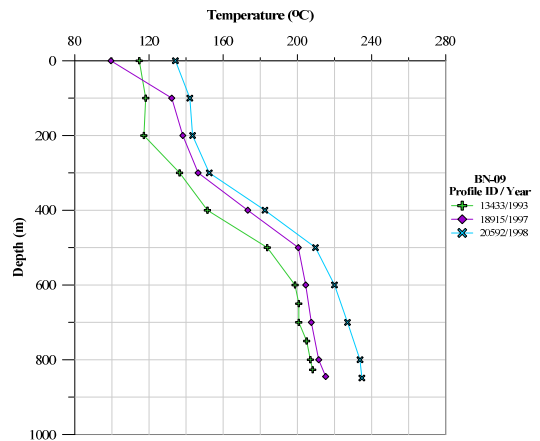
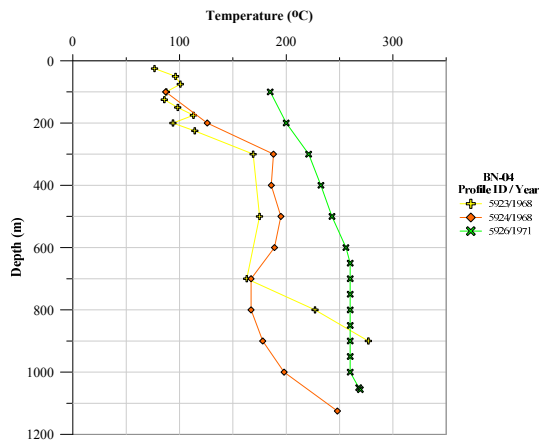
- Gudmundsson, Á., Mortensen, A.K., Hjartarson, A., Karlsdóttir, R. and Ármannsson, H. 2010: Exploration and utilization of the Námafjall high temperature area in N-Iceland. *Proceedings World Geothermal Congress Bali, Indonesia*.
- Gunnarsson, I., Arnórsson, S., 2000: Amorphous silica solubility and the thermodynamic properties of H₄SiO₄ degrees in the range of 0 degrees to 350 degrees C at P-sat. *Geochim. Cosmochim. Acta*, 64-13, 2295-2307.
- Hauksson, T., and Benjamínsson, J., 1997: *Well performance and chemical analysis of water and steam from well discharges*. Landsvirkjun - National Power Company, Reykjavík, report (in Icelandic), 70 pp.
- Hauksson, T., and Benjamínsson, J., 1995: *Krafla and Bjarnarflag. Production of wells and chemical composition of fluids from wells and power plant*. Landsvirkjun - National Power Company, Reykjavík, report (in Icelandic), 64 pp.
- Hauksson, T., and Benjamínsson, J., 1989: *Krafla and Bjarnarflag. Production of wells and chemical composition of fluids from wells and power plant*. Landsvirkjun - National Power Company Reykjavík, report (in Icelandic), 51 pp.
- Hauksson, T., and Benjamínsson, J., 2000: *Krafla and Bjarnarflag. Production of wells and chemical composition of fluids from wells and power plant*. National Power Company, report (in Icelandic), 66 pp.
- Helgeson, H.C., 1967: Thermodynamics of complex dissociation in aqueous solution at elevated temperatures. *J. Phys. Chem.*, 71, 3121-3136.
- Hersir G.P., and Árnason, K., 2009: Resistivity of rocks. Presented at "Short Course on Surface Exploration for Geothermal Resources", organized by UNU-GTP and LaGeo, in Ahuachapan and Santa Tecla, El Salvador, 17-30.
- Hjartarson, A., Sigurdsson Ó., Gudmundsson Á., Ármannsson, H., Karlsdóttir R., 2005: *Numerical modeling of the geothermal system in námafjall and response prediction of 30-90 mw electrical generation in Bjarnarflag*. ÍSOR, Reykjavík, report ÍSOR 2004/009 (in Icelandic), 123 pp.
- Hönnun, 2003a: *The Bjarnarflag power plant 90 MWe and the 132 kV Bjarnarflag power transmission line 1 in Skútustadahreppur. Environmental Impact Assessment*. Landsvirkjun, Reykjavík, report, LV-2003/123, 116 pp.
- Hönnun, 2003b: *The Bjarnarflag power plant up to 90 MWe and the 132 kV Bjarnarflag power transmission line 1 in Skútustadahreppur. Environmental Impact Assessment*. Landsvirkjun, Reykjavík, scoping document, LV-2003/052, 46 pp.
- Hönnun, 2003c: *The Bjarnarflag power plant 90 MWe and the 132 kV Bjarnarflag power transmission line 1 in Skútustadahreppur. Environmental Impact Assessment*. Landsvirkjun, Reykjavík, LV-2003/123, appendices, 267 pp.
- Hönnun, 1996: *A geothermal power plant at Bjarnarflag. Environmental Impact Assessment. Initial environmental impact assessment for a 2×20 MWe geothermal power plant in Bjarnarflag and a 132 kV high voltage transmission line between the Krafla power plant*. Landsvirkjun, Reykjavík, 101 pp.
- Holland, T. J. B., Powell, R., 1998: An internally consistent thermodynamic data set for phases of petrological interest. *Journal of Metamorphic Geology*, 16-3, 309-343.

- Horne, R.N., Satik, C., Mahiya, G., Li, K., Ambuso, W., Tovar, R., Wang, C., and Nassori, N., 2000: Steam-water relative permeability. *Proceedings World Geothermal Congress 2000, Kyushu-Tohoku, Japan*, 2609-2615.
- Hreggvidsdóttir, H., 1987: *The greenschist to amphibolite facies transition in the Nesjavellir hydrothermal system, Southwest Iceland*. University of Stanford, Stanford, MSc thesis.
- Ingebritsen, S.E., Geiger, S., Hurwitz, S. and Driesner, T., 2010: Numerical simulation of magmatic hydrothermal systems. *Reviews of Geophysics*, 48, 33 pp.
- Isabyrie, E., 1994: Borehole geology and hydrothermal alteration in well B-9, Námafjall geothermal field, NE-Iceland. Report 5 in: *Geothermal Training in Iceland 1994*. UNU-GTP, Iceland, 89-121.
- Jakobsson, S. P. 1979. Petrology of recent basalts of the Eastern Volcanic Zone, Iceland. *Acta Naturalia Islandia*, 26, 1-103.
- Jóhannesson, H. and K. Saemundsson 1998. *Geological map of Iceland. Bedrock geology, scale 1:500.000*. Náttúrufræðistofnun Islands, Reykjavík (2nd edition).
- Johnson, J. W., Oelkers, E. H., Helgeson, H. C., 1992: SUPCRT92 - A software package for calculating the standard molal thermodynamic properties of minerals, gases, aqueous species, and reactions from 1-bar to 5000-bar and 0-degrees-C to 1000-degrees-C. *Computers and Geosciences*, 18, 899-947.
- Karingithi, C. W., Arnórsson, S., and Gronvold, K., 2010: Processes controlling aquifer fluid compositions in the Olkaria geothermal system, Kenya. *J. Volcanol. Geoth. Res.*, 196, 57-76.
- Karlsdóttir, R., 2002: *Námafjall. TEM-resistivity measurements 2001*. Orkustofnun, Reykjavík, report OS-2002/057 (in Icelandic), 68 pp.
- Karlsdóttir, R., 1993: *Námafjall. TEM-resistivity measurements 1992*. Orkustofnun, Reykjavík, report OS-93022/JHD-12, 34 pp.
- Kristmannsdóttir, H., 1979: Alteration of basaltic rocks by hydrothermal activity at 100-300°C. In: Mortland, M.M., and Farmer, V.C. (editors), *International Clay Conference 1978*. Elsevier Scientific Publishing Co., Amsterdam, 359-367.
- Kristmannsdóttir, H., 1978: *Alteration of bedrock in the Krafla geothermal system*. Orkustofnun, Reykjavík, report OSJHD 7854 (in Icelandic).
- Kristmannsdóttir, H. and Ármannsson, H., 2004: Groundwater in the Lake Mývatn area, northern Iceland. *Chemistry, Origin and Interaction, Aquatic Ecology*, 115-128.
- Larsen, G., Gronvold, K., and Thorarinnsson, S., 1978: *Volcanic eruption through a geothermal borehole at Námafjall, Iceland*. Nordic Volcanological Institute, Science Institute, Reykjavik, report RH-78-10, 22 pp.
- Li, K. and Horne, R.N., 2004a: An analytical scaling method for spontaneous imbibitions in gas-water-rock systems. *SPEJ*, 9-3, 322-329.
- Li, K. and Horne, R.N., 2004b: Experimental study of gas slippage in two-phase flow. *SPERE*, 409-414.
- Lonker, S. W., Franzson, H., Kristmannsdóttir, H., 1993: Mineral-fluid interactions in the Reykjanes and Svartsengi geothermal systems, Iceland. *American Journal of Science*, 293, 605-670.

- Mortensen, A., Egilson, T., Gautason, B., Gunnarsson, H., and Ingólfsson, T., 2008: *Bjarnarflag- well BJ-14. 3rd stage: Drilling of production section from 847 m to 2506 m depth*. ÍSOR – Iceland GeoSurvey, Reykjavik, report ÍSOR -2008/039 (in Icelandic).
- Nicholson, H., Condomines, M., Fitton, J.G., Fallick, F.E., Grönvold, K., and Rogers G., 1991: Geochemical and isotopic evidence for crustal assimilation beneath Krafla, Iceland. *J. Petrol.*, 32, 1005-1020.
- Noorollahi, Y., 2005: *Application of GIS and remote sensing in exploration and environmental management of Námafjall geothermal area, N-Iceland*. University of Iceland, M.Sc. Thesis, 176 pp.
- Ólafsson, M., and Kristmannsdóttir, H., 1989: The influence of volcanic activity on groundwater chemistry within the Námafjall geothermal system, North Iceland. In: Miles D.L. (editor), *Water-Rock Interaction, WRI-6, Balkema, Rotterdam*, 537-540.
- O’Sullivan, M., Pruess, K., and Lippmann, M., 2001: State of the art of geothermal reservoir simulation. *Geothermics*, 30-4, 395-429.
- Orkustofnun and VGK, 1994: *A geothermal power plant at Bjarnarflag. Feasibility study*. Landsvirkjun, Reykjavík, report, 71 pp.
- Pálsson, B., Gunnarsson, Á., Ingason, K., Gudmundsson, Á., Hjartarson, H., and Júlíusson, B.M., 2010: Development of the 400 MW Northeast Iceland geothermal project. *Proceedings World Geothermal Congress, Bali, Indonesia, 25-29 April 2010*.
- Pálmason, G., and Saemundsson, K., 1974: Iceland in relation to the Mid-Atlantic Ridge. *Ann. Rev. Earth Planet. Sci.*, 2, 25-63.
- Plummer, L.N., Busenberg, E., 1982: *The solubilities of calcite, aragonite and vaterite in CO₂-H₂O solutions between 0 and 90°C, and evaluation of the aqueous model for the system CaCO₃-CO₂-H₂O*. *Geochim. Cosmochim. Acta*, 46, 1011-1040.
- Pokrovskii, V. A., Helgeson, H. C., 1995: Thermodynamic properties of aqueous species and the solubilities of minerals at high pressures and temperatures: The system Al₂O₃-H₂O-NaCl. *American Journal of Science*, 295-10, 1255-1342.
- Pruess, K., 2002: *Mathematical modeling of fluid flow and heat transfer in geothermal systems*. UNU-GTP, Reykjavík, Iceland, report 3, 92 pp.
- Ragnars, K., Saemundsson, K., Benediktsson, S., Einarsson, S.S., 1970: Development of the Námafjall area, northern Iceland. *Geothermics*, 2, 925-936.
- Remoroza, A.I., 2010: *Calcite mineral scaling potentials of high-temperature geothermal wells*. University of Iceland, Reykjavík, Faculty of Science, MSc thesis, 99 pp.
- Rivera Ayala, M. A. 2010: *Coupled geothermal reservoir wellbore simulation with a case study for the Námafjall field, N-Iceland*. University of Iceland, Reykjavík, MSc thesis, UNU-GTP, Iceland report 2, 66 pp.
- Robie, R.A., Hemingway, B.S., 1995: *Thermodynamic properties of minerals and related substances at 298.15 K and 1 bar (105 Pascals) pressure and at higher temperatures*. U.S. Geol. Survey, Bull. 2131, 461 pp.
- Rodas, M.A., 2010: *Preliminary environmental impact assessment for the geothermal field Chachimbiro in Ecuador. A case comparison with Bjarnarflag geothermal field in Iceland*. University of Iceland, Reykjavík, MSc.thesis, 147 pp.

- Rosenkjaer, G.K., 2011: *Electromagnetic methods in geothermal exploration. 1D and 3D inversion of TEM and MT data from a synthetic geothermal area and the Hengill geothermal area, SW Iceland*. University of Iceland, Faculty of Earth Sciences, Reykjavík, MSc thesis.
- Saemundsson, K., 1991: The geology of the Krafla system. In: Gardarsson, A., and Einarsson, Á. (eds.), *The nature of Lake Mývatn* (in Icelandic). The Icelandic Society of Natural Sciences, Reykjavík, 25-95.
- Saemundsson, K. 1979: Outline of the geology of Iceland. *Jökull*, 29, 7-28.
- Scott, S.W., 2011: *Gas chemistry of the Hellisheidi geothermal field*. University of Iceland, MSc Thesis. REYST report 08-2011, 69 pp.
- Sigurdsson, Ó., 1993: *The geothermal system in Bjarnaflag. Evaluation of temperature, pressure and well productivity*. Orkustofnun, Reykjavík, report OS-93016/JHD-08 B, 45 pp (in Icelandic).
- Sólnes, J., Sigurdsson, T.M. and Einarsson, H. 1995: *A geothermal power plant at Bjarnarflag. An overview of environmental impact and a draft initial environmental impact report for a 20 MWe geothermal power plant at Bjarnarflag*. Landsvirkjun, Reykjavík, report, 138 pp.
- Sorey, M.L., Grant, M.A. and Bradford, E., 1980: Nonlinear effects in two-phase flow to wells in geothermal reservoirs. *Water Resour. Res.*, 16, 767-777.
- Stefánsson, A. and Arnórsson, S., 2002: Gas pressures and redox reactions in geothermal fluids in Iceland. *Chem. Geol.*, 190, 251-271
- Sveinsbjörnsdóttir, Á.E., 1992: Composition of geothermal minerals from saline and dilute fluids – Krafla and Reykjanes, Iceland. *Lithos*, 27, 301-315.
- Sverris saga, 1920: History of king Sverrir. G. Inderbro, 150 pp.
- Thórarinnsson, S., 1979: The postglacial history of the Mývatn area. *Oikos*, 32, 17-28.
- Thórdarson, T. and Larsen G., 2007: Volcanism in Iceland in historical time: Volcano types, eruption styles and eruptive history. *J. Geodynamics*, 43, 118-152.
- Thóróddsson Th.F. and Sigbjarnarson G. 1983: *The Lake Mývatn diatomite plant. Groundwater studies*. Orkustofnun, Reykjavík, report OS-83118/VOD-10 (in Icelandic), 25 pp.
- Ushakov, S., 2000: Interpretation of geochemical data from fumaroles and wells in the Námafjall geothermal field, Iceland and from fumaroles in the Mutnovsky geothermal field, Kamchatka, Russia. Report 18 in: *Geothermal training in Iceland 2000*. UNU-GTP, Iceland, 385-398.

APPENDIX I: TEMPERATURE PROFILES OF NÁMAFJALL WELLS



APPENDIX II: FLUID / GAS CHARACTERISTICS AND SELECTED CONSTITUENT CONCENTRATIONS AT 10 BAR-A / 180 °C AS A FUNCTION OF PRODUCTION TIME

